Antti Karjalainen

Framework for a positron microscope

School of Science

Thesis submitted for examination for the degree of Master of Science in Technology.

Espoo February 16, 2015

Thesis supervisor:

Prof. Filip Tuomisto

Thesis instructor:

D.Sc. Klaus Rytsölä

Aalto University
School of Science

AALTO UNIVERSITY
SCHOOL OF SCIENCE

ABSTRACT OF THE
MASTER'S THESIS

Author: Antti Karjalainen

Title: Framework for a positron microscope

Date: February 16, 2015 Language: English Number of pages:8+75

Department of Applied Physics

Professorship: Nuclear engineering Code: Tfy-56

Supervisor: Prof. Filip Tuomisto

Instructor: D.Sc. Klaus Rytsölä

Positron annihilation spectroscopy is an efficient method for studying defects, especially vacancies. The resolution of positron microscopy is restricted by the diffusion length of positrons (typically 0.1-0.2 µm). In practice, spatial resolutions up to 1 µm have been reached. A positron microscope can be used for studying defects in e.g. cracks in metal and optoelectronic components.

In this thesis, three existing positron microscopes are reviewed. They all possess a spatial resolution below 5 µm with an acceptable count rate. The Münich positron microscope is a pulsed positron beam and is able to measure positron lifetime. It has one remoderation stage for reducing the beam spot size and the spatial resolution of it is 2 µm. The positron microscopes in Bonn and Takasaki measure Doppler broadening of annihilation radiation of positrons with resolutions of 1 µm and 3.9 µm, respectively. They both utilise optical columns of commercial SEMs for focusing the positron beam. The Münich and Bonn positron microscopes can also be used as scanning electron microscopes.

Based on the comparison of the existing positron microscopes, the structure of a new positron microscope for the needs of the Aalto positron group is proposed. The structure is based on the Bonn positron microscope with some modifications, such as an additional objective lens below the sample. Some of the modifications require verification of their feasibility.

A commercial SEM (ZEISS/Opton, DSM 950), which will be utilised as the optical column of the positron microscope, was initialised and tested. A roadmap for the design and construction of the new positron microscope is outlined.

Keywords: positron, annihilation, microscope, microprobe, review, design

AALTO-YLIOPISTO
PERUSTIETEIDEN KORKEAKOULU

DIPLOMITYÖN
TIIVISTELMÄ

Tekijä: Antti Karjalainen

Työn nimi: Pohjatyö positronimikroskooppia varten

Päivämäärä: February 16, 2015 Kieli: Englanti Sivumäärä:8+75

Teknillisen Fysiikan Laitos

Professuuri: Ydintekniikka Koodi: Tfy-56

Valvoja: Prof. Filip Tuomisto

Ohjaaja: TkT. Klaus Rytsölä

Positroniannihilaatiospektroskopia on herkkä ja tehokas menetelmä hilavirheiden, etenkin vakanssien, tutkimiseen. Positronien diffuusiopituus (tyypillisesti 0.1-0.2 µm) asettaa rajan positronimikroskooppien resoluutiolle. Olemassa olevilla positronimikroskoopeilla on päästy 1 µm resoluutioon. Positronimikroskooppi soveltuu hilavirheiden tutkimiseen esimerkiksi metallien murtumissa ja optoelektroniikan komponenteissa.

Tässä työssä käydään läpi kolmen olemassa olevan positronimikroskoopin rakenne ja toiminta. Kaikkien positronimikroskooppien resoluutio on parempi kuin 5 µm pulssitaajuuden vielä ollessa käyttökelpoinen. Münchenin positronimikroskooppi on pulssitoiminen ja siten pystyy mittaamaan positronien elinaikaa. Se sisältää yhden remoderointi-vaiheen positronisuihkun koon pienentämiseksi ja sen resoluutio on 2 µm. Bonnin ja Takasakin positronimikroskoopit mittaavat molemmat annihilaatiosäteilyn Doppler-levenemää resoluutioilla 1 µm (Bonn) ja 3.9 µm (Takasaki). Ne käyttävät kaupallisen pyyhkäisyelektronimikroskoopin optista kolumnia positronisuihkun fokusointiin näytteeseen. Münchenin ja Bonnin mikroskoopit pystyvät toimimaan myös pyyhkäisyelektronimikroskooppeina.

Olemassa olevien positronimikroskooppien ominaisuuksien ja suorituskykyjen vertailun pohjalta valittiin rakenne ja ominaisuudet Aalto-yliopiston positroniryhmän uutta positronimikroskooppia varten. Lähtökohdaksi valittiin Bonnin positronimikroskooppi, jonka rakenteeseen ehdotettiin muutamia muutoksia, kuten erillisen magneettilinssin lisäämisestä näytteen alle. Ehdotetuista muutoksista osan käyttökelpoisuus vaatii jatkoselvitystä.

Työn aikana kaupallinen elektronimikroskooppi (ZEISS/Opton, DSM 950), jota on tarkoitus käyttää positronimikroskoopin optiseksi kolumnina, valmisteltiin käyttökuntoon ja testattiin. Positronimikroskoopin toteuttamiselle hahmoteltiin etenemissuunitelma.

Avainsanat: positroni, annihilaatio, mikroskooppi, vertailu, suunnittelu

Preface

I would like to thank Filip for the interesting topic for my thesis; my group for the patience to answer to an innumerable load of questions during my thesis, especially Klaus; the help from Würzburg: Torsten, Danny, Sebastian, Frank and, of course the walking positron microscope encyclopedia, Matz; academic sources of inspiration [36, 50]; my brother for a coffee package in my hour of need and Anna for regular, deep and meaningful conversations in a completely platonic manner.

The total amount of cola containers and the itemisation of the consumed cola products are shown below in Figure 0 and Table 0. The making this Master's thesis took 43.98 litres of cola. The most consumed cola in volume was Pepsi MAX (14 l), while in the number of containers the most consumed cola product was a Rio cola can (11 × 0.33 l). The total consumption is equivalent to a consumption of 6.3 l per a month (7 in total), 1.6 l per a week or 0.31 l per a day. The average daily cola consumption of almost a 0.33 l can suggests a mild level of cola addiction.

Figure 0: The amount cola, which was consumed during the thesis. One 0.35 l Coca Cola bottle was sacrificed as a liquid coolant container, two 0.5 l and one 1.5 l Pepsi Max bottles as canisters for used oil and two 0.33 l Rio Cola cans were turned into mini speaker enclosures. Those bottles and cans are not included in the figure.

Table 0: The amount of cola consumed during this thesis. The minor amounts of orange and lemon lemonade can be considered as measurement technical artefacts and should be neglected from the analysis.

Type	Number	Volume (l)
Coca-cola		(8)
0.35 l bottle	10	3.5
1.5 l bottle	3	4.5
Coca-cola ZERO		(3.35)
1.5 l bottle	2	3
0.35 l bottle	1	0.35
Coca-cola light		(6)
1.5 l bottle	4	6
Pepsi		(7.5)
1.5 l bottle	5	7.5
Pepsi Next		(1.5)
1.5 l bottle	1	1.5
Pepsi MAX		(14)
1.5 l bottle	8	12
0.5 l bottle	4	2
Rio cola		(3.63)
0.33 l can	11	3.63
Sprite		~~(0.33)~~
0.33 l bottle	1	~~0.33~~
La Rita, orange lemonade,		~~(0.33)~~
0.33 l can	1	~~0.33~~
In total		43.98

Otaniemi, 27.1.2015

Antti J. Karjalainen

About citations in this thesis

In order to achieve unambiguous citation without having a citation in every sentence, a method to cite multiple sentences unambiguously has to be defined. In this thesis, citations outside sentences refer to all sentences up to the previous citation or the beginning of the paragraph are cited from the source:

> Nullam eu tellus tellus. Suspendisse at nunc bibendum, luctus libero at, rutrum dolor. [C]
>
> Cum sociis natoque penatibus et magnis dis parturient montes, nascetur ridiculus mus [D]. Aliquam tempor ornare odio vitae rutrum. Nullam porta et massa sed tempus. In vel quam sit amet mi consectetur sollicitudin. [E]

Citations inside a sentence refer to the sentence above:

> Lorem ipsum dolor sit amet, consectetur adipiscing elit [A]. Cras quis maximus ante [B].

Contents

Symbols and abbreviations

Symbols

Z	atomic number of an element

Abbreviations

BPM	Bonn scanning positron microprobe
CDBS	coincidence (positron) Doppler broadening spectroscopy
cps	counts per second (1/s)
DBS	(positron) Doppler broadening spectroscopy
DFT	density functional theory
FWHM	full width at half maximum
HMA	high momentum analysis
linac	linear accelerator
LLNL	Lawrence Livermore National Laboratory
LTS	(positron) lifetime spectroscopy
MPM	Münich scanning positron microprobe
PAS	positron annihilation spectroscopy
SEM	scanning electron microscope
SPM	scanning positron microscope/microprobe
TPM	Takasaki scanning positron microscope

1 Introduction

A defect in a solid matter means a local interruption in the periodic structure of the solid. Depending on their concentration and type, defects can have a major impact on the properties of the solid. For example, the modification of the properties of semiconductors by introducing defects, i.e. doping, is a cornerstone of the modern semiconductor industry. However, also unintentional defects can have as significant effects as the intentional ones. Unintentional defects can arise from the growth methods of the material, as byproducts of intentional doping or from the material treatments.

Defects can be classified by their dimensions. The simplest defect structure is a point defect where the periodicity is disrupted only by a single atom. Point defects, i.e. vacancies, substitutional and interstitial atoms, are classified as zero-dimensional defects. The defects, which extend in one dimension, are referred to as line defects and the defects extending in two dimensions are referred to as planar defects.

The defects in solids can be studied in several different ways, such as with electrical, optical or particle beam methods. Electrical measurements can provide information on the concentrations of free-carriers, deep carrier traps and both ionised donors and acceptors. Optical spectroscopies measure absorption and emission characteristics of the material, which originate from emissive transitions of charge carriers between the energy states of the solid. Unlike electrical and optical measurements, particle beam methods can damage in the sample under measurement. For example, secondary ion mass spectroscopy (SIMS) is a destructive particle beam method. It measures the mass-to-charge ratios of sputtered ions. Transmission electron microscopy can detect individual extended defects but can also damage the sample. Also, non-destructive beam methods exist, such as positron annihilation spectroscopy (PAS).

PAS is a sensitive method for studying defects with open volume, starting from individual vacancies, but it is also able to detect negatively charged defects. PAS can detect individual point defects at concentrations of 10^{15} cm^{-3} and can separate the defect structures of different sizes and concentrations. Measurements on different temperatures can further yield information on the charge states of the defects. Coincidence type Doppler broadening PAS together with density functional theory (DFT) calculations enables identification of the atoms surrounding the defects.

The usual PAS techniques have a lateral resolution of the order of millimeters. The positron diffusion length (typically 100-200 nm) limits the maximal spatial resolution of PAS techniques. However, cracks in metals and some semiconductor devices possess defect structures with characteristic spatial dimensions in the micrometer range, which are unreachable with conventional PAS techniques but achievable within the physical resolution limit. Hence, there is motivation for a PAS measurement device with a resolution of few micrometers. The first high spatial resolution positron beam was constructed by Brandes *et al.* in 1987. It produces a beam with dimensions of 10 µm×50 µm and 8000 positrons/s [1]. Three positron microscopes with beam diameters below 5 µm have later been built [2–4]. Two of them utilise electron optics of commercial scanning electron microscopes. The mi-

croscopes produce images of the measured quantity by scanning the sample with a sample stage. Therefore, they are also referred to as scanning positron microscopes (SPMs).

The goal of this work is to produce guidelines for the structure of a new SPM based on a commercial scanning electron microscope (ZEISS/Opton, DSM 950). The requirement for the SPM is a positron beam with a diameter smaller than 10 µm with at least 50 counts per second (cps). After meeting these conditions, the effort of the construction should be minimised.

First in this manuscript, the basic theory concerning PAS measurements and SPMs is introduced. Then, existing SPMs are reviewed and their characteristic features and performances are compared. Next, the structure of the new SPM is proposed based on the comparison of the existing SPMs. Finally, a roadmap for the design and construction of the SPM is outlined. During this thesis, the scanning electron microscope was initialised and tested. A concise documentation of the DSM 950 is presented in Appendix A.

2 Positron annihilation spectroscopy

Positrons can be used to identify the concentration and the type of defects starting from concentrations of around 1 ppm or 10^{15} cm^{-3}. The electron density and the atomic structure of defect sites can be studied by implanting positrons into the sample and measuring the lifetime positrons or the energy spectrum of the annihilation radiation.

The positrons annihilate either in delocalised bulk states or localised states in potential wells. Positron annihilation spectroscopies yield information of the sites where positrons annihilate. Common positron traps are defects with open volume but also negative ions and dislocations act as shallow traps for positrons. Detailed reviews of positron annihilation spectroscopies are given for instance in [5] and [6].

2.1 Basic theory of positron annihilation studies

When a positron is injected into a material it loses its kinetic energy in collisions within a few picoseconds (Figure 1). Afterwards, the positron lives in a thermal equilibrium with its surroundings and diffuses in the solid. The positron may get trapped into potential wells, such as vacancies or negative ions. The total lifetime of positrons in a solid is usually of the order of a hundred picoseconds and it ends in an annihilation with an electron. The positron lifetime depends on the electron density around the positron. Due to the conservation of momentum, the momentum of annihilating positron-electron pair is transferred to the annihilation gammas, which makes possible to use the energy of the annihilation gamma photons to study the concentration and type of the defects in the solid. The two main branches of the positron annihilation spectroscopies are positron lifetime spectroscopy (LTS) and Doppler broadening spectroscopy (DBS). [5]

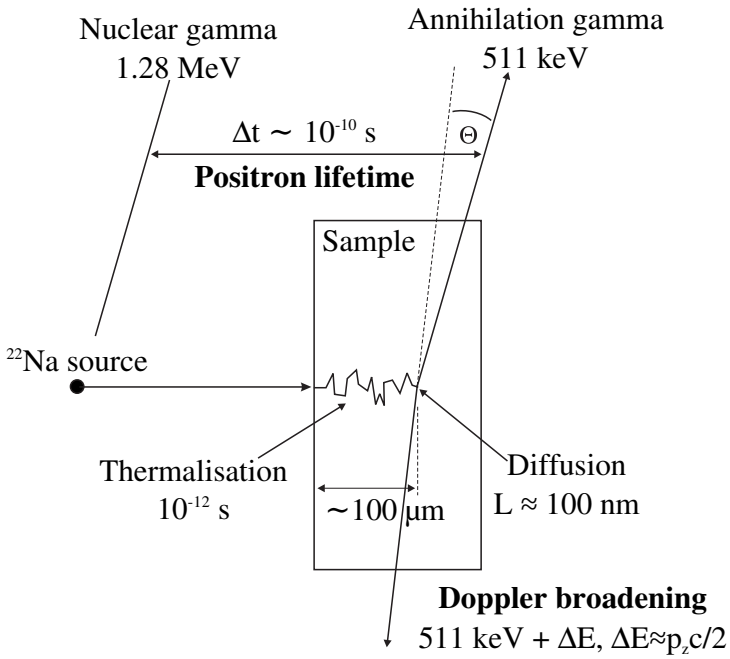

Figure 1: A schematic of the positron annihilation measurements.

2.1.1 Positron production and stopping

Positrons are usually obtained from radioactive β^+ sources but also reactor and linear accelerator (linac) sources based on pair production exist. The most usual radioactive source isotope nowadays is ^{22}Na, which has the following decay chain

$$^{22}\mathrm{Na} \rightarrow {}^{22}\mathrm{Ne}^* + \mathrm{e}^+ + \nu \quad (1)$$

$$^{22}\mathrm{Ne}^* \rightarrow {}^{22}\mathrm{Ne} + \gamma_{1.28\ \mathrm{MeV}}, \quad (2)$$

where Ne* refers to a Ne-atom with an excited nucleus, e^+ to a positron, ν to a neutrino and $\gamma_{1.28\ \mathrm{MeV}}$ to a gamma quantum of 1.28 MeV. Both reactor and linac sources generate a high flux of high energy gammas (>1 MeV) and produce positrons via pair production [7,8]. These sources produce greater positron fluxes than radioactive sources ($\lesssim 10^9$ 1/s) but such facilities are rare and expensive.

The positron energy distribution from beta decay can be approximated with Fermi's golden rule [9]

$$\frac{\mathrm{d}\lambda}{\mathrm{d}K} = \frac{C}{c^5}\sqrt{K^2 + 2mc^2K}(K_{max} - K)^2(K + mc^2), \quad (3)$$

where λ refers to the decay constant, K to the kinetic energy of the emitted positron, c to the speed of light, m to the mass of a positron, K_{max} to the total energy released in the decay (maximum kinetic energy of positrons) and C is a constant. The kinetic energy distribution of positrons emitted from ^{22}Na ($K_{\mathrm{max}} = 543$ keV), calculated using equation 3, is shown in Figure 2a.

The stopping profile of positrons, with the energy spectrum of a beta decay, in a material, with a density of ρ, follows approximately an exponential stopping profile

$$p(x) \approx \alpha e^{-\alpha x} \tag{4}$$

where

$$\alpha \approx 16 \frac{\rho[\mathrm{g/cm^3}]}{(K_{max}[\mathrm{MeV}])^{1.4}} \mathrm{cm}^{-1}. \tag{5}$$

In equation 5, $\rho[\mathrm{g/cm^3}]$ refers to the density of the solid in units of $\mathrm{g/cm^3}$ and $K_{\mathrm{max}}[\mathrm{MeV}]$ to the maximum kinetic energy of positrons emitted in the beta decay in units of MeV. The stopping profile of positrons emitted by ^{22}Na in Si, calculated with equations 4 and 5, is shown in Figure 2b. The mean stopping depth $(1/\alpha)$ in Si is 110 µm. As roughly one half of the positrons annihilate within the first 100 µm, positrons emitted from a radioactive source can only be used to study bulk materials. [6]

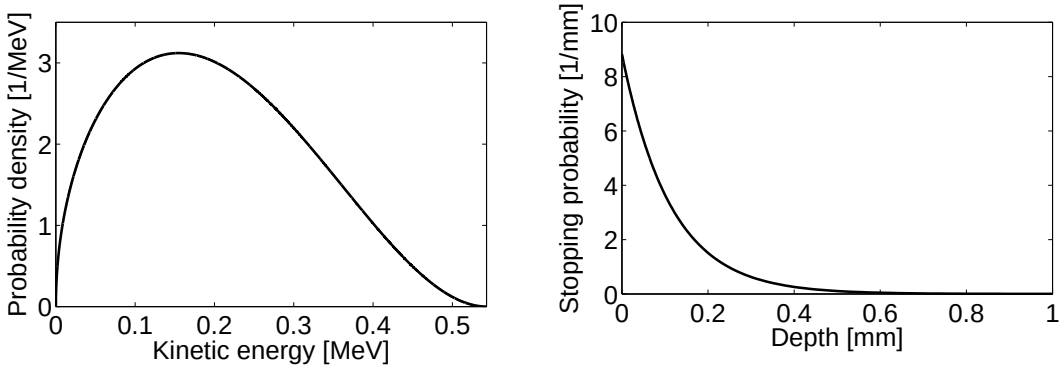

(a) energy distribution (b) stopping profile

Figure 2: 2a: The emission probability distribution of positron from ^{22}Na decay with respect to their kinetic energy. Calculated according equation 3.
2b: Stopping profile of positrons from ^{22}Na decay in Si, according equations 4 and 5.

In order to achieve any depth resolution, a monoenergetic positron beam is required. The stopping distribution of positrons with a low kinetic energy ($K < 50$ keV) in a material, with a density ρ, can be described with a derivative of a Gaussian function

$$p(x) \approx \frac{2x}{x_0^2} e^{-(x/x_0)^2} \tag{6}$$

with a mean stopping depth of

$$\bar{x} \approx 0.886 x_0 = A(K[\mathrm{keV}])^n, \tag{7}$$

where $A = 4/\rho \cdot \mathrm{\mu g/cm^2}$ and $n \approx 1.6$. The width of the positron stopping profile increases with the kinetic energy of positrons, as seen in Figure 3. The mean stopping depth for 20 keV positrons in Si is 2 µm. [5]

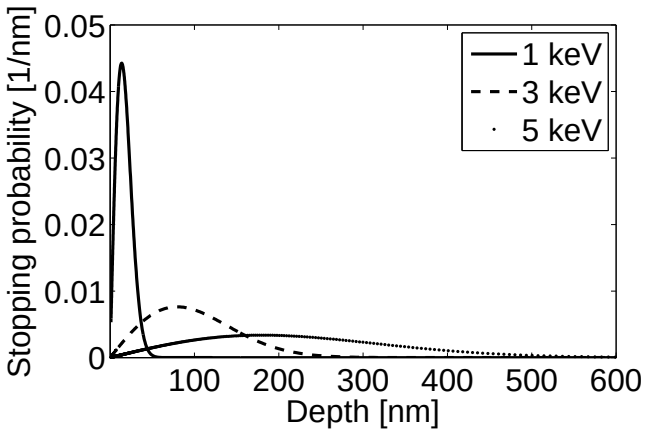

Figure 3: The stopping profile of positrons with kinetic energies of 1, 3 and 5 keV in Si, according equation 6.

After positrons have lost their kinetic energy, i.e. they have been thermalised, they diffuse in the solid until getting trapped or annihilated. The positron diffusion length (L_+) is dependent on the diffusion constant (D_+) of positrons in a solid and on the positron lifetime (τ)

$$L_+ = \sqrt{6D_+\tau}. \tag{8}$$

The diffusion constant is typically largest for a perfect lattice and decreases when the defect concentration increases. The defects, which trap positrons, decrease the diffusion length most. For a typical diffusion constant of $D_+ \approx 1.5$ cm^2/s at room temperature and a positron lifetime of $\tau \approx 100$ ps, the positron diffusion length is around 0.3 µm which corresponds roughly to 500 lattice sites. During the diffusion, positrons can be trapped into potential wells. Depending on the depth of the potential well, the thermal energy of the positrons may be enough to induce significant detrapping. With positron trapping models one can describe positron trapping for instance as a function of temperature, as described in [5, 6].

2.1.2 Positron moderation

Monoenergetic positrons can be produced in a process called moderation, where positrons with a wide energy spread (e.g. a beta spectrum of ^{22}Na) are injected into a material with a negative positron work function, such as W, Ni or solid Ne. The injected positrons thermalise in the material within few picoseconds. The positrons, which reach the surface with diffusion, are ejected perpendicularly to the surface normal with the energy corresponding to the work function of positrons in the moderator material, typically a few eV. The small non-normal momentum component of the emitted positron comes from the momentum of positron before the emission. For a thermalised positron, the typical kinetic energy in room temperature is approximately 25 meV, which is significantly smaller than the work function for example in W (3 eV). Thus, moderated positrons are emitted practically perpendicular to

the surface. Also, the total kinetic energy of the emitted moderated positrons is practically equal to the work function of the moderating material.

Moderating efficiency is typically defined as the amount of moderated slow positrons divided by the amount of positrons produced in the source. The exact moderator efficiency values defined this way are somewhat imprecise, but the reason for this is purely practical: the amounts of the absorbed and scattered positrons are not well known, and their determination would warrant an additional study. Besides the moderator material, the value of the efficiency of a moderator depends on the crystal quality, the energy spectrum of the primary positrons and the geometry of both the moderator and the source.

Moderation can be done in transmission geometry with thin moderator films (Figure 4a) or in reflection geometry with thick moderator blocks (Figure 4b). The reflection geometry has yielded better efficiencies ($3 \cdot 10^{-3}$ for a W single crystal with ^{58}Co source [10]), but the positron source shadows the center of the moderated positron beam and the reflection geometry cannot be used in positron microscopes. Today, monoenergetic positron beams usually use transmission geometry moderation, which does not have the shadowing effect.

Among thin film moderators, the best moderation efficiency has been obtained with solid Ne, $3 \cdot 10^{-3}$ for ^{22}Na [11], while efficiencies for W and Ni thin films have been reported as one order of magnitude lower: $6 \cdot 10^{-4}$ and $5 \cdot 10^{-4}$ for ^{22}Na, respectively [12]. Higher efficiencies in transmission geometry have been obtained with cone moderator geometries (Figure 4c): $5 \cdot 10^{-3}$ for a solid Ne [13] and $1.4 \cdot 10^{-3}$ for a W cone moderators [14]. A tungsten moderator with a thin film attached to a single crystal cone has yielded an efficiency of $1.7 \cdot 10^{-3}$ [15].

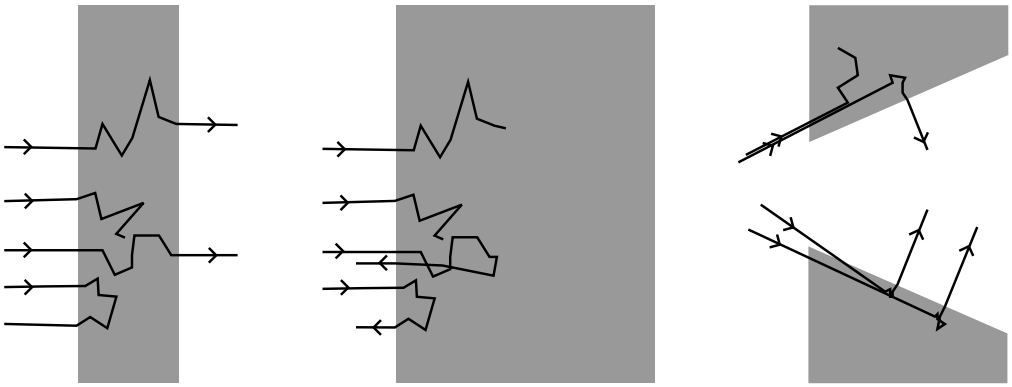

(a) thin film (b) reflection (c) cone

Figure 4: Schemes of different moderator geometries: thin film (4a), reflection (4b) and cone (4c) moderator. Black lines represent trajectories of positrons. Dimensions are no in scale. Moderators are typically rotationally symmetric.

A quantity called longitudinal energy spread

$$E_{\parallel} = \frac{p_{\parallel}^2}{2m_e} \tag{9}$$

is typically used to also describe the angular spread of positrons, because this quantity can be easily measured by slowing particles down with an axial electrostatic field. The longitudinal energy variation of moderated positrons has been reported to be an order of magnitude higher for a solid Ne moderator (an FWHM of approximately 0.6 eV) [11, 16] than for W and Ni moderators (90 meV for W and 25 meV for Ni) [17]. For a W cone moderator, the longitudinal energy spread has been measured to be twice the energy spread of a W thin film moderator [14]. Recently, an efficiency of $\sim 10^{-2}$ has been reported for a solid Ne cone moderator but with an FWHM energy spread of 2 eV [18].

The documented efficiencies of solid Ne moderators are fivefold compared to the efficiencies of W moderators of the same geometry, but the longitudinal energy spread of the moderated positrons is correspondingly larger. The solid Ne moderator requires cryogenic cooling to 4 K [11], which accelerates the surface contamination of the moderator. Hence, solid Ne moderators require regular regrowth. Threefold moderating efficiencies have been reached with moderators of cone geometry compared to the thin film moderators of the same material but with a correspondingly increased longitudinal energy spread of the moderated positrons. Usually, W thin film are used as moderators because of their simplicity.

In a typical monochromatic slow positron beam, a thin film moderator is attached in front of a positron source, which is usually NaCl with ^{22}Na isotope. The moderated positrons are extracted from the moderator with an electric field. The guiding of the positron beam can be performed both electro- and magnetostatically. A simple solenoid magnet or Helmholtz coils around the beam line are mainly used as they are relatively simple to construct. If transmission moderation geometry is used, most of the positrons will penetrate the moderator without thermalisation. Thus, it is necessary to filter the unmoderated, fast positrons from the positron beam. The filtering can be performed for instance by E×B -filter or by bending the beam with a magnetic field.

2.2 Positron lifetime spectroscopy

Positron lifetime spectroscopy (LTS) is one of the two main branches of the positron annihilation spectroscopies. In an LTS measurement setup, the lifetime of positrons is measured. A typical LTS setup uses ^{22}Na as the source because the decay of ^{22}Na produces almost simultaneously a gamma quantum of 1.28 MeV. This 1.28 MeV gamma can be used to start a timer, whereas the 511 keV annihilation gamma can be used to stop the timer. The time between the start and the stop gammas is approximately the positron lifetime.

Each annihilation state produces an exponential lifetime distribution, $N_i e^{-t/\tau_i}$. The time resolution of the measurements setups is finite and in good setups it is approximately Gaussian. The measured lifetime spectrum is a convolution of the resolution function, $g(t)$, and the sum of individual lifetime components

$$N(t) = g(t) * \sum_i N_i e^{-t/\tau_i}. \tag{10}$$

However, due to trapping kinetics, the measured lifetimes, τ_i, are not straightforwardly the lifetimes of the different annihilation sites. With trapping models and knowledge of the concentration and types of the defects, the actual lifetimes of annihilation sites can be calculated. [5, 6]

The positron lifetime spectrum can be used to calculate the mean positron lifetime or to fit multiple lifetime components in the data. The positron lifetime in open volume type defects (vacancies, voids) is larger than in a bulk state because of the smaller electron density, and the positron lifetime increases as the size of the open volume increases. The positron lifetime in dislocations is similar to the bulk but the existence of dislocation traps can still be detected via kinetic trapping models and temperature resolved LTS measurements. The positron lifetime data can also be compared to the results of DFT-calculations. [5, 6]

A conventional LTS setup is illustrated in Figure 5. It utilises a sandwich-geometry, where the ^{22}Na positron source is placed between two identical samples and two scintillator-photomultiplier detectors: one detector for the start gamma and another for the stop gamma. Both detectors require an energy selection. In an analogous setup, the start and stop signals are fed into constant-fraction-timing-discriminators (CFDs). A CFD transforms long, wide pulses of the detector into narrow, sharp ones, which are more suitable for timing purposes. The timing signals of CFDs are fed into a time-to-amplitude converter (TAC). The stop signal is delayed with a constant delay due to measurement technical reasons. The analogous signal of the TAC is then read and digitised with a multichannel analyser (MCA).

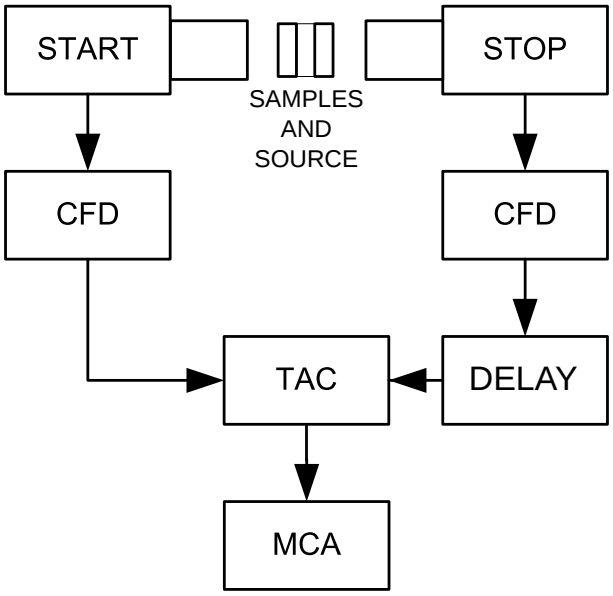

Figure 5: A diagram of an analogous lifetime setup. The components of the setup are discussed on the page 8.

In a digital measurement setup, the pulses from the detectors are directly digitised and further processing is done with a computer. Pulsed monoenergetic positron beams enable performing positron lifetime measurements with a depth resolution.

In a pulsed slow beam, the start signal is acquired from the bunching system of the beam.

The resolution function of a conventional LTS setup is fairly Gaussian while in pulsed positron beams it can be significantly non-Gaussian. A Gaussian resolution function does not change the centre of mass of the lifetime spectrum, i.e. the mean lifetime, or the fitted values of the exponential lifetime components. [5] Although the stop-signal detection system of a pulsed slow beam would be similar to conventional LTS setups, the total resolution function of a pulsed beam is usually distorted to non-Gaussian by the temporal structure of the positron pulses.

2.3 Doppler broadening of annihilation radiation

Doppler broadening spectroscopy (DBS) is based on the energy shift of the annihilation gamma quanta due to the total momentum of the annihilated positron-electron pair. If the annihilative electron-positron pair was in rest in reference to the gamma detectors, both the annihilation gamma quanta ($E_{\gamma 1}, E_{\gamma 2}$) would only have the mass energy of the pair

$$E_{\gamma 1} = E_{\gamma 2} = m_e c^2 = 511 \text{ keV}, \tag{11}$$

where m_e is the mass of an electron and c is the speed of light. When the pair has a non-zero total momentum, the energies of the annihilation gamma quanta have a Doppler shift

$$E_{\gamma 1} = m_e c^2 + \Delta E \tag{12}$$

$$E_{\gamma 2} = m_e c^2 - \Delta E, \tag{13}$$

where the Doppler shift (ΔE) is

$$\Delta E \approx \frac{c p_L}{2}, \tag{14}$$

and where p_L is the "longitudinal" momentum component of the electron-positron pair i.e. in the direction of the gamma quantum. The momentum of a thermalised positron is typically negligible compared to the momentum of electrons in a solid and, thus, the total momentum of the electron-positron pair approximately corresponds to the momentum of the annihilated electron. DBS does not require time resolved-measurements and, thus, it can be performed with both the beta decay spectra and slow positron beams. [5]

A Doppler spectrum can be analysed either as such or integrated over its peak or wing regions. The integral over low momentum shifts of a Doppler spectrum is referred to as S-parameter. The value of S-parameter correlates to the fraction of positrons annihilating with low momentum electrons and, thus, mainly the annihilations with low momentum valence electrons contribute to S-parameter. The second employed integral is over the wing region, W-parameter, which gives the fraction of annihilations with high momentum electrons. Core electrons solely cause the annihilations of W-parameter region. S- and W-parameters are usually normalised by dividing them with the respective parameters of the bulk material. The normalising is sometimes troublesome if no defect-free bulk exist. [5, 6]

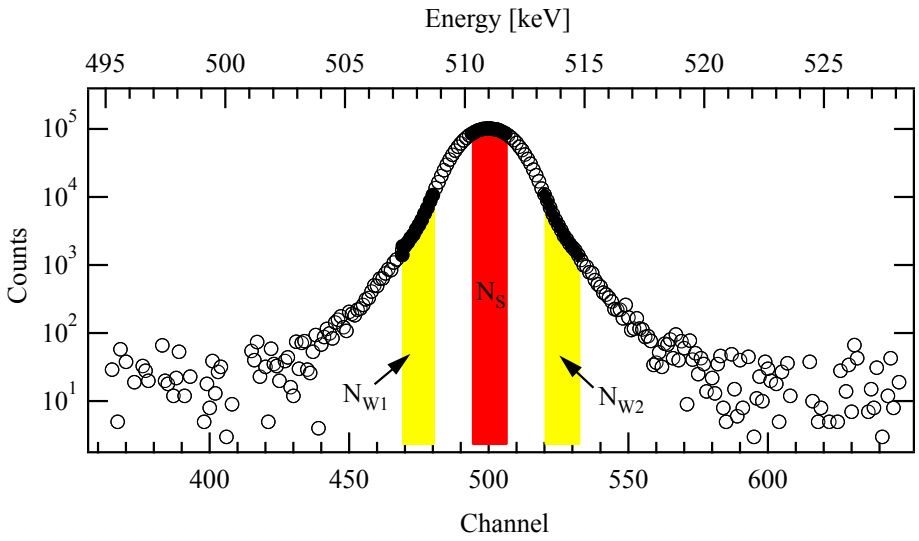

Figure 6: Raw Doppler broadening data from a positron annihilation measurement. Labels of the picture have been translated. [19].

An integral over a momentum region has a lower statistical error than the original measurement points and, thus, a lower number of counts is enough to achieve the same level of accuracy in S- or W-parameters compared to analysing the Doppler spectrum itself. The fraction of annihilations and also the signal-to-noise ratio decreases with increasing momentum shift. An acceptable S-parameter can be determined from 10^5 counts and W-parameter from 10^6 counts while the analysis of the Doppler spectrum itself usually requires a coincidence measurement of $3 \cdot 10^7$ counts.

The energy of annihilation gammas is measured with high purity Ge detectors. The energy resolution of a Ge detector is usually 1.0-1.5 keV at 511 keV, which is significant as compared to the total broadening of the annihilation peak, 2-3 keV. The resolution function of the Ge detector affects the measured shape of the annihilation peak. [5]

The peak-to-background ratio of a DBS measurement is relatively low (10^2) but the background can be suppressed with experimental and signal processing methods. By introducing two gamma detectors on opposite sides of the sample and demanding a time coincidence, the peak-to-background ratio can be increased by two orders of magnitude to about 10^4. The other detector used for time gating can be one of a lower energy resolution, such as a scintillator-photomultiplier one. An even higher peak-to-background ratio is reached if it is also demanded that the sum of the energies of the gamma photons is approximately equal to the rest energy of electron positron pair

$$E_1 + E_2 \approx 2m_e c^2 = 1.022 \text{ MeV}. \tag{15}$$

The execution of the energy condition requires the use of two Ge detectors but enhances the peak-to-background ratio to 10^6. [5] Usually, coincidence measurements are utilised in order to have a proper signal-to-noise ratio at high momenta. In practice, the count rate of a coincidence measurement is roughly an order of magnitude

lower than for a single detector measurement.

A possible method of obtaining a Doppler spectrum of a higher peak-to-background ratio with a single Ge detector, the high momentum analysis (HMA), was suggested by Haaks *et al.* [20–22]. It is based on subtracting multiple detector artefacts from the measured data. The requirements for the HMA are that the data has no significant background from gammas with higher energy than 511 keV and that the contribution of energy-dependent detection efficiency of Ge detectors is taken into account. DBS data of $1.1 \cdot 10^8$ counts of pure Cu measured with a single Ge detector and treated with the HMA is shown in Figure 7 with reference data from CDBS measurements. The result of HMA is comparable to CDBS reference up to $35 \cdot 10^{-3}$ m_0c. [22] The HMA has been utilised with the Bonn scanning positron microprobe (BPM) up to a Doppler broadening of $25 \cdot 10^{-3}$ m_0c [23].

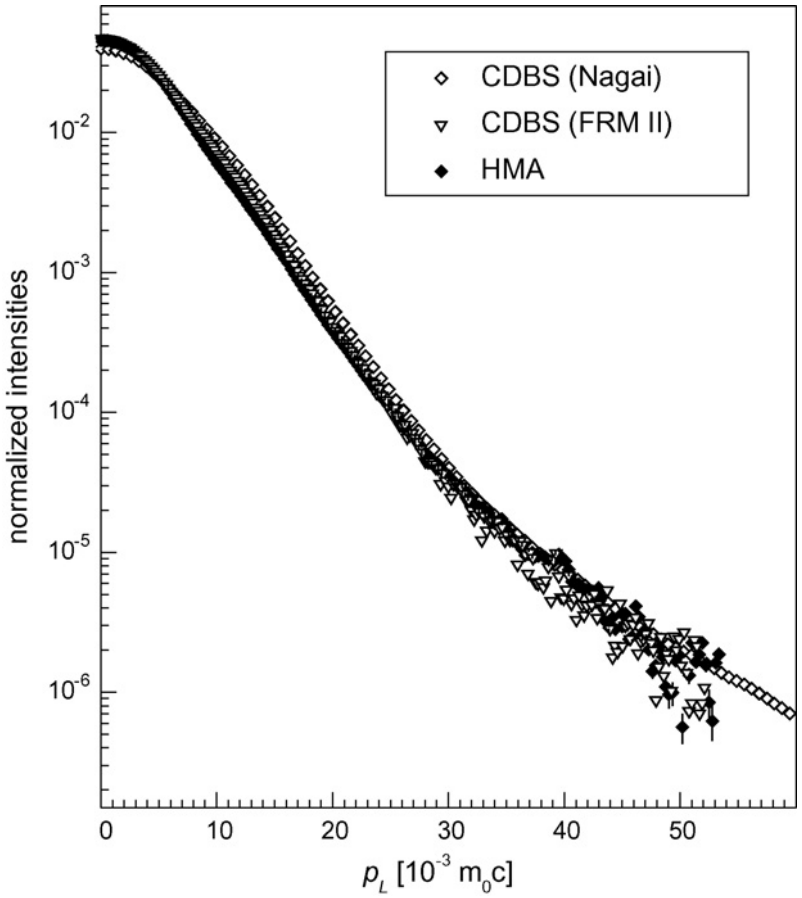

Figure 7: A Doppler spectrum of Cu obtained with a single Ge detector and treated with the high momentum analysis (HMA) and raw Doppler spectra of two reference coincidence Doppler broadening measurements (CDBS) [22].

2.4 Scanning positron microscope

A scanning positron microscope (SPM) is a device, which is able to perform PAS studies with a high lateral resolution (<10 µm) and scanning over the sample area, producing one, two or three dimensional image of the measured quantity, such as S-parameter or mean lifetime. As mechanical fractures exhibit defect structures with sizes in the micron range, SPMs are suitable for studying fatigue and cracks. Electrical components of suitable size, such as laser diodes, form another set of applications for SPMs.

A scanning positron microscope is also referred as a scanning positron microprobe or an SPM. It should be noted that the Münich research group also abbreviates the Münich scanning positron microscope as the SPM [3, 37, 46, 47]. In this work, the Münich scanning positron microscope is referred to as the MPM (Münich positron microscope) to separate it from other SPMs, the Bonn positron microprobe (BPM) and the Takasaki positron microscope (TPM).

An SPM is schematically illustrated in Figure 8. It consists of a microbeam apparatus, which implants positrons into the sample, and a gamma detector, which measures the data from the annihilation radiation. The data is acquired from the whole volume volume where positrons annihilate.

The most relevant characteristics of an SPM are the spatial resolution, the count rate and the resolution of the measured quantity (energy or time) (Figure 8). The last is the feature of the detector, which is also the most easily replaceable part. The depth resolution is defined by the stopping profile and diffusion of positrons, while in lateral direction the beam spot size, lateral scattering and diffusion length determine the resolution. The shape of the stopping profile and the lateral scattering depend on the acceleration voltage and the target material density. The diffusion length is solely a feature of the target material. The microbeam apparatus itself affects the spatial resolution via the beam spot size and the acceleration voltage (Figure 8).

The relation between the beam spot size and the count rate of an SPM is continuous. The smallest acceptable count rate defines the smallest usable beam spot size of the SPM. Because the acceleration of positron to the desired energy between 1 and 30 keV is relatively simple, in practice, the only interesting character of the actual positron microbeam apparatus is the connection between the positron flux and the beam spot size.

2.4.1 Limitations of an SPM

As to particle optics, the differences between the scanning positron and electron microscopes (SPMs and SEMs) are that the accelerating voltage is inverse, positrons gyrate to the opposite direction in the same magnetic field and the flux of moderated positrons is smaller by a factor of 10^{10}. Among these the last one bears the most difficulty to SPMs: obtaining a positron beam with a small diameter with still an acceptable count rate.

Besides the low positron fluxes, the spatial resolution of an SPM is also degraded from the resolution of its electron counterparts by the fact that in PAS the measured signal originates from the whole interaction volume, as illustrated in Figure 8. The

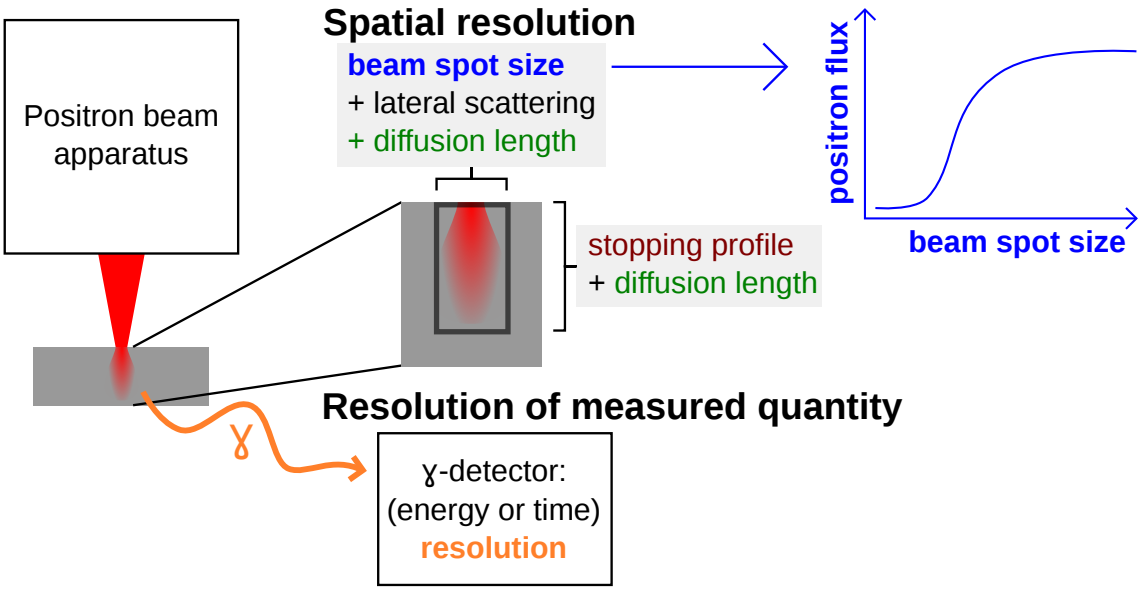

Figure 8: The most important features of a positron microscope.

diffusion lengths of positrons in solids range from a few to hundreds of nanometers and, therefore, even a point-like injection of positrons results in probing a volume determined by the diffusion. A beam diameter of 1 µm can be considered as a reasonable maximum spatial resolution because the positron flux decreases towards smaller beam spot sizes and below 1 µm the relative effect of the diffusion to the beam spot size starts to significantly increase.

The depth resolutions of SPMs is even more strongly restricted due to the stopping profile of positrons in solids. For low implantation energies ($K < 5$ keV) the stopping profile of positrons is relatively compact (<500 nm). As positrons with higher implantation energies penetrate deeper, the width of the stopping profile also increases accordingly. As an example, Figure 9 shows the main features of the stopping profile of positrons with kinetic energies of 1-30 keV in Si. The figure shows the mean stopping depth and both the lower and upper limits, which confine the middle 80 % of the positrons. The relative width of the stopping profile stays constant though the mean stopping depth changes. Thus, the absolute depth resolution decreases with increasing implantation energy. Sputtering and low-angle wedging of samples have been utilised to overcome the low depth resolution of SPMs [24], but they are destructive methods and impose the problem of whether the surface preparation can affect the measured data.

A fraction of implanted positrons is scattered back from the sample. The positrons back-scattered from a sample can either annihilate at the sample chamber walls or, if they feel an accelerating electric field, be re-accelerated to the sample. In a DBS measurement, the annihilations in the walls result in a contribution to data, which cannot be removed. In a lifetime measurement, both result in a formation of a second peak after a time interval, which depends on the implantation energy. To reduce the contribution of the scattered positrons to the data, the space above the

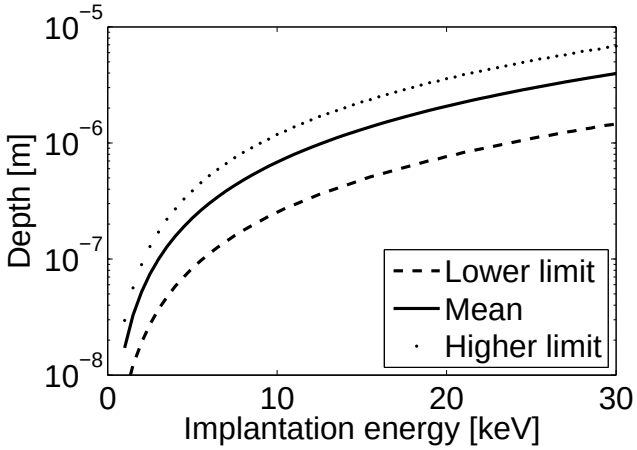

Figure 9: Stopping of positrons in Si calculated with equation 6. The limits confine the middle 80 % of the positrons.

sample should be empty of matter until a sufficient distance ($\sim$ 100 mm). However, the aberrations of magnetic lenses increase with the focal length and, thus, limit the maximum usable focal length. If the objective lens is located inside the optical column, there is a trade-off between the effects of the aberrations of the objective lens and the contribution of scattered positrons.

2.4.2 Remoderation

Liouville's theorem states that the volume of the phase space occupied by a particle beam (space containing both the spatial and momentum dimensions) is not changed by conservative forces, such as static magnetic or electric fields [25]. When a particle beam is collimated in the spatial space with a static magnetic or electric lens, the momentum distribution of the beam diverges. Hence, many lenses in series cannot provide an arbitrary reduction of the beam diameter. Furthermore, an arbitrary high magnification also has downsides. A high magnification results in a high angular divergence and a small depth of focus. A single magnetic lens of an SPM has been reported to obtain a focus with a diameter of 10^{-2} of the diameter of the parallel beam [39].

In order to have reasonable count rate, a small particle beam has to have a high intensity. An efficient spatial collimation of a beam requires a parallel incoming beam. Both of these factors are taken into account in the concept of beam brightness

$$B = \frac{dN}{dtdAd\Omega}, \tag{16}$$

which describes the particle flux per unit time dN/dt over an area of dA within a solid angle $d\Omega$. As a result of Liouville's theorem, the beam brightness is not changed by static magnetic or electric fields. A positron source of a high brightness is very crucial for SPMs.

In order to achieve a smaller beam diameter with the same positron sources without removing excessive amounts of positron flux with apertures, the concept of remoderation (also known as brightness enhancement) was developed. In a remoderation stage, a positron beam is focused on a moderating material. Positrons thermalise and significant fraction of them is re-emitted due the negative work function, in the direction of the surface normal. The area of the emissions is the same as for the beam spot albeit slightly increased due to positron diffusion. The remoderation process is non-conservative and, thus, can increase the beam brightness (Figure 10). Also multiple, subsequent remoderation stages can be used. For monochromatic positron beams, remoderation efficiencies greater than 20 % have been observed [3].

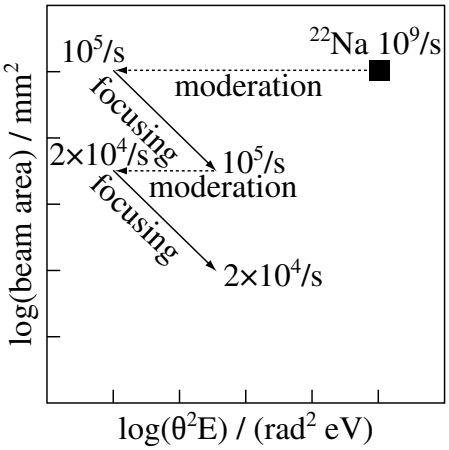

Figure 10: Positron beam brightness and count rate during moderation, focusing and remoderation steps [26].

3 Existing scanning positron microscopes

This chapter describes the structure and the operation of the scanning positron microscopes (SPMs) built in Bonn and Münich, Germany, and the one built in Takasaki, Japan. The plans for an SPM in Lawrence Livermore National Laboratory, USA, are also considered though the SPM was not constructed. A scanning positron beam was considered as an SPM if the spatial resolution reached below 10 µm.

Some device-related data of this chapter might be outdated. Especially, in the case of the Münich scanning positron microscope, most of the literature regarding the device structure and performance was published in the mid-1990's. Some improvements in the performance and changes in the device structure might have taken place within the past two decades.

3.1 Scanning positron microscope in Bonn

The Bonn scanning positron microprobe (BPM) is based on a commercial scanning electron microscope (ZEISS/Opton, DSM 960 (A)) and can operate both as a scanning electron microscope (SEM) with a resolution of 12 nm and as a positron microscope to measure Doppler broadening of annihilation radiation with a resolution of 1 µm. In the BPM this dual operation is performed by a magnetic prism between the electron and positron sources, which directs both beams into the optical column of the SEM as illustrated in Figure 11. The positron source of the BPM is a radioactive source with a transmission moderator consisting both a W thin film and a W cone. The moderating efficiency of the moderator is $1.7 \cdot 10^{-3}$. With a 370 MBq ^{22}Na positron source and a beam diameter of 1 µm, the count rate of the 511 keV photopeak is 50 cps, which increases to 2000 cps with a 20 µm beam diameter. [15] Presently, the BPM is located in the University of Würzburg.

3.1.1 Constructional details

Figure 12 shows a picture of the BPM. The construction of the BPM consists of a T-shaped beam line, which occupies a floor space of 2 m×1.8 m. The height of the BPM is 2.4 m. The *in-situ* annealing chamber of the BPM is an additional horizontal 2 m long vacuum vessel, perpendicular to the beam lines and connected to the positron source of the BPM. As the BPM is less compact than an ordinary SEM, vibrations cause both the positron and electron beam spots to wobble over few micrometers at the sample [27]. The decoupling of the BPM from building vibrations is carried out by mounting the BPM on a 80 mm thick aluminum plate, which is hung on springs. In total, the BPM demands a floor space of 2 m×3 m and a height of 2.4 m for the microscope itself and 1.8 m×0.5 m for the console of the SEM.

The sample and source chambers and the beam guide for the electron and positron branches were made of µ-metal, which has a high magnetic permeability [27]. The sample chamber of the SEM was modified as the Ge detector has to be placed right under the sample to cover a maximal space angle. [15]

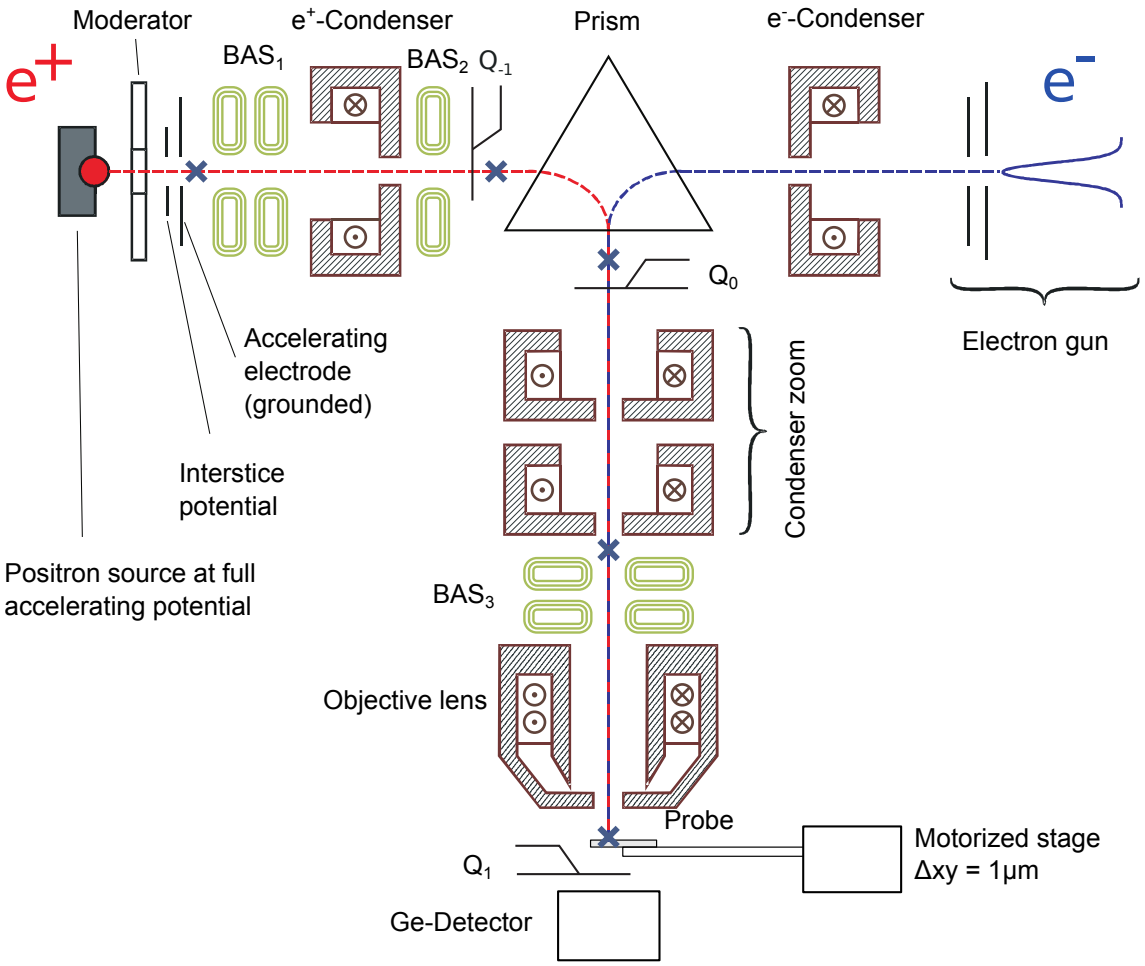

Figure 11: Diagram of the Bonn positron microprobe (BPM) [15]. BAS stands for a beam alignment system, which is capable of parallel and angular displacement of the beam. Q_{-1}, Q_0 and Q_1 are scintillator-photomultiplier detectors for measuring the positron flux. The blue crosses are the cross-over points of the positron beam. [15]

3.1.2 Positron source

The positron source of the BPM is attached to a holder shown in Figure 13. The source consists of NaCl with ^{22}Na isotope and has a specific activity of 12 TBq/g. The thickness of the source is only approximately 200 µm. Typically, the activity of the positron source is 370 MBq. The ^{22}Na salt is sealed within a Au-holder, a Ta-alignment pin and a 3 µm Ti-foil. The location of the source holder is adjustable in all three dimensions. [15]

The moderator of the BPM consists of a 500 nm thick W thin film and a W single crystal with a conical hole, as illustrated in Figure 13 [15]. Also the surface of the cone hole acts as a positron moderator and it yields roughly a 1/3 of the count rate of the BPM [27]. The moderator is positioned 10 µm in front of the source to maximise the solid angle of the moderator seen by the source. The lifetime of the moderator in the vacuum of 10^{-5} Pa is roughly half a year. [15]

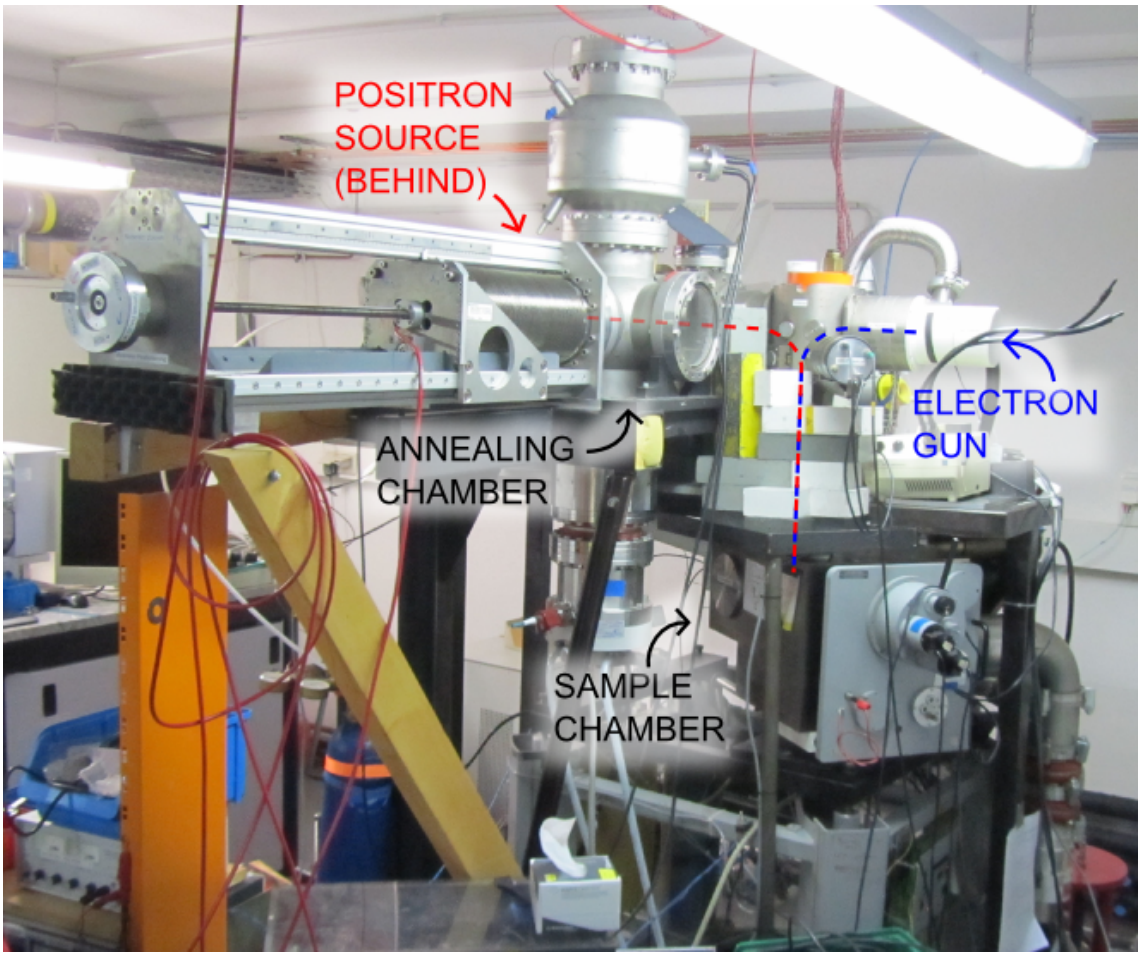

Figure 12: The BPM in the University of Würzburg. The main elements are overlaid in the image. The *in situ* annealing chamber is in front of the positron source.

The moderator can be transferred between the source-site and the *in-situ* annealing chamber with a linear manipulator. In the annealing chamber, the moderator can be heated with a simple tungsten filament electron gun up to 3000 °C. There is also a gas inlet for an oxygen treatment during the annealing. [15]

The moderated positrons are accelerated within 600 µm distance from the source in two stages (Figure 13). The whole source is raised to the acceleration potential in order to have the sample-end of the BPM grounded. [15] An intermediate potential of approximately 10 % of the total accelerating voltage is applied to the electrode just in front of the moderator (Figure 13) to pull the moderated positrons from the surface of the moderator [2, 15]. The second accelerator electrode is grounded and accelerates the positrons to their full kinetic energy [15].

The shape of the moderator surface, the locations of both electrodes and the potential of the interstitial electrode affect the location and the quality of the first cross-over of the beam and the quality of the positron beam after it. The positron beam profile originating from the film and the surface of the cone was simulated by

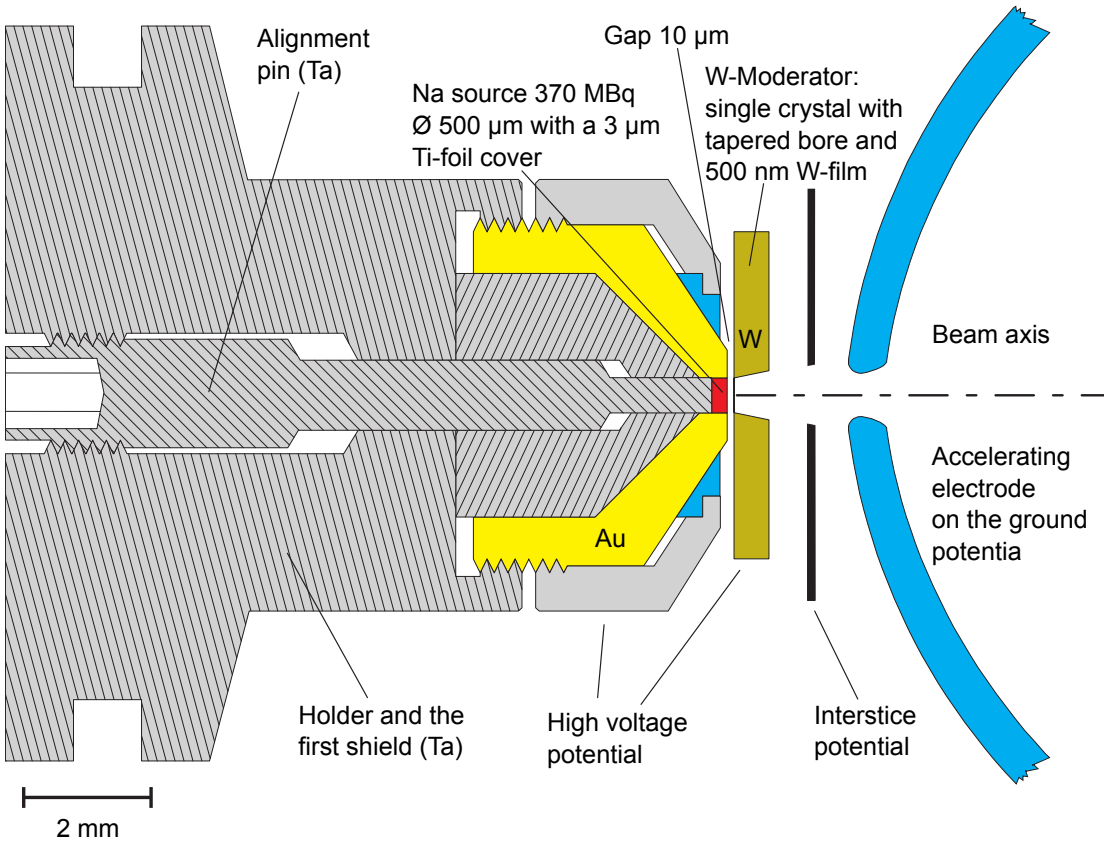

Figure 13: A sketch of the positron source and the moderator [15]. The ^{22}Na source salt is inside a golden holder with 500 µm hole in diameter and is enclosed by a tantalum plug from behind and by a 3 µm thick titanium foil attached with a clamping ring from the front. The source holder is adjustable in all three dimensions. The acceleration voltage is applied in two stages over the distance of 600 µm.

M. Haaks with Simion 7 software. In the simulation the interstice potential was 1.4 keV and the total accelerating potential was 30 keV. Figure 14 shows some results of the simulations. [15] It can be seen that the positrons originating from the film are significantly more parallel than the ones originating from the surface of the cone. [15]

3.1.3 Beam transportation

Figure 11 shows a diagram of the BPM with its optical elements. There are two additional condenser lenses (ZEISS [27]) besides the ones in the optical column of the BPM, one for the positron and one for the electron branches. The positron beam branch also has two additional beam alignment systems (ZEISS [27]), which can transversely displace the beam or change the beam angle. They consist of air coils perpendicular to the beam axis. [15]

The magnetic prism (shown in Figure 11) bends both positron and electron beams 90° downwards into the optical column of a commercial scanning electron microscope (ZEISS/Opton, DSM 960 (A)). The BPM uses a magnetic prism (ZEISS

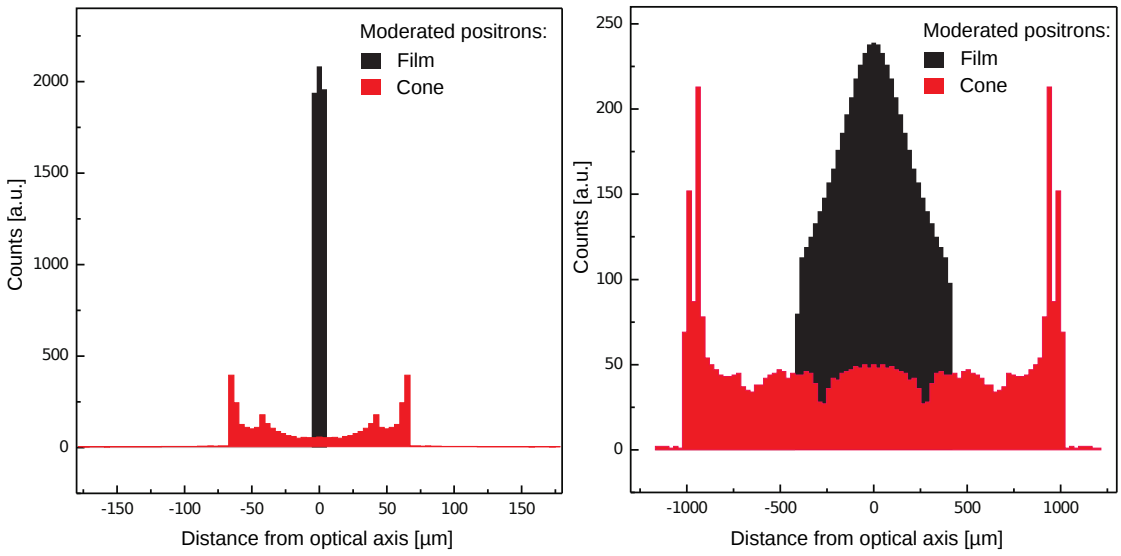

(a) first cross-over (b) entering plane of the condenser

Figure 14: Simulated (Simion 7) beam profiles of positrons re-emitted from the thin film (black) and the cone surface (red) at the first cross-over (14a) and the entering plane of the first condenser lens (14b). The total accelerating potential of the simulation was 30 keV and the interstice potential was 1.4 keV. [15] It should be noted that the positrons moderated by the thin film are significantly more parallel.

[27]), which is designed for two-stage energy filtering of electrons in a transmission electron microscope. For the positron and electron beams of the same energy, the magnetic field density in the prism is approximately the same. The magnetic prism also filters the unmoderated, fast positrons.

The optical column of the SEM consists of condenser lenses, an aperture (not shown in Figure 11), a beam alignment system and a zoom lens. The sample chamber is free of magnetic fields starting from 2 mm below the zoom lens. In the BPM, the distance between the sample and the optical column is typically 5 mm. The field-free sample chamber enables studying of ferromagnetic materials. The sample is attached to a motorised stage. The positron image is acquired by scanning the sample with fixed positron beam parameters, not by using the scanning coils of the SEM-column. [15] This is due to the second-order corrections of the SEM scanning coils designed for the opposite gyration direction of electrons [27]. The stage has an accuracy of 1 µm and is controllable by the measuring software. The SEM-operation and the coordinate system of the stage enable recovery of the locations of interest even after removing the sample from the BPM. [15]

There are three Q-detectors for counting the positron flux: one before and after the prism and one below the sample stage [15]. The Q-detectors consist of scintillator material and two parallel photomultiplier tubes operated in coincidence mode [27]. The Q-detectors can be used to monitor the positron flux when adjusting the beam parameters or aligning the optical components [15].

In a cross-over the beam is at focus. The locations of the first and second cross-over can be adjusted by the potentials of the accelerating electrodes and the current of the positron branch condenser lens. The second cross-over determines the location of the third cross-over just below the magnetic prism. The beam can be operated with and without a cross-over in the SEM optical column. The final cross-over, or the final focus, is located at the sample site. [15]

Figure 15 shows the count rate of the Q_1-detector as a function of the currents of the condenser lenses of the optical column. There are three regions in the graph divided by two black lines: a region where the beam does not have a cross-over inside the column ("I: No cross-over"), a region where the beam has a cross-over ("II: Cross-over") and a region where the beam cannot be properly focused because the focus is located further than what is the distance to the sample site. [15]

The maximum count rate (2000 cps with a 370 MBq positron source) is achieved if the beam is operated in the region II of Figure 15 with no cross-over in the optical column. However, in this operating area, the beam diameter is 20 µm at minimum. Smaller beam diameters can be achieved when operating the BPM in the region with a cross-over in the optical column (region I in Figure 15). The beam diameter can be reduced up to till 1 µm (50 cps with 370 MBq positron source) if the BPM is operated in the region denoted by point P_2 and the adjacent arrow (Figure 15). [15]

During a measurement, the parameters of the beam alignment systems are monitored. A simple algorithm adjusts the optical parameters of the BPM between individual measurement points in order to compensate possible drifts of the parameters. [15]

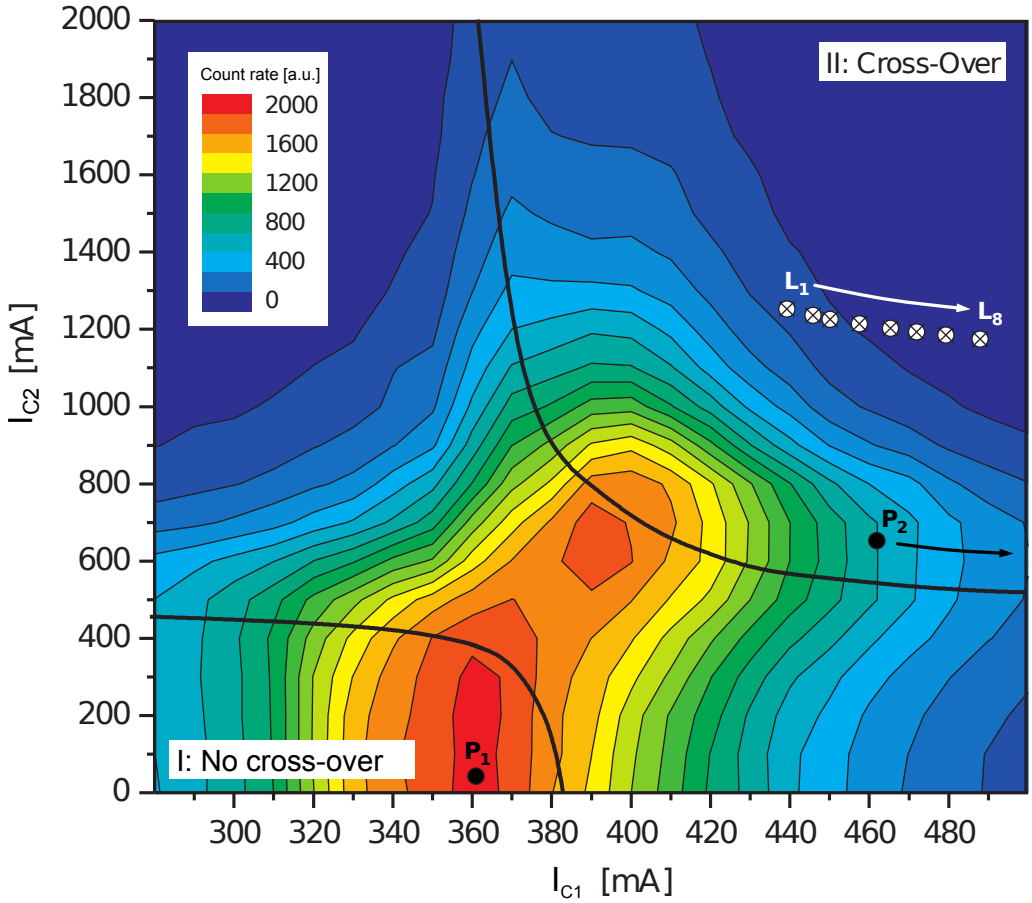

Figure 15: The count rate of the BPM as a function of the currents of the condenser lenses [15]. The black lines divide the plot to sections with either no beam cross-over (I: No cross-over), one beam cross-over (II: beam cross-over) and the rest where the beam cannot be focused because the focal length is longer than the beam path. The white circles L_1-L_8 stand for default condenser lens currents of the SEM operation. P_1 denotes the operating point of the high flux positron beam with a diameter 20 µm. Smaller beam diameters are located in the direction of the arrow next to the point P_2. [15]

3.1.4 Performance and research

The BPM uses a Ge detector with a detection probability of 60 % at 0.5 MeV and an energy resolution of 1.05 keV at 477.6 keV (^{7}Be) with both analogous and digital stabilisations. The detector covers a solid angle of $\Omega/4\pi \approx 0.3$. With a 370 MBq ^{22}Na source, the detector photopeak count rates are 50 and 2000 for 1 µm and 20 µm beam diameters, respectively. [15]

The BPM has been mostly used for studying fatigue and deformation in metals. In order not to be dominated by properties of grain boundaries of a solid, beam sizes 20-100 µm were usually used. [2, 23, 28–35] The high momentum analysis (see page 11 for more details) has been successfully applied with the BPM [23, 35].

One example of the measurement results acquired with the BPM is presented in Figure 16 [29]. Figure 16a shows the normalised S-parameter in the vicinity of a fatigue crack tip, which was produced by cyclic deformations of over 4000 cycles on AISI 321 stainless steel. The measurement was performed with 30 keV implantation energy, 20 µm resolution and 150 µm step size. The insets 16b and 16c show SEM images from the crack tip and a reference view 1 mm away from the crack tip, respectively. The area, where slip lines are visible, is circumfenced with a purple line in Figure 16a. [29] The normalised S-parameter is elevated even at the region, where there are no visible signs of deformation.

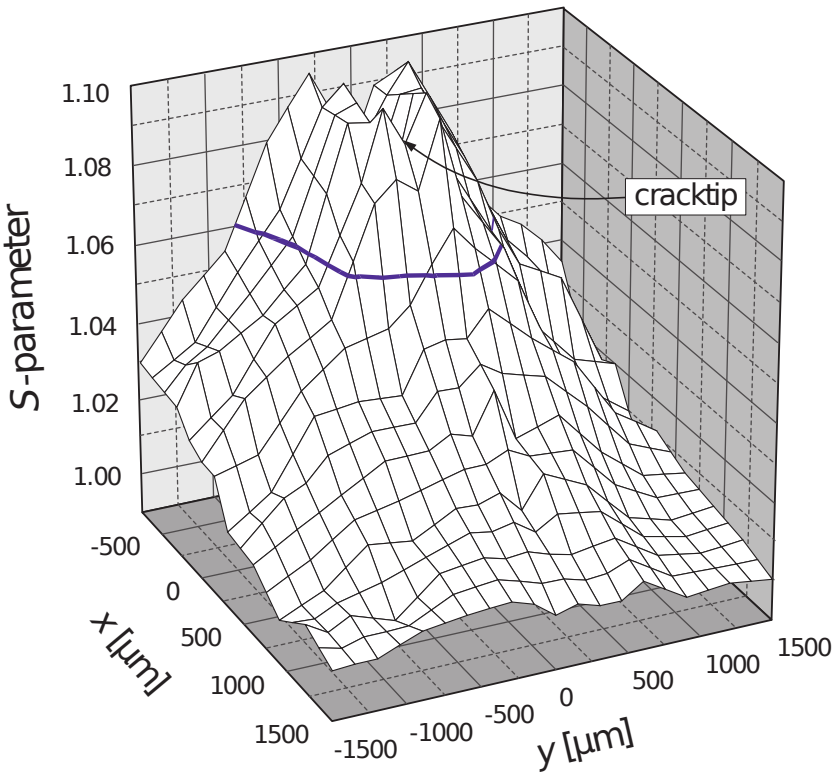

(a) The relative S-parameter around a crack tip

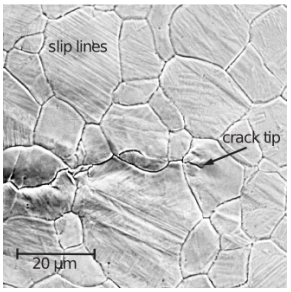

(b) SEM-image of the crack tip

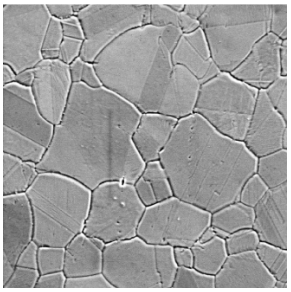

(c) SEM-image 1 mm away from the crack tip

Figure 16: Measured SPM and SEM images from deformed AISI 321 steel [15]. The purple line in Figure 16a limits an area where slip lines are visible.

3.2 Scanning positron microscope in Münich

The Münich scanning positron microscope (MPM) is a positron microscope, which measures positron lifetime, and has a reflection remoderator and "single pole" magnetic lenses (see chapter 3.2.2). The MPM also possesses an electron gun with a 0.5 µm beam diameter. [3, 37] Figure 17 shows the structure of the MPM. The positron beam is bunched in three steps within the primary beam and the optical column. [37] Originally, the MPM has been operated with a 1.1 GBq ^{22}Na source, but its merging to the NEPOMUC positron reactor source has been initiated (see chapter 3.2.4). With a 1.1 GBq ^{22}Na source, the MPM can operate with a 2 µm resolution for 1-20 keV beam energy and a 255 ps time resolution (FWHM). An area of 600 µm×600 µm can be scanned. It takes 7 days to scan a 45 µm×45 µm area with 2 µm resolution and $1{\cdot}10^5$ cts/pixel. [38] This corresponds to a count rate of approximately 80 cps.

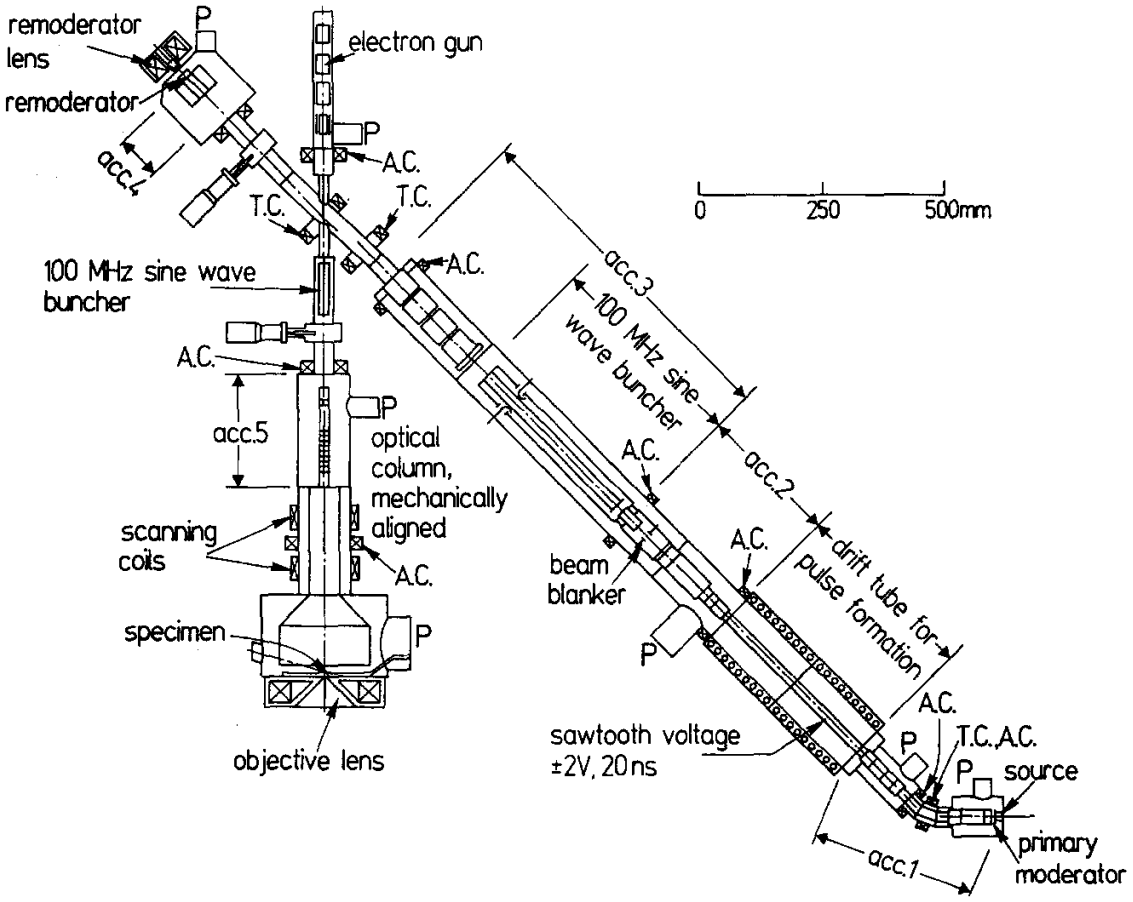

Figure 17: Diagram of the Münich scanning positron microscope (MPM) [37]. A.C. stands for alignment coils, T.C. for toroidal deflection coils, P for pumps and acc.1-acc.5 for accelerating sections.

3.2.1 Positron source and primary beam

Originally, the positron source of the MPM has been 1.1 GBq ^{22}Na [38]. The MPM has been transferred to research reactor FMR II in Garching, Germany, to be connected to a reactor based positron source NEPOMUC (more discussed in chapter 3.2.4) [38].

A 1 µm thick W(100) moderator with an efficiency of $6 \cdot 10^{-4}$ has been used in the MPM [39]. *In situ* annealing system of the moderator consists of a 50 W electron gun, a valve between source chamber and the main vacuum system and a separate vacuum pump at the source chamber. After moderator, the positron beam is bent 45° with a toroidal coil. The bending magnet filters unmoderated positrons from the beam. The beam is then accelerated and injected into a drift tube with an energy of 20 eV. [39]

The 37 cm long drift tube contains a 50 MHz sawtooth prebuncher in a homogenous axial magnetic field of 0.5 mT. The drift tube has field terminators at both ends and in the centre. The sawtooth wave has an amplitude of 4 V, a rise time of less than 2 ns and it bunches positrons from a 20 ns segment into bunches with an FWHM of 4 ns with an efficiency of 70 %. A detailed description of the electronics of the prebuncher is given in [40]. The whole bunching process of the primary beam is illustrated in Figure 18. After the beam leaves the prebuncher, the positron beam is accelerated to energy of 800 eV. [39]

A beam blanker, also referred to as a chopper, deflects positrons outside the prebunched pulse with a perpendicular electric field. It operates with an amplitude of 5 V, is switched on for about 15 ns of the 20 ns period and has a rise time shorter than 2 ns (Figure 18). The width of the pulse can be adjusted to match the width of the prebunched beam. [41]

The main buncher of the primary beam operates with a 100 V and 100 MHz sine wave (Figure 18). The buncher is a resonant cavity with an active gap. The buncher is thermally compensated and the drift of the resonance frequency between 20 °C and 90 °C is less than $4 \cdot 10^{-4}$. The quality factor of the cavity is 450. [39] After the main buncher, the third electric lens system accelerates the positron beam to the desired energy and focuses the beam into a 3 mm spot. The focus is located 520 mm from the last electrode. [39]

The primary beam of the MPM is a stand-alone beam with a final energy of 5 keV, a spot diameter of 3 mm and a temporal FWHM of below 350 ps [39]. With a magnetic “single pole” lens, the beam has reached a lateral FWHM of <15 µm. [39]

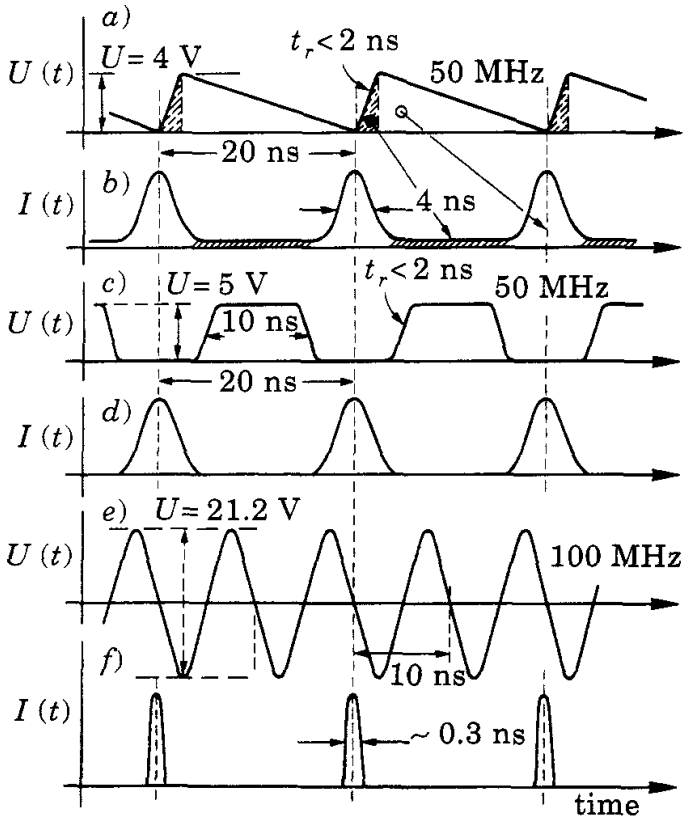

Figure 18: The timing scheme of the MPM primary beam [39]: a) sawtooth voltage in the drift tube, b) pre-bunched beam at the exit of the drift tube, c) rectangular voltage of the blanker, d) beam at the entrance of the main buncher, e) 100 MHz sine wave of the buncher, f) beam bunches at the remoderator.

3.2.2 Remoderation and deflection

The reflection remoderator of the MPM is located 640 mm from the third accelerator (section acc. 3 in Figure 17) [37]. It uses a magnetic "single pole" lens for focusing the beam onto the remoderator surface and a simple two-tube electrostatic lens for accelerating the re-emitted positrons to 200 eV [42]. The magnetic "single pole" lenses of the MPM are designed such that one of the two magnetic poles has the desired optical properties, while the other pole is not being used. A schematic drawing of the remoderator-lens system is shown in Figure 19. The total efficiency of the remoderator-lens system is about 20 % [38]. A detailed description of the remoderator structure and the positron optics in the vicinity of the remoderator can be found in [42, 43].

Due to the low energy of the remoderated positron beam, the remoderated beam passes many cross-overs. [42] In order to minimise the spherical aberration of the remoderated beam [44], the "single pole" lens is designed such that the magnetic field lines approximate straight, monopole field lines at the focus, which is located few centimetres in front of the pole shoe [42] (Figure 20). The lens focuses the 3

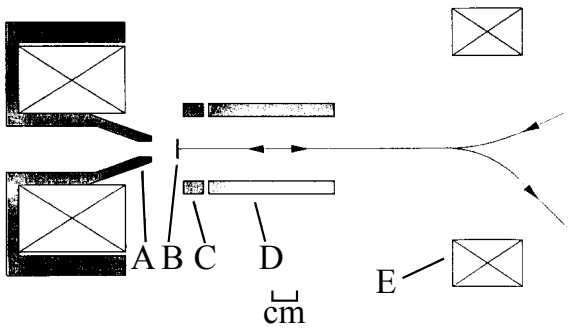

Figure 19: The remoderator-lens system of the MPM: A = "single pole" magnetic lens, B = remoderator, C,D = accelerator, E = magnetic deflector [42].

mm primary beam diameter into a 20 µm spot. The deceleration of 200 eV of the primary beam over the last few centimetres has a negligible effect on the incoming 5 keV beam. [43]

The remoderator is cooled below 100 K. The cooling of the remoderator decreases transverse energy spread of the remoderated beam and, thus, increases the brightness of the beam threefold. A liquid nitrogen cryostat was built to be a part of the electrostatic accelerator, as shown in Figure 21a. The temperature of the cryostat walls is lower than the temperature of the remoderator, which reduces the amount of absorbed residual gases on the remoderator surface. This slows down the degradation of the remoderator efficiency. [43]

The remoderated positrons are accelerated to 200 eV with a two-tube lens. The re-emitted beam has a low energy, so the remoderator lens system is shielded from external magnetic fields. The remoderated beam is deflected into the optical column with a toroidal deflection coil from the fifth or sixth cross-over approximately 400 mm away from the remoderator (Figure 21b). [45].

Also the incoming primary beam is deflected by the deflection coil above the optical column, although by a smaller angle. In order to conserve the direction of the primary beam, an identical deflection coil is located in the path of the primary beam before the coil above the column, with an opposite excitation. An external view of the remoderation chamber with the deflectors is shown in Figure 21b. [43]

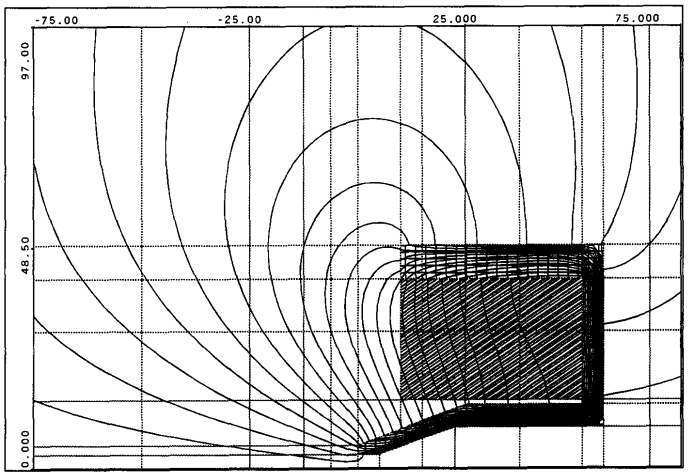

Figure 20: Simulated magnetic field lines of the "single pole" magnet in the remoderator of the MPM [42]. The label coordinates are presented in millimetres.

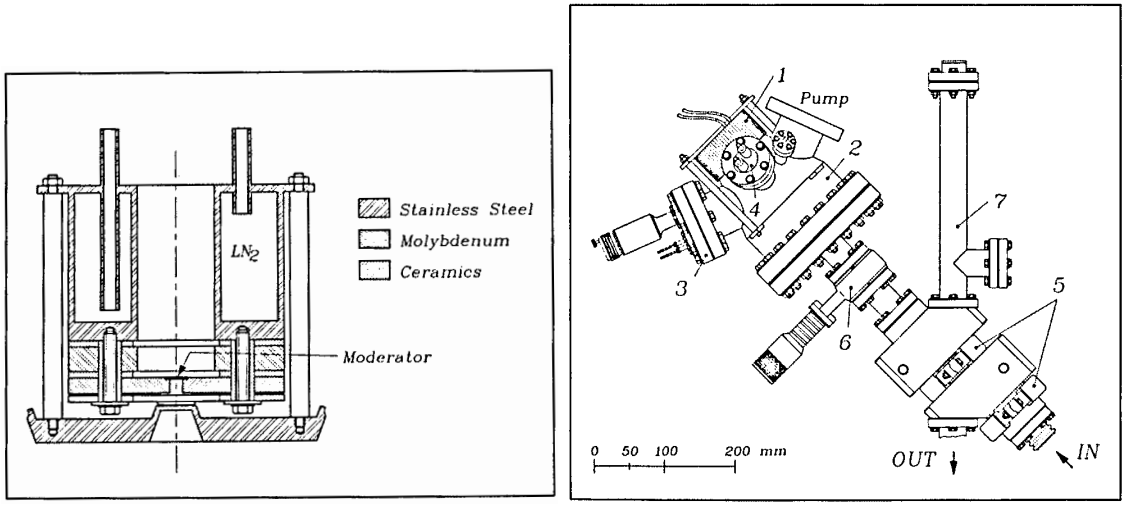

(a) (b)

Figure 21: 21a: A diagram of the remoderator-lens system. An electrostatic accelerator is integrated in the liquid nitrogen cryostat. The cryostat cools the remoderator below 100 K. [43]
21b: An external view of the remoderator unit of the MPM [43]: 1 = "single pole" lens, 2 = remoderator housing, 3 = linear motion and electrical inlets for annealing the remoderator, 4 = liquid nitrogen inlet, 5 = toroidal deflection coils, 6 = gate valve, 7 = additional source (e.g. electron gun), IN = incoming primary beam, OUT = remoderated beam.

3.2.3 Optical column

In the MPM, the optical column of a commercial SEM was not used for the construction. The MPM uses a configuration where the objective (or probe forming) lens is located below the sample. This enables a longer distance between the optical column and the sample than would be possible with an objective lens within the optical column. The large free space above the sample suppresses the contribution of the scattered positrons. They would cause additional, delayed peaks in the lifetime spectrum, which would complicate the use of fitting algorithms.

The optical column of the MPM consists of a final accelerator and scanning coils (Figure 22). The distance between the sample and the edge of the optical column is 100 mm. The detector is located on the center axis of the lens, partially inside the lens. The sample, the last stage of the accelerator, the internal cage and the sample holder are held at high voltage whereas the vacuum chamber walls are grounded. The optical column of the MPM is shielded with µ-metal and large Helmholtz coils surrounding the column. [45] The structure and optics of the column are described in details in [45].

The final accelerator accelerates positrons from the energy of 200 eV to the implantation energy between 1 and 20 keV [38, 45]. Because the optical properties of the accelerator vary with acceleration voltage, the accelerator is coupled with an electrostatic einzel lenses. The accelerator has 3 different modes for different acceleration energies. The structure of the accelerator and potentials of the different modes are shown in Figure 23. For energies from 1 to 4 keV, the MPM uses a a zoom lens. For energies from 4 to 7 keV, there is a 4-electrode accelerator, while in the third region from 7 to 30 keV, the accelerator uses an 8-electrode accelerator. [45]

The scanning coils of the MPM are saddle coils with a 30° angle and a 120 mm diameter winding outside the vacuum system. The aberration of the scanning coils can be neglected because the aberrations of the objective lens dominate the total aberration. [45] The scanning coils are discussed in detail in [45].

There were multiple requirements for the objective lens of the MPM [45]:

- an axial field strong enough to focus 30 keV positrons (the initially specified maximum),
- room for a scintillator detector inside the pole shoe of the lens,
- space for the sample manipulator between the focus and the pole of the lens and
- only a small field behind the lens at the location of the photomultiplier tube.

A side-gap "single pole" lens was chosen as the objective lens of the MPM and is shown with the simulated field lines in Figure 24a. A specific feature for the side-gap lens is a small gap in the pole shoe, which results in a very short lens field in front of the lens. The optimal focus of the side-gap lens is 9 mm in front of the lens. The lens needs an excitation of 4000 Ampere-turns to focus 30 keV positrons. The pole shoe of the side-gap lens saturates with currents required to focus 30 keV electrons,

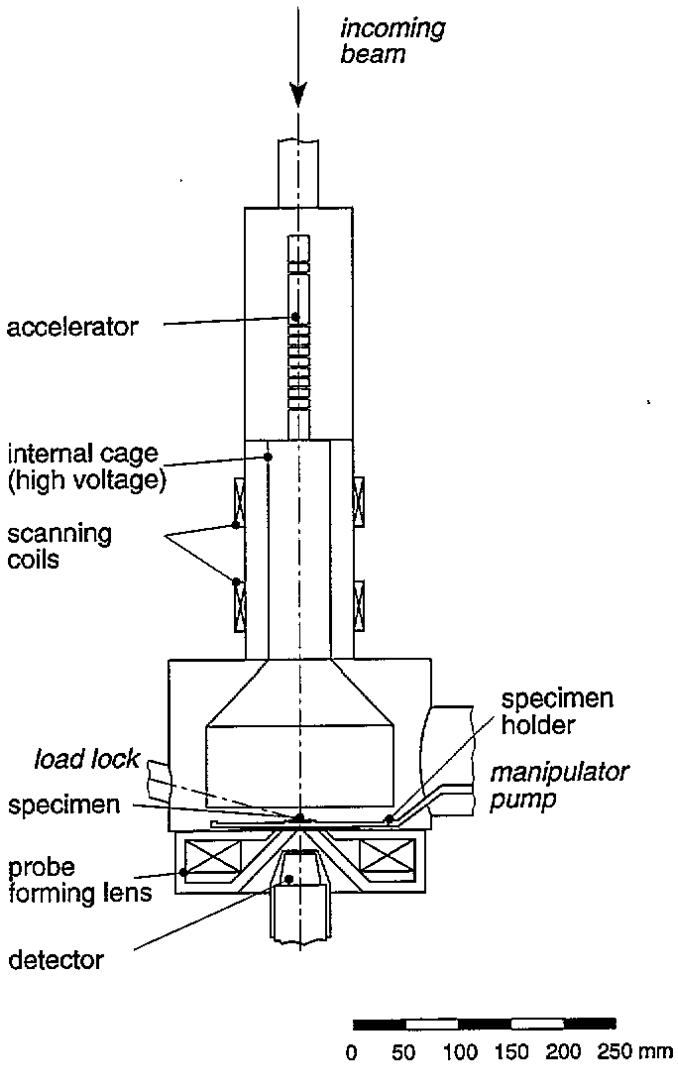

Figure 22: A diagram of the optical column of the MPM [45].

and the photomultiplier requires a double-walled shielding. The maximum power loss of the coil is 200 W and water cooling was applied, as seen in Figure 24b. [45]

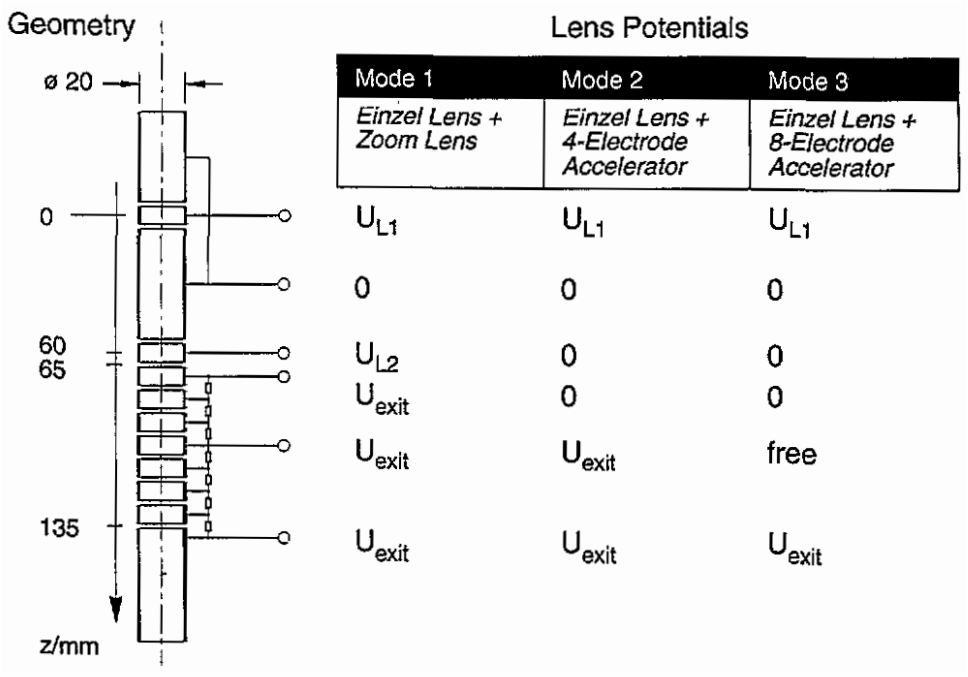

Lens Potentials

Mode 1	Mode 2	Mode 3
Einzel Lens + Zoom Lens	*Einzel Lens + 4-Electrode Accelerator*	*Einzel Lens + 8-Electrode Accelerator*
U_{L1}	U_{L1}	U_{L1}
0	0	0
U_{L2}	0	0
U_{exit}	0	0
U_{exit}	U_{exit}	free
U_{exit}	U_{exit}	U_{exit}

Figure 23: The structure and electrode potential of the final accelerator of the MPM [45].

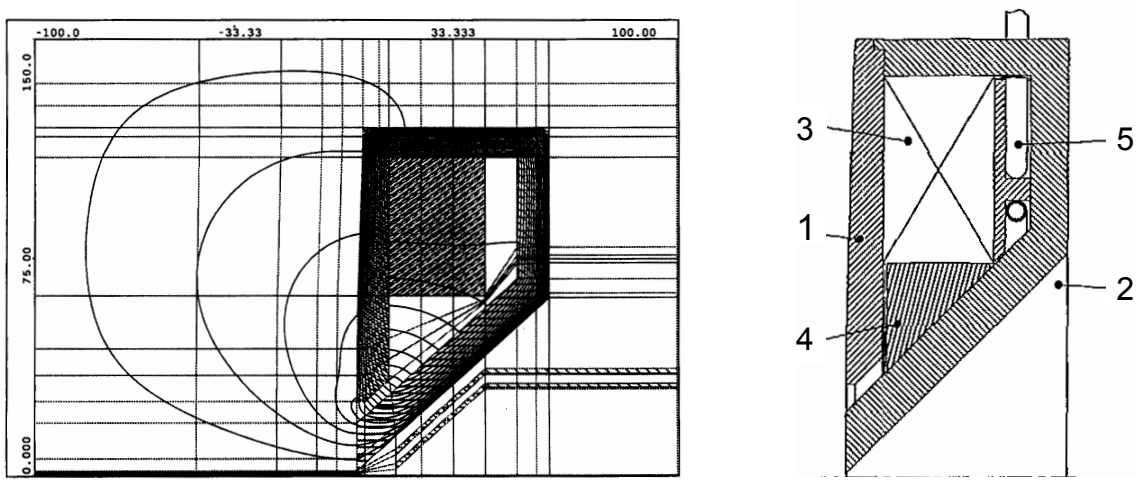

(a) field line simulation (b) diagram

Figure 24: 24a: Simulated field lines of the side-gap lens [42], used as the objective lens of the MPM. The lens is located 9 mm below the sample surface.
24b: A diagram of the side-gap objective lens of the MPM: (1) top plate, (2) assembly of pole shoe body and central cone, (3) coil, (4) centering ring, (5) water cooling [45].

3.2.4 Merging into NEPOMUC positron facility

As the major problem of positron microscopy is the low flux of moderated positrons, the MPM is being upgraded into the high intensity positron facility source NEPOMUC at the research reactor FRM II in Garching, Germany. The MPM has been transferred to FRM before 2008. [38] In 2011, preliminary test runs with the MPM were reported without results being published [48]. The building of the final reactor beam line is estimated to be finished in August 2014 [49]. Until 15 December 2014, no publications were found about completing the beam line or having the MPM operational.

The major advantage of replacing a radioactive positron source with the NEPOMUC positron beam is the increased positron flux. It has been estimated that the increased positron flux enables improving the lateral resolution of the MPM from 2 µm to 100 nm and still having an count rate which is higher by a factor of 60 than with the isotope source. [38] In 2014, the intensity of the remoderated positron beam of the NEPOMUC was $3 \cdot 10^7$ e^+/s with a beam diameter of 1.9 mm. [49]

The phase space of the NEPOMUC beam has been estimated to be 10^3 higher than the MPM is able to use. Thus, the primary column of the MPM is planned to be replaced with two sets of bunchers and accelerators and an additional remoderator stage, as shown in Figure 25. The first unit of the modified beam line is a sawtooth wave prebuncher. It is followed by a sine wave buncher. Then, the positron beam is extracted from the guiding magnetic field of the NEPOMUC beam and accelerated to 5 keV into the additional remoderator. The remoderated beam is bent with a magnetic prism into a beam blanker and a buncher.

The potential of the NEPOMUC beam lines are grounded and, after the 5 keV acceleration, the static potential of the beam line is -5 keV. This is different from the previous primary beam. In order to be able to use the same electrostatic potentials at the sample end of the MPM, the potential of the positron beam line is changed by passing the beam through an rf-elevator. The rf-elevator enables having a DC-potential difference across it and lets the positron bunches through unchanged. Besides the DC-potential difference, the gaps of the elevator also have a high frequency AC-voltage. The positron bunches pass the rf-gaps when the sum of the DC- and AC-voltages is zero and the gaps are free of accelerating fields. [38]

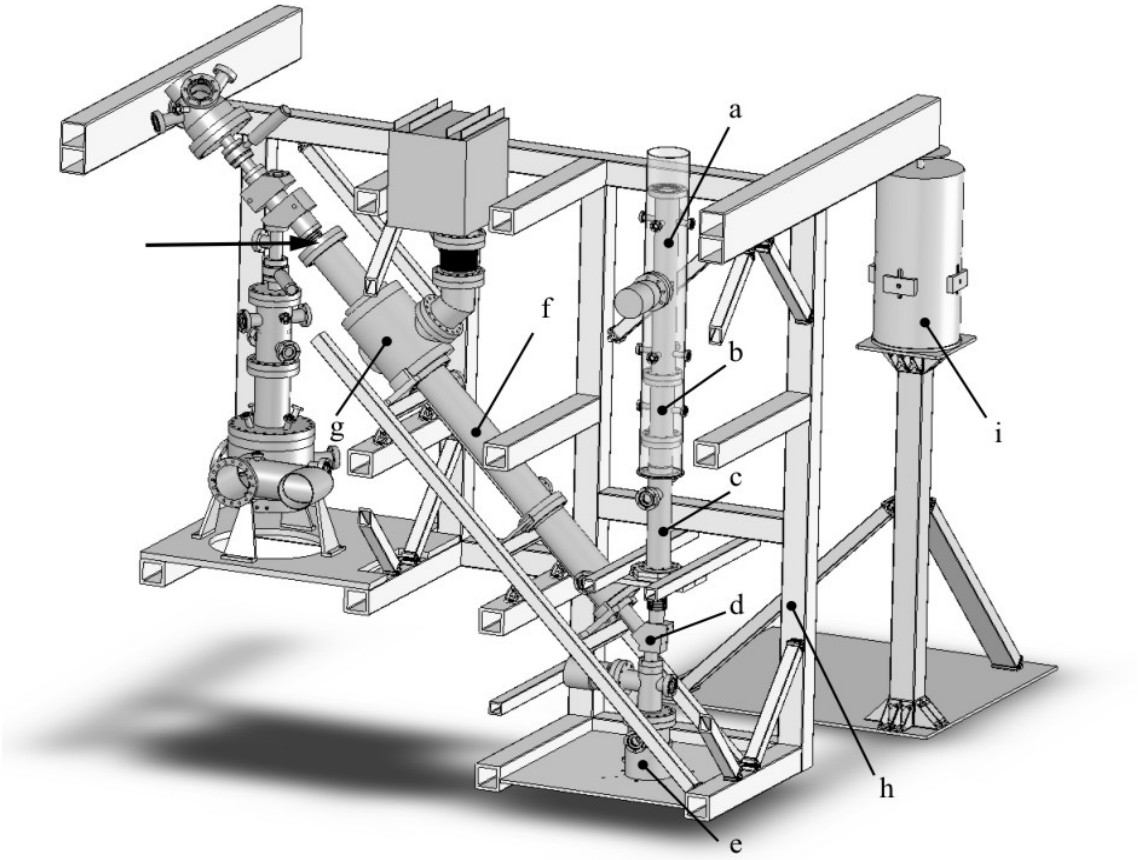

Figure 25: The interface connecting the MPM to the NEPOMUC beam line [38]. a) pre-buncher, b) buncher, c) electrostatic accelerator to 5 keV, d) magnetic prism, e) reflection remoderator, f) rf-accelerator, h) support, i) vibration isolator (only one of four is shown).

3.2.5 Performance and research

The MPM operates with positron implantation energies 1-20 keV and has reached a spatial resolution of 2 µm [3, 38]. The count rate with 2 µm beam diameter is 80 cps while using a 1.1 GBq ^{22}Na source [38]. With larger beam diameters higher count rates can be achieved: with a 5 µm beam diameter a count rate of 170 cps has been reported, but without the source activity [46]. An FWHM time resolution of 255 ps has been obtained [38]. The maximum scanning area of the MPM is 600 µm×600 µm. The MPM also possesses an electron beam with a diameter of 0.5 µm. Both beams coincide within approximately 30 µm.

The results obtained with the MPM have been reported in [3, 24, 46, 47]. Next, a study performed with the MPM in 2002 on fatigue cracks of cold-rolled electrolytic copper is described in more detail. The cracks were generated with symmetrical tension-compression loading and the fracture area was polished with polishing grits of sizes down to 50 nm [46].

Lifetime mapping around the fatigue crack was performed with implantation

energies of 5 keV (Figure 26a) and 16 keV (Figure 26b). In scans with both implantation energies the area, where the mean lifetime is elevated, is approximately 100 µm wide and is symmetrical with respect to the crack. The mean lifetime away from the crack approaches 230 ps with a 5 keV implantation energy, while in the measurement with 16 keV it approaches 210 ps. This is a sign of back diffusion. The diffusion length of positrons was estimated to be 50 nm from the Figures 26a and 26b. [46]

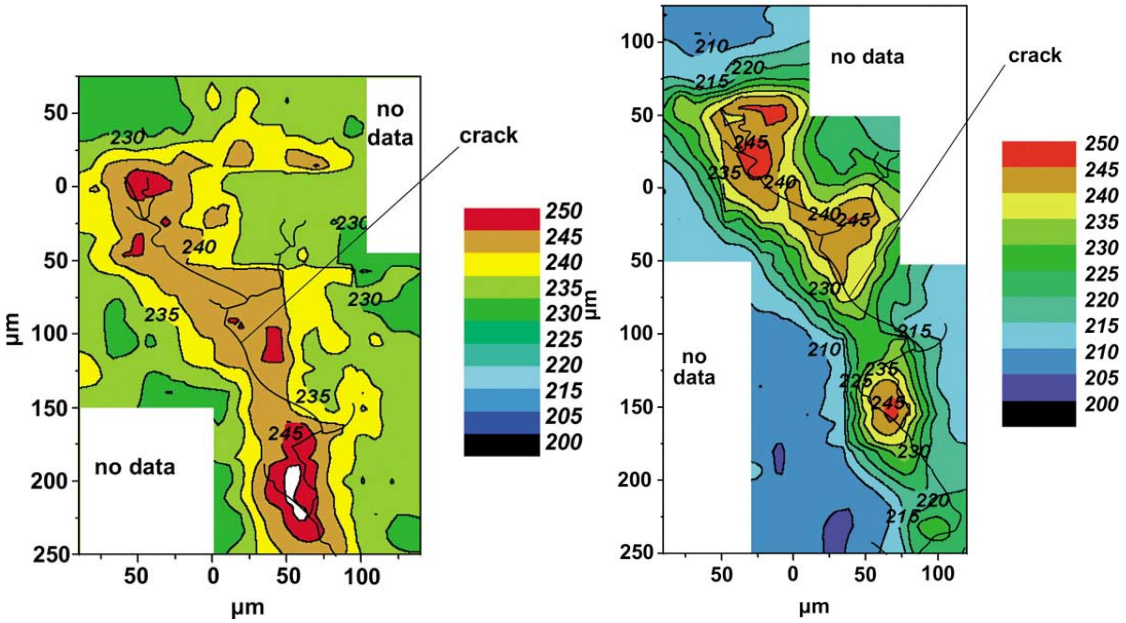

(a) 5 keV implantation energy

(b) 16 keV implantation energy

Figure 26: Map of mean positron lifetime [ps] in Cu with 5 and 16 keV positron implantation energies. Crack line from an optical image is overlayed on the lifetime map [46].

A line scan with a positron implantation energy of 16 keV was performed perpendicular to the crack with a measurement time of 9000 s/point (about $1.5 \cdot 10^6$ events per point). The mean lifetime and results of a two-component fitting are shown in Figure 27. The second lifetime, τ_2, was fixed to 400 ps because in unconstrained fits it varied between 360 and 420 ps. Both, the mean lifetime and the intensity of the second (400 ps) component I_2 indicate plastic deformation in the vicinity of the crack. [46]

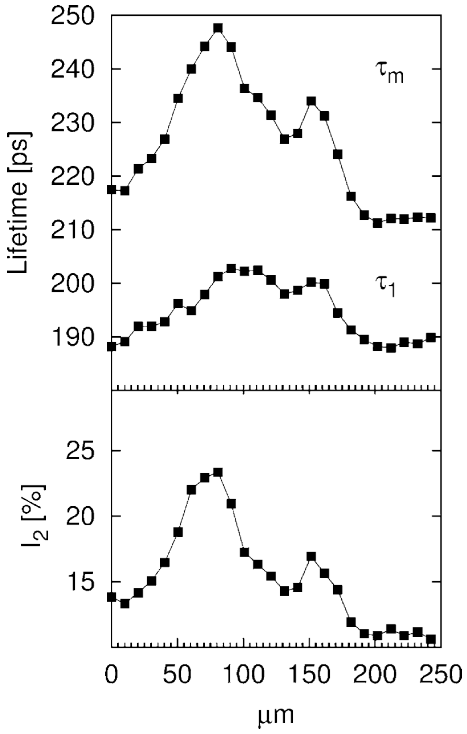

Figure 27: Results of a two-component lifetime fit to the line scan across the fatigue crack in Cu with a positron implantation energy of 16 keV [46]. The second lifetime component was fixed to τ_2=400 ps. [46]

3.3 Scanning positron microscope in Takasaki

The positron microscope in Takasaki (TPM), Japan, measures Doppler broadening of annihilation radiation and utilises an optical column of an SEM (Figure 28). The TPM uses a ^{22}Na source and a solid Ne moderator. The positron beam is deflected with a magnetic prism into an optical column of a commercial scanning electron microscope (TOPCON CORPORATION, SM-300). The TPM has reached beam diameters of 3.9 µm with a count rate of 30 cps and 15 µm with a count rate of 150 cps when using a 55 MBq source. The TPM also includes an electron gun (F in Figure 28), but it has not been reported to operate as an SEM. [4] A beam pulsing system has been prepared for the TPM [4], but no studies using the pulsing system have been published so far.

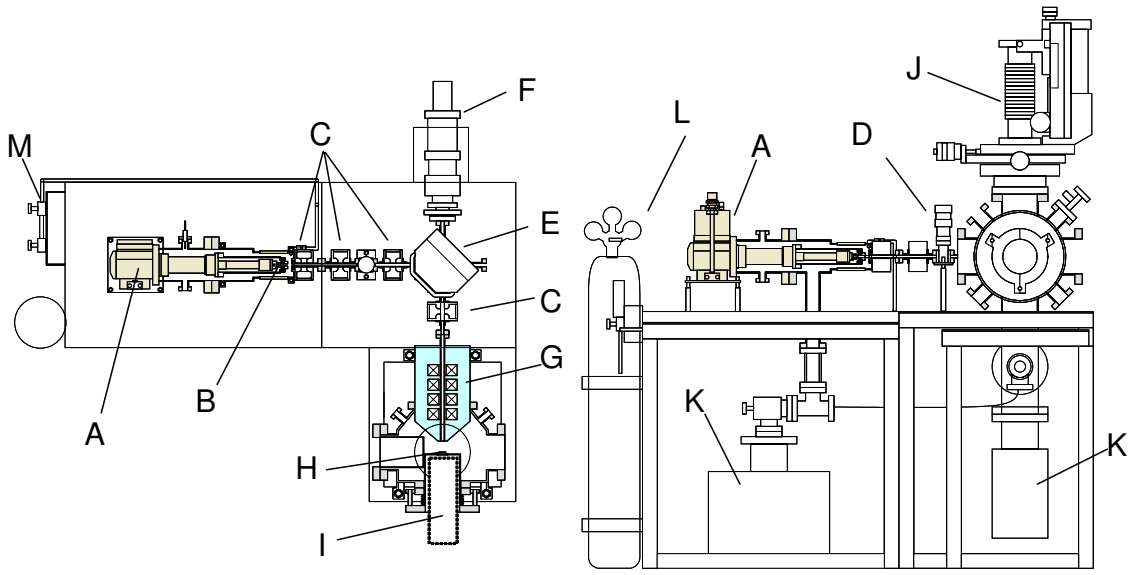

Figure 28: A schematic drawing of the SPM in Takasaki [16]. (A) cold head, (B) positron source, (C) magnetic lenses, (D) gate valve, (E) bending magnet, (F) electron gun, (G) optical column of an SEM, (H) sample holder, (I) Ge detector, (J) sample stage, (K) vacuum pumps, (L) Ne-gas container, (M) mass flow controller.

3.3.1 Positron source

The positron source of the TPM is NaCl with ^{22}Na isotope placed inside a 2 mm diameter hole in a block made of W and Cu (Figure 29a). The source is sealed in a capsule with a 5 µm thick Ti foil. The reported source activities range from 37 to 330 MBq [4, 16, 51, 52]. The positron source is mounted on a radiation shielded cold head and cooled down to 4 K (Figure 29c). [4] A solid neon film is grown on the source window as a moderator [4, 11].

The moderated positrons are extracted with an electrostatic lens system consisting of 5 parts at different potentials, shown in Figure 29b [4, 53]. The lens system

accelerates the positron beam to the final kinetic energy, which can be varied from 0 to 20 kV. The beam line starting from the anode is grounded. Figure 29b shows simulated positron trajectories and electric potentials in the electrostatic lens system at an accelerating voltage of 10 kV. [53]

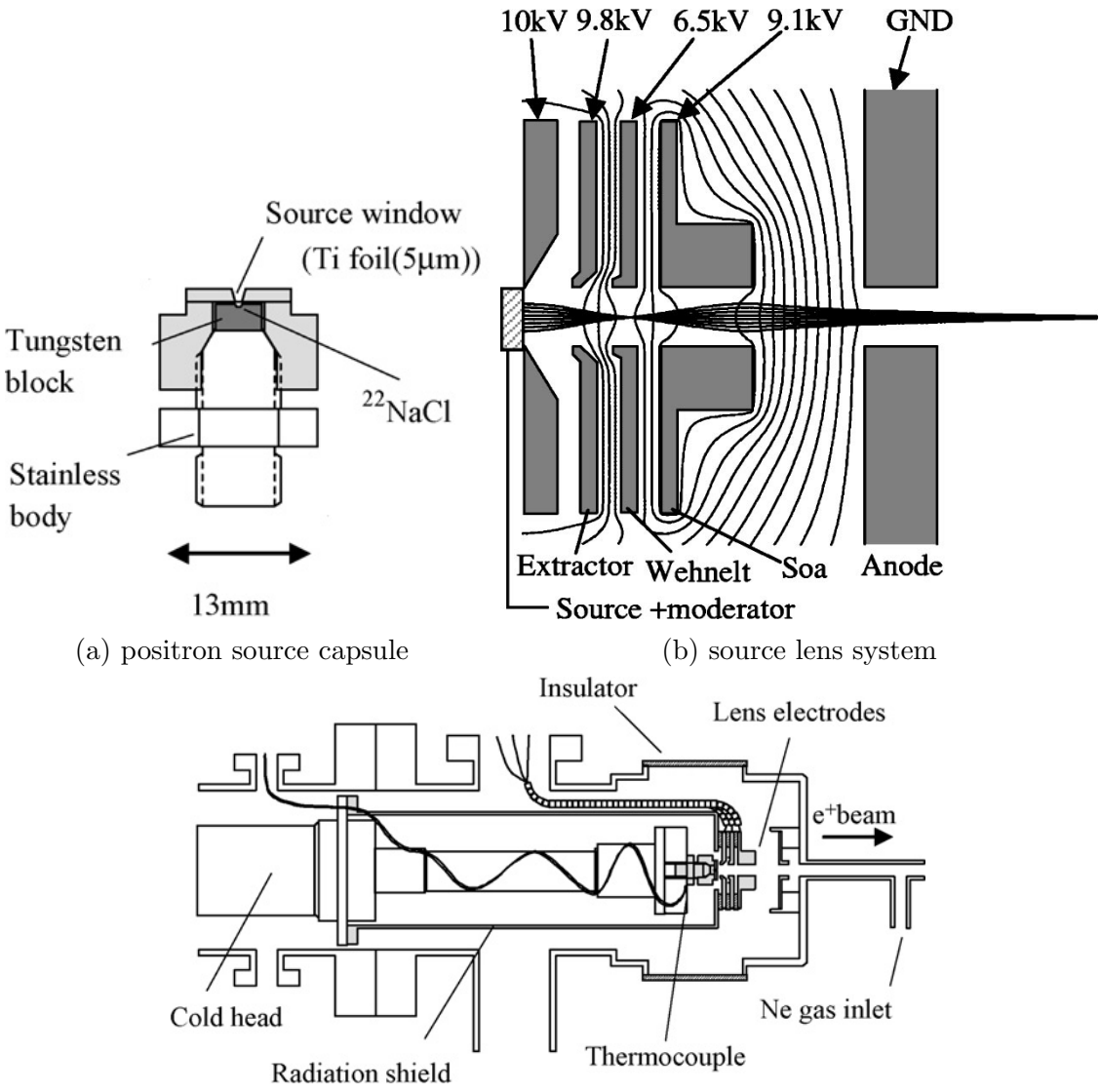

(a) positron source capsule

(b) source lens system

(c) positron gun

Figure 29: 29a: A schematic drawings of the positron source capsule of the TPM [4].
29b: A diagram of the source lens system of the TPM. The positron trajectories and the electrostatic potentials were simulated with SIMION. The contour spacing of electric potential is 1 kV. [53]
29c: A diagram of the positron gun of the TPM. The source capsule is installed on the cold head. The thermocouple is attached to the source capsule. [4].

3.3.2 Beam transportation

After the positron beam leaves the source lens system, it is first guided by three magnetic lenses (Figure 28). The positron beam is then bent 90° with a magnetic prism to filter out the unmoderated positrons and shield the gamma detector from gamma rays from the source. Next, the positron beam is injected into an optical column of a commercial SEM (TOPCON CORPORATION, SM-300). The column consists of a projector, middle and objective lens. The distance between the column and the sample is approximately 10 mm. There is a possibility to use a collimator with a hole diameter of 0.5 mm in front of the objective lens. [4]

3.3.3 Bunching system

A bunching system can be connected to the TPM between the positron source and the magnetic prism (Figure 30). When using the bunching system, the moderated positrons are only accelerated to 10 eV in the positron gun and then transported into the bunching system within a DC guiding magnetic field. The bunching system consists of a 50 MHz prebuncher with non-linear sawtooth wave, a 25 MHz parallel-plate sine wave chopper and a 200 MHz one-gap main buncher. The chopper passes bunches of approximately 2 ns. The wave form driven to the main buncher consists of the 200 MHz sine wave and its third harmonic. [4]

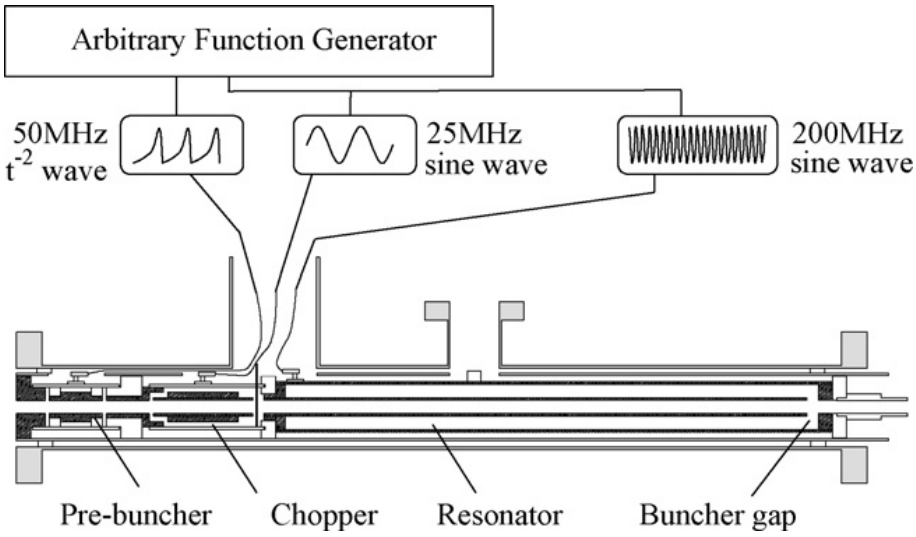

Figure 30: A schematic drawing of the beam bunching system of the TPM [4].

After bunching, the pulsed positron beam is extracted from the guiding magnetic field by accelerating and focusing the beam with magnetic lenses, as shown in Figure 31. After extracting the pulsed beam from the guiding magnetic field of the bunching system, the beam in guided through magnetic lenses (C in Figure 28), the magnetic prism (E) and focused onto the sample through the optical column (G). [16]

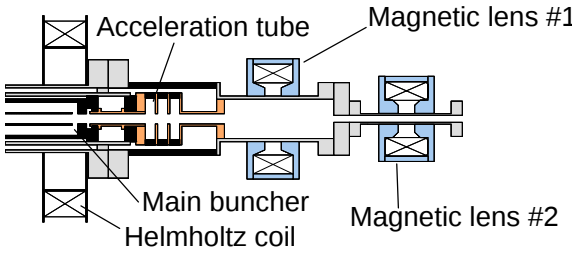

Figure 31: A schematic drawing of the section where the positron beam is extracted from the guiding magnetic field of the bunching system. [16]

3.3.4 Performance and research

The positron beam diameter was measured to be 15 µm with a count rate of 150-200 cps for a 55 MBq ^{22}Na source when the collimator was not used. After attaching a collimator with a hole diameter of 0.5 mm, a beam diameter of 3.9 µm was measured but the count rate was reduced to 30-40 cps. [4]

The temporal structure of the positron bunches was tested with a high-speed microchannel plate (Hamamatsu F4655-13) with a time resolution of approximately 25 ps. An FWHM of 140 ps and a peak-to-background ratio of >1000 were measured for the positron bunches. The count rate and the beam spot size with the pulsing system were not reported. [4]

The image is laterally scanned by moving the sample with a sample stage with an accuracy of 1 µm. The annihilation radiation is measured with a Ge detector placed behind the sample. The detector has a detection efficiency of 65 % and an energy resolution of 1.85 keV at 1.33 MeV peak of ^{60}Co. [4]

Some of the results obtained with the TPM can be found in [51,52,54–56]. Only a positron beam energy of 20 keV has been used [51, 52, 54–56], while the beam diameters range from 10 to 20 µm [54–56]. The most common application of the TPM has been the study of stress in stainless steel. Therefore, the large beam spot sizes may have been chosen to average the data over metal grains and prevent the distortion of the data by the grain boundaries of polycrystalline metals.

Next a study on stress-corrosion cracking (SCC) is described in more detail. The sample was first annealed at 1150 °C, quenched in water and then re-annealed at 400 °C. The sample was sensitised at 650 °C for 24 h in vacuum. Then, a plastic deformation up to a strain of 14 % was applied with 150 MPa tensile stress at room temperature. [55]

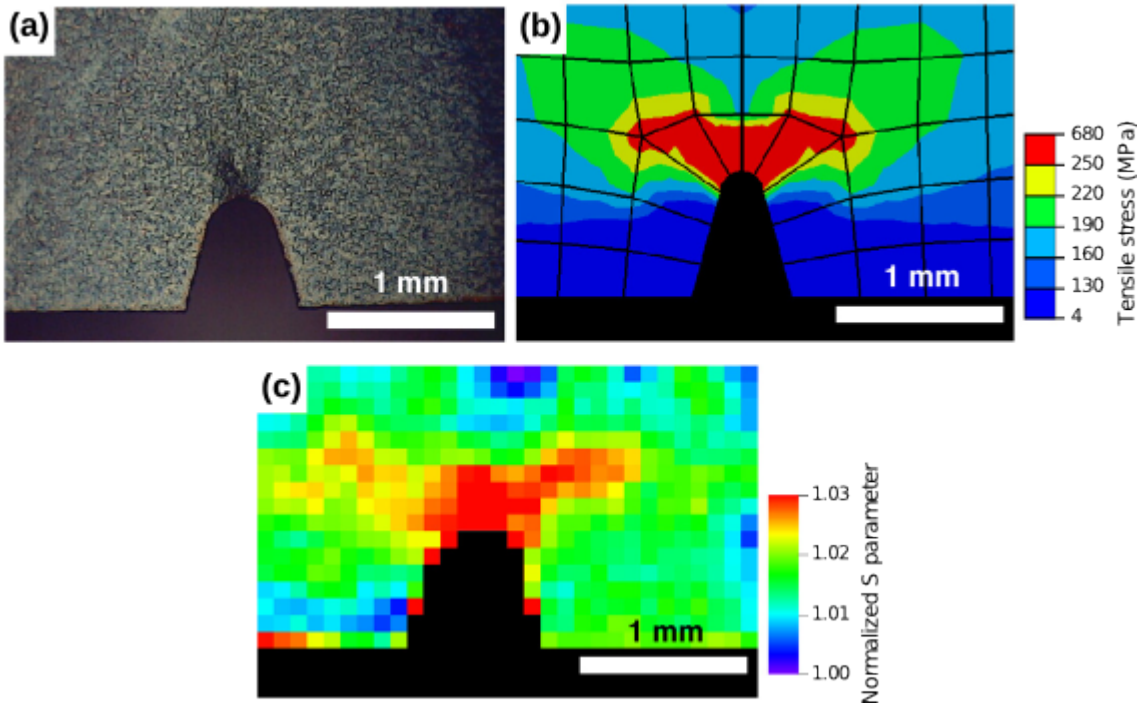

Figure 32: The steel sample after the annealing procedures, the sensitization and the plastic deformation [55]: (a) an optical image, (b) tensile stress distribution calculated with finite-element method and (c) an S-parameter map with a 20 keV implantation energy and a 20 µm beam diameter.

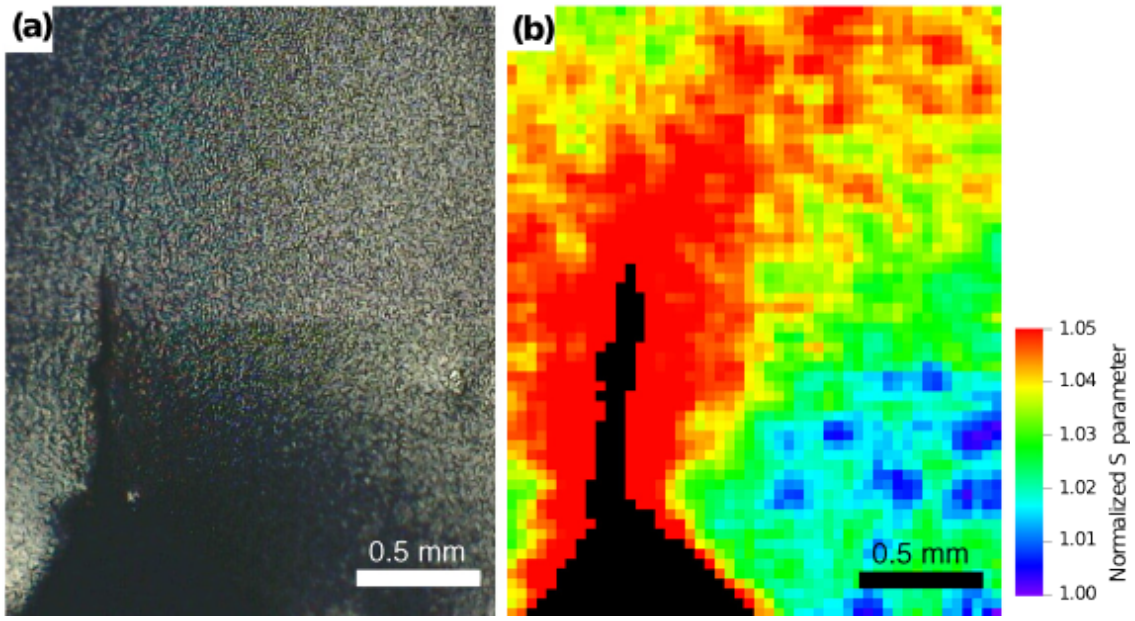

Figure 33: The steel sample after applying the stress-corrosion-cracking: (a) an optical image, (b) an S-parameter map with a 20 keV implantation energy and a 20 µm beam diameter. [55]

Figure 32 shows an optical image, a tensile stress finite-element calculation and an S-parameter map of the steel sample. The steel sample was measured with a 20 keV implantation energy and a 20 µm beam diameter. Even though the applied total stress (150 MPa) was lower than the yield stress of the type 304 steel (250 MPa), the simulation shows that the local stress in the vicinity of the notch exceeds the yield stress. The S-parameter map from the TPM measurement shows an elevated S-parameter all around the starting notch but the highest S-parameter is observed at roughly the areas where the simulated local stress was greater than the yield stress. [55]

Next, a corrosion treatment was applied to the sample. Figure 33 shows an optical microscopy image and an S-parameter map of the notch after the SCC crack propagation. The S-parameter map shows an elevated S-parameter 200-400 µm around the crack tip. [55]

3.4 Plans of a scanning positron microscope in Livermore

A positron lifetime microprobe was planned in 1990s at Lawrence Livermore National Laboratory (LLNL) in the USA. In 1999, the linear accelerator (linac) in LLNL was capable of producing 10^{10} moderated positrons per second. The LLNL microprobe was planned to feature a 1 µm resolution, an event rate of $2 \cdot 10^5$ cps and a 20 MHz beam repetition frequency. The suggested applications of the LLNL microprobe include deformation studies, buried interfaces, electro-migration of defects in integrated circuits and *in situ* annealing. [57]

According to references [57–59] published in 1997-1998, the primary beam line from the source of the moderated positrons to the microprobe was being tested in the 1998. No publications about the LLNL microprobe published after the year 1999 were found.

3.4.1 Positron source and primary beam

The positron source of the LLNL is an electron linac capable of a 400 mA electron beam current with a repetition rate of 300 Hz. The electrons are stopped in a water-cooled tungsten target, which provides a shower of bremsstrahlung photons. The pair-production of MeV photons is an intense positron source. These positrons are moderated in well-annealed 25 µm tungsten foils arranged in the form of "Venetian blinds". [57] With the full power of the linac, 10^{10} moderated positrons per second are produced [57, 59].

The moderated positron beam is guided into an experimental hall with an axial magnetic field of 6 mT [57]. The beam transport contains a curved section to stop gammas and the unmoderated positrons from source. The experimental hall has a 4.5 m thick shielding from the positron production target. [59] The moderated positron beam has a temporal width of 3 µs and a repetition rate of 300 Hz. The energy spread of the beam is approximately 4 eV. [57]

The moderated 3 µs pulses contain $3 \cdot 10^7$ positrons each, which could saturate the detection system. The initial 300 Hz pulsed beam is turned into a quasi-continuous

beam with a penning trap stretcher. The trap converts 3 µs pulses into 3 ms pulses and reduces the energy spread of positrons from 4 eV to 20 meV. [57] [59]

The trap is followed by a 20 eV accelerator consisting of 30 electrodes equal spacings and voltage differences. Right after the accelerator, there is a two-gap buncher section, which produces 1 ns wide pulses every 50 ns. Every bunch contains approximately 500 positrons. A 1 GHz waveform generator provides a non-linear sawtooth voltage for the buncher. [57] The combination of the linac, the pulse stretcher and the buncher allows production of either 1 ns bunches of 500 positrons with a 20 MHz repetition rate, 3 µs bunches of $3 \cdot 10^7$ positrons with a 300 Hz repetition rate or a quasi-continuous beam with a flux of 10^{10} e^+/s. [59]

After the bunching, the positron beam is accelerated to 2 keV before the termination of the guiding magnetic field. The extraction of the beam from the guiding field is done with a magnetic grid consisting of 36 tapered fins pointing towards the center, a construction resembling the spokes of a wheel. The grid has a diameter of 5 cm and it is made of a high permeability stainless steel. The spokes are cut to three different distances from the center, and the transmission of the grid is >90 %. [57] The magnetic field density 2 mm after the grid was measured to be 30 µT [59]. Beyond, the beam is guided only electrostatically [57].

After the grid, the primary beam has a diameter of 1.2 cm, a half-angle below 1°, an energy of 2 keV, a pulse width of 1 ns and a repetition rate of the 20 MHz. [59] A switchyard is located 40 cm after the magnetic field termination. The switchyard can either pass the beam to the microprobe, divert the beam to other experiments or measure the beam profile with a microchannel plate. [59]

3.4.2 Microprobe optics

The actual microprobe consists of four beam columns, three remoderators, a chopper, two bunchers, a beam deflection system and an electron gun for SEM operation (Figure 34). In the LLNL microprobe, only electrostatic focusing is used because magnetic lenses would interfere with the nearby beam lines. [57]

The first remoderator is located on the axis of the incoming beam line, 190 cm after the magnetic grid. The re-emitted positron beam is guided to the second, 50 cm long column, which contains a chopper section. The chopper is located in a cross-over of the beam, and it consists of 4 mm×4 mm parallel plates with a 6 mm separation. The second column produces a spot diameter of 150 µm on the second remoderator at the end of the second column. The third column is also 50 cm long and contains the main buncher, which compresses the width of the positron bunches from 1 ns to 100 ps. The main buncher operates with an 80 MHz and 30 V sine-wave. The spot diameter on the third remoderator is 15 µm. The final, optical column is 113 cm long, houses a buncher, an accelerator and a 12-pole deflection system. The positron beam can be accelerated to a beam energy of 1 to 50 keV. The sample can be scanned with beam diameter down to 1 µm. The use of the final column buncher allows a pulse width below 100 ps but degrades the minimum final spot size to 7 µm. The estimated evolution of the positron beam of the LLNL microprobe is summarised in Table 1. [57]

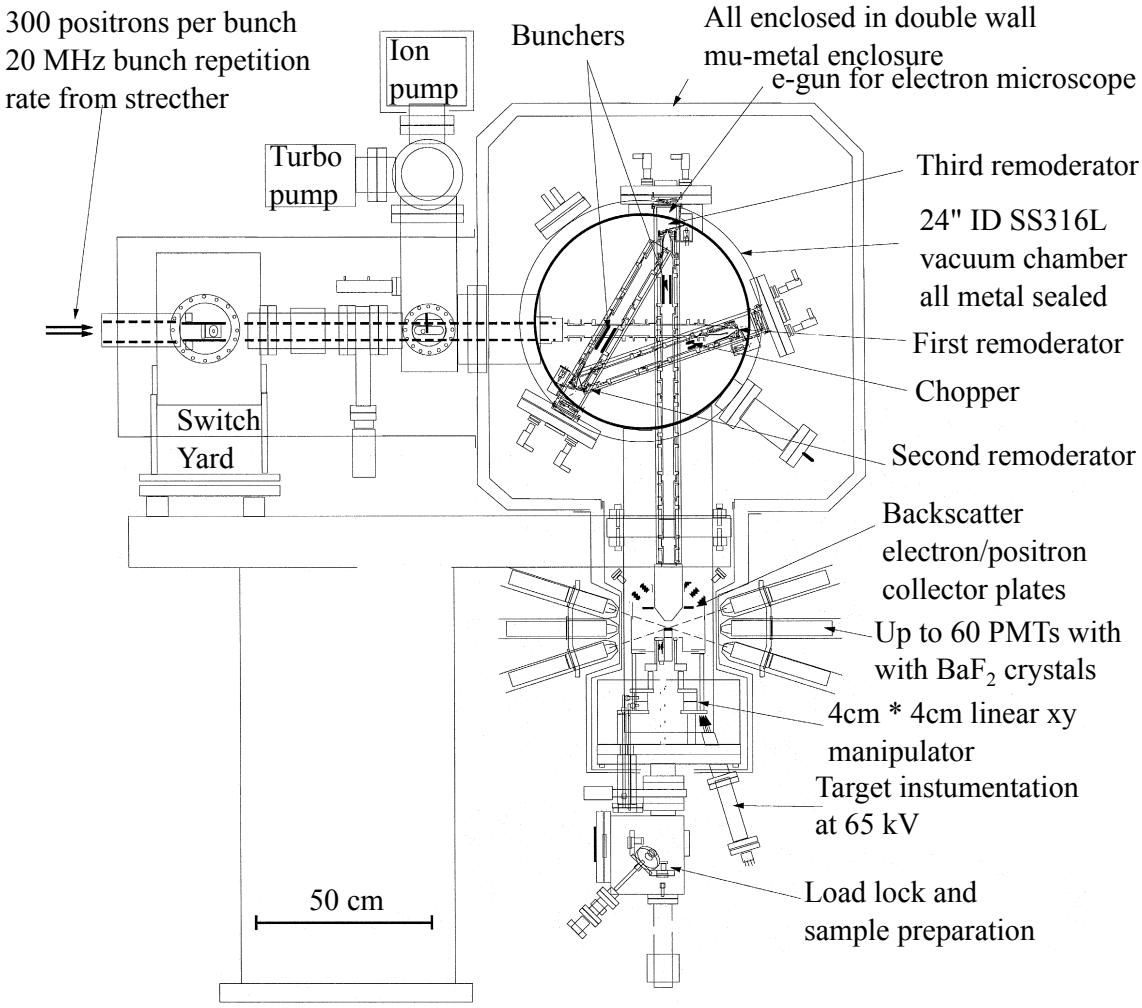

Figure 34: A diagram of the SPM planned, but not built, at LLNL [57].

Table 1: The beam diameters and the positron fluxes during the beam line [57, 58]. The use of the buncher of the final column suppresses the width of positron pulses below 100 ps but degrades the minimum spot size to 7 µm.

Stage	Beam diameter	Pulse width	Positron flux
Primary beam	1.5 cm	3 µs	10^{10}
First remoderator	3 mm	1 ns	$5 \cdot 10^9$
Second remoderator	400 µm	1 ns	-
Third remoderator	50 µm	100 ps	$2 \cdot 10^8$
Sample	1 µm/7 µm	100 ps/<100 ps	$1 \cdot 10^7$

Each remoderator compresses the beam 10-fold in diameter and 20-fold in brightness. The positron beam is accelerated to 5 keV between the remoderators. The remoderators are placed behind 25 µm thick stainless steel foils with holes slightly larger than the anticipated beam spot size. This allows the alignment of the beam to the centers of the optical columns and removes the halo surrounding the beam. The remoderators can be annealed *in situ* by flipping them and heating with electrons guns to 2000 °C. [57]

The amount of annihilation radiation from the remoderators, the grids and the chopper is several orders of magnitude higher than the signal from the target. Thus, the lengths and the layout of the columns are designed such that annihilations from the remoderators, the magnetic grid, the accelerating grids and the stopper of the chopper occur within a 10 ns window during the 50 ns cycle. Then, a positron bunch is implanted into the sample, and there is a 40 ns window without background annihilations. [57] Also, the locations of all radio frequency elements are optimised to reduce coupling effects. [59]

3.4.3 Technical details

The vacuum enclosure of the microprobe is made of SS316L and SS304 stainless steels. The electrostatic lenses are Au-plated Al, the electric insulators and lens carriers are alumina ceramics and radiation shielding is non-magnetic W alloy. [57]

The microprobe is located inside a 3-D Helmholtz coil, which decreases the Earth's magnetic field from tens of µT to hundreds of nT. The microprobe columns are shielded with a double walled µ-metal enclosure, which reduces the AC-magnetic fields inside the microprobe from 100 nT to about 1 nT. [57] The lens systems are designed to produce an odd number of cross-overs in each column and the locations of the cross-overs are adjusted to compensate the beam spot shift due to residual AC magnetic fields. [59]

The electric potential of the remoderators and optical columns increase in steps of 5 kV, so all the electrical equipment located after the first remoderator float at 5, 10 or 15 kV. The target potential is between 16 and 65 kV above the ground potential depending on the implantation energy. [57]

3.4.4 Planned performance

The lifetime spectra are measured with an array of up to 30 pairs of BaF_2 detectors, which operate in coincidence mode. The enclosure around the target is designed to be large enough to discriminate the annihilations from the chamber walls. [59] The 250 ps time resolution of the BaF_2-detectors allows the identification of annihilations in the chamber walls based on asymmetric time-of-flight delays. The positron flux at the target is 10^7 e^+/s, which results roughly in a two day measurement time for a typical 3D-mapping. An electron gun located behind the third remoderator allows SEM studies in the classical manner. [57]

4 Design of a new positron microscope

This chapter will first compare the different characteristics and performance of the existing SPMs. Next, the design of an SPM is discussed on a general level. Then, a specific structure for the needs of our group is proposed. The suggested structure consists of the most suitable starting point among existing SPMs and a list of suggested modifications. At the end of the chapter, a roadmap for the design and construction is outlined.

4.1 Comparison of the existing scanning positron microscopes

Due to the completely self-made structure, the remoderation and the beam pulsing, the construction of the MPM appears to be significantly more laborious than the construction of the BPM or the TPM. The major differences between the BPM and the TPM seem to favour the BPM: the moderator solution of the TPM is more complicated, while it does not significantly enhance the performance, and the angle of the electron gun in the TPM may cause problems for the electron image. The TPM is not reported to be able to operate as an SEM.

All three SPMs have reached beam spots smaller than 5 µm with a count rate higher than 30 cps, as shown in Table 2. However, the beam spot intensity of the TPM is an order of magnitude smaller than what attained with the BPM and the MPM.

Table 2: A performance comparison of the existing SPMs. The characteristics have been described in more detail in chapter 3. The value for the moderator efficiency of the TPM is for another moderator of the same type [11]. [4, 15, 38, 46]

	BPM		**MPM**		**TPM**	
source activity (MBq)	370		1 100	?	55	
- diameter (mm)	0.5		?		2	
moderator	W: 0.5 µm + cone		1 µm W(100)		Solid Ne	
- efficiency	$1.7 \cdot 10^{-3}$		$6 \cdot 10^{-4}$		$(3 \cdot 10^{-3})$	
remoderator	———		reflection W		———	
- efficiency	———		20 %		———	
beam diameter (µm)	1	20	2	5	3.9	15
- count rate (cps)	50	2000	70	170	30	150
- intensity (cps/µm^2)	60	6	20	9	3	0.8

4.1.1 The specific characteristics of the Münich positron microscope

The MPM is significantly more complex than the BPM and the TPM because unlike them it has a beam pulsing and a remoderation stage as well as it does use an SEM-column.

The MPM may have problems with a small depth of focus because all of the samples measured with the MPM in [3, 24, 46, 47] were surface-polished. For a comparison, none of the studies done with the BPM or the TPM include polishing the surfaces of samples [2, 23, 28–35, 51, 52, 54–56]. The need for polished sample surfaces is most likely explained by the small depth of focus, which is most probably related the objective lens below the sample.

The objective lens below the sample may prevent measuring magnetic samples. Because the objective lens of the MPM is located below the sample, the focusing magnetic field penetrates the sample. If the sample is magnetic, it may disturb the magnetic field and the degrade the beam spot.

Having an objective lens below the sample allows a longer distance between the optical column and the sample that would be possible with an objective lens within the optical column. This suppresses the contribution of the backscattered positrons. The distance between the sample and the optical column is below 10 mm for both the BPM and the TPM while for the MPM it is 100 mm.

4.1.2 Comparison of the beam intensities

The structure of the MPM is significantly different from the others because of the beam pulsing and remoderation stages. The beam lines of the BPM and the TPM, on the other hand, are quite similar (chapters 3.1 and 3.3), while there is a significant difference in the beam intensities. Both have a bend of 90° with a magnetic prism and an optical column of a commercial SEM. The SEMs themselves were capable of creating electron beams with diameters 100-fold below the attainable positron beam diameters [15, 60]. Therefore, the SEM-columns should be equally suitable and not affect the differences of the performances of the BPM and the TPM. The beam line of the TPM is a bit longer but appropriate magnetic transport does not affect the beam.

The beam intensities for beam diameters between 1 and 20 µm of the TPM are an order of magnitude smaller (Table 2). The main differences related to the positron beam intensities between the BPM and the TPM are the moderator material and the activity and the diameter of the positron source. The activity of the positron source of the TPM is an order of magnitude smaller, while the diameter of the positron source of the TPM is fourfold. The activity per source area of the TPM is only one percent of that of the BPM. The lower beam intensity of the TPM probably results from the lower activity and the larger diameter of the positron source.

4.1.3 The angle of the electron gun

In an SPM configuration where the electron gun is on the optical axis of the optical column, as in the MPM and the TPM, the residual magnetic fields of the magnetic prism may disturb the electron beam. If the electron and positron sources are located on opposite sides of the optical column with a 90° angle to it, both beams are operated with roughly the same magnetic field and such a problem does not exist.

The TPM has not been reported to be capable of operate as an SEM though it possesses an electron gun and a column of an SEM. The only use of the electron gun of the TPM is reported in [52], where it was used for electron beam induced current (EBIC) imaging. The resolution of the EBIC image was $\sim$ 100 µm, which suggests an electron beam spot of the same size. The SEM operation of the MPM has been used in one [3] study out of four [3, 24, 46, 47]. For a comparison, SEM images were taken with the BPM in four studies [28, 29, 31, 34] out of ten [2, 23, 28–35].

The TPM appears to have problems with the electron beam while the BPM seems to be free of such problems. Thus, a configuration, where the electron gun is at a 90° angle to the axis of the optical column, is preferable.

4.2 General design of a scanning positron microscope

The necessary parts of an SPM include a positron source, a moderator, an accelerator, an energy filter, lenses, a method to scan the sample and a gamma detector. In practice, due to low fluxes of moderated positrons, an SPM needs also a supporting measurement method for lateral and vertical positioning of the sample (see chapter 4.2.2). Figure 35 shows the basic building blocks of an SPM.

During the design of an SPM, the parameters, which affect the use of the SPM most, should of course be paid the most attention. The clearest deficiency of SPMs is the low count rate due to the lack of high brightness sources of moderated positrons. The intensity of the moderated positrons depends on the activity and cross section of the source, and the efficiency of the moderator. The energy spread of the moderated positrons is solely a feature of the moderator. Also focusing lenses affect the beam spot size. The spherical and the chromatic aberrations of the magnetic lenses define the quality of the focus. However, if the optical column of an SEM is used, the lenses may be impossible to replace with improved lenses.

The possible positron sources of an SPM are radioactive sources, or nuclear or accelerator facilities. Essential for the positron source is to emit as many positrons as possible from a small area and not to have an excessively high level of gamma emission. The optimisation of the geometry of a radioactive positron source is discussed in chapter 4.2.1. The positron beams of nuclear or accelerator facilities typically have too large diameters and energy spreads to be directly used as the positron source of an SPM. Therefore in practice, a facility source needs a remoderation stage.

In order to have a high count rate in a small beam spot, the moderated positrons of an SPM need to have a high brightness, i.e. the moderator has to emit a lot of positrons with a low energy spread. A low energy spread facilitates the focusing and the positrons, whose trajectories deviate too much from the optical axis, are removed from the beam by the apertures of the beam line. The BPM has a moderator with both a W thin film and a single crystal cone and the proportion of the count rate produced by the cone was reported to be 1/3 [27]. By combining that with the individual moderating efficiencies of a thin film ($6 \cdot 10^{-4}$ [12]), single crystal cone ($1.4 \cdot 10^{-3}$ [14]) and their combination ($1.7 \cdot 10^{-3}$ [15]), the result suggests that the positrons moderated by the W single crystal cone reach the final beam spot of

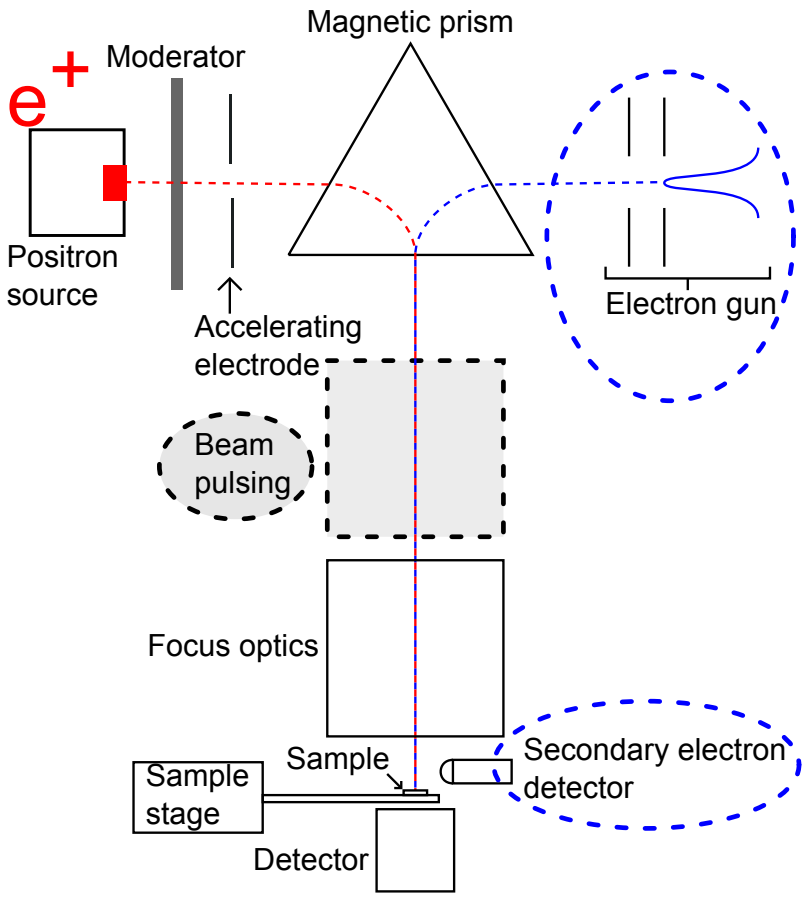

Figure 35: Basic building blocks of an SPM. There are not any unconditional reasons why the accelerating electrode would need to locate right after the moderator. The beam pulsing is only required if lifetime is measured. An SEM appears to be the most suitable supporting measurement method and, thus, an electron gun and a secondary electron detector are also included.

an SPM half as often as the positrons from the thin film part of the moderator. Only a 1/3 of the count rate of the BPM was reported to be generated by the cone moderator , although according to the reported moderating efficiencies, the fraction should be roughly $1.4 \cdot 10^{-3}/1.7 \cdot 10^{-3} \approx 4/5$. Although the efficiencies are measured in different setups of different geometries and, hence, already the definition of the efficiency causes some inconsistency, the reported moderating efficiencies are additive within an acceptable accuracy: the efficiency of the moderator with both a thin film and single crystal core is the sum of the individual efficiencies $6 \cdot 10^{-4} + 1.4 \cdot 10^{-3} = 2 \cdot 10^{-3} \approx 1.7 \cdot 10^{-3}$. It seems that the higher momentum spread of the positrons moderated by the cone causes an additional reduction of $\sim 1/2$ during the optical path of the BPM. Thus, positrons with a larger energy spread are less valuable for SPMs.

The addition of a cone moderator, besides the thin film, does not worsen or remove the positrons emitted from the thin film, while it produces additional mod-

erated positrons. In the case of the BPM, the addition to count rate is 50 % . Therefore, the optimal moderator for an SPM has both a thin film and a (single crystal) cone.

The selection of the moderator material of an SPM is a trade-off between efficiency and energy spread. The efficiency of solid Ne moderators is five-fold compared to W moderators of the same geometry but they also have an order of magnitude higher energy spread of moderated positrons. Ni moderators have been reported to have a significantly lower energy spread and a slightly lower efficiency than W moderators. Additionally, a relatively low annealing temperature is sufficient for Ni as even the melting temperature is 1455 °C [61], whereas the annealing temperature of W can be as high as 3000 °C. A relatively high efficiency ($1.7 \cdot 10^{-3}$) has been reported for the W moderator of the BPM, which has both a thin film and a single crystal cone, while its the energy spread has not been reported to induce any problems [15].

The design of the accelerator of an SPM needs to mainly concentrate on preventing the unidealities of the accelerator. The acceleration of charged particles is trivial, but a particle accelerator also has particle optical properties, which have to be either minimised or utilised into the optics of the SPM. All the existing scanning positron microscopes have one or more electrostatic accelerators.

The energy filtering of the moderated and unmoderated positrons is performed by bending the beam with a magnetic field in all the existing SPMs. It appears to be the simplest option and, in addition, it allows the use of an electron beam as the supporting measurement method. The need for it is further discussed in chapter 4.2.2.

Charged particles can be bunched with time depended potential applied between a single or multiple gaps. Typically, prebunchers consisting of multiple acceleration gaps are used for the first bunching of the beam while the final bunching is done with a single gap buncher. The optimal bunching voltages require production of arbitrary waveforms. Because the typical repetition rates of SPMs are tens of MHz, the arbitrary waveforms of the repetition rate contains Fourier components with notably high frequencies. Sine wave voltages are hence used because they are easier to produce and they can approximate the linear region of optimal bunching waveforms. The unidealities of the bunching spread some of the positrons outside the bunches. These unbunched positrons can be removed from the beam, for example with a transverse electric field. [62]

The use of an SEM-column seems to be the most cost-efficient solution for the focusing optics of an SPM. The BPM and the TPM have shown that SEM-columns can be utilised in SPMs [2, 23, 28–35, 51, 52, 54–56]. In the existing SPMs where an SEM-column is used, the scanning of the sample is performed by moving the sample with a sample stage with a fixed location of positron beam focus, instead of using the scanning coils of the SEM-column. A possible reason for this are the higher-degree corrections of the SEM scanning coils relating to the gyration of electrons [27]. The opposite gyration direction of positrons would result in a larger spot. The scanning of the sample with a sample stage does not significantly increase the complexity or the cost of an SPM.

In order to reduce the contribution of the annihilations of scattered positrons, the space above the sample should be free of matter. Therefore, the only feasible location for the gamma detector is opposite the incoming beam. In order to maximise the detection efficiency of annihilation gammas, the detector has to be as close to the sample as possible. An option is to surround the sample with numerous detectors located $\sim$ 100 mm distance around the sample. This option would demand tens of gamma detectors and significantly increase both the cost and the complexity of the SPM. The gamma detector has to be shielded from the gamma radiation of the positron source.

4.2.1 Design of the radioactive positron source of a scanning positron microscope

The features of a positron source relevant for the SPM are the area and intensity of positron emission and the amount of gamma emission. The intensity of positron emission depends on the specific activity of and the length of the source as well as on the stopping length of positrons in the source material.

The reasonable length of the source material is limited by the positron stopping length in it. The thicker the source is, the more probable it is for an average positron to be annihilated in the source. After a certain length of the source material ($l_{s,max}$), an increase on the length increases the gamma background of the detector more significantly than the positron emission.

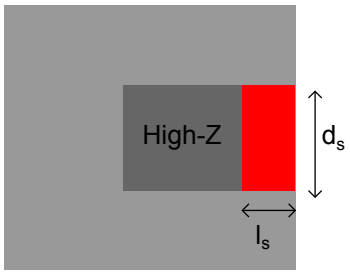

Figure 36: A schematic drawing of an isotope positron source of an SPM.

The optimal source diameter (d_s) is a trade-off between the gamma background, the count rate and the cost. In a simple picture the focusing of an SPM can be divided into two operating modes. In the first mode the apertures of the beam line are not being used, or their contribution is minor, and the resulting beam spot is large and has a high flux. In the second mode, the apertures strongly restrict the size of the positron beam yielding a smaller beam diameter and count rate.

If the activity per volume and the length of the source are kept constant, an increase of the source diameter approximately linearly increases the size of the beam of the first mode and the count rate quadratically. The same diameter of the beam of the second mode should be attainable with the same count rate. The increased amount of annihilations in the apertures and the source can increase the background of the detector. If the source diameter is decreased when keeping the conditions

fixed, a beam of the first mode contracts while the beam of the second mode should stay constant.

In this simple picture, the diameter of the source is proportional to the diameter of the beam of the first mode, while it does not have effect on the beam of the second mode. The positron emission intensity determines the intensity of the positron beam and, thus, also the smallest diameter of the positron beam, which still has a feasible positron flux for practical use. As a source of a larger diameter also "includes" a smaller source, the only reasons to reduce the source diameter are be the reduction of the background or the cost of the source.

The source material of the highest possible specific activity should be used because it linearly increases the positron emission intensity. High-Z material in the source holder, especially right behind the source, enhances the positron emission intensity by backscattering positrons emitted into the wrong direction. The optimal diameter of a positron source can be determined either with simulations or experimentally. A sufficient simulation requires simulation of almost the whole instrument. The source diameters of the BPM and the TPM are 500 µm and 2000 µm, respectively. The beam intensities for the BPM are an order of magnitude higher than for the TPM at beam diameters of 1-20 µm. If no more precise data concerning the diameter of the positron source of a new SPM is available, a diameter around 500 µm should be preferred.

4.2.2 Supporting measurement technique

In an SPM, the lateral and vertical positioning of the sample can be done significantly faster with other measurement techniques, such as an SEM or an atomic force microscope. This is due to the low fluxes of moderated positrons, resulting low count rates and long measurement times.

First, attaining a focus by observing the sharpness of the image of the sample, as is done in SEMs, would be too time-consuming. A measurement of even a simple 20×20 pixel map takes 11 hours with a typical count rate of 100 cps and only 10^4 counts/pixel, for a rough mean lifetime or S-parameter. The focus can be attained much faster with a beam profile monitoring setup, using for example a knife-edge method or a beam profile detector. If a supporting measurement technique can be used for determining the distance of the sample surface, an SPM can be focused only once for one distance, preferably halfway of the working distance. Afterwards, the samples can be adjusted in the vertical direction until the surface of the sample is at the same distance as the focus according the supporting technique.

The other SPM operation, which can be done significantly faster with a supporting technique is the finding of the locations of interest of the sample. For example, with a count rate of 100 cps, it would take 12 days to measure a map of 100×100 pixels with only 10^4 counts per pixel. With a supporting technique, positron measurements can be applied only to the regions of interest.

A supporting technique of an SPM has be capable of providing the vertical coordinate of the sample surface, with an accuracy better than the depth of focus of the SPM, and have a lateral resolution of 1 µm. An apparent option for a sup-

porting technique is an SEM, as has been done in the BPM and the MPM. The standard secondary electron (SE) detector provides an image of the surface topology of the sample and is suitable for this application. The vertical distance of the sample surface can be determined with the focus. The attaining of the focus can be automatised with modern focus algorithms. First, the focus parameters for vertical distances of interest, such as the distance of the positron focus, can be tabulated. Then, the sample can be shifted to the vertical location desired. If necessary, the vertical location of even individual positron pixels (>1 µm×1 µm) can be acquired, because a standard SEM can distinguish approximately 100×100 pixels from that area. A map of 100×100 pixels is well sufficient for finding a focus.

A dual operational SPM-SEM can further be equipped with other SEM detectors, such as backscatter electron, energy dispersive X-ray or cathode luminescence detectors, for a material specific resolution without affecting the positron imaging. A detector can be attached to a linear manipulator if necessary. The manipulator allows moving the detector closer during the SEM operation to maximise the collection efficiency of the detector, and further away during the SPM operation when a large free space in front of the sample is required to suppress the contribution of scattered positrons.

There is no reason why other techniques could not be used as supporting techniques of an SPM as well. One option is a scanning probe device (SPD) capable of atomic force microscopy (AFM) or scanning tunneling microscopy (STM). However, the duration of a typical scan with AFM is few minutes where an SEM can provide tens of images in a second. Also, an SPD does not usually fit between the optical column and the sample of an SPM. Only in the MPM there is enough space for an SPD, but the SPD would anyway block the positron beam. If an SPD is used as the supporting technique of an SPM, a linear manipulator stage is required. Either the sample or the SPD has to be moved when changing from the use of the SPD to the positron beam or vice versa (Figure 37).

Both an SEM and an SPD have the necessary resolution for lateral and vertical positioning of the sample. The imaging with an SPD is significantly slower than with an SEM and the use of an SPD would require additional manipulators. If there is no additional motivation for the use of an SPD, an SEM outperforms present SPDs as the supporting technique of an SPM.

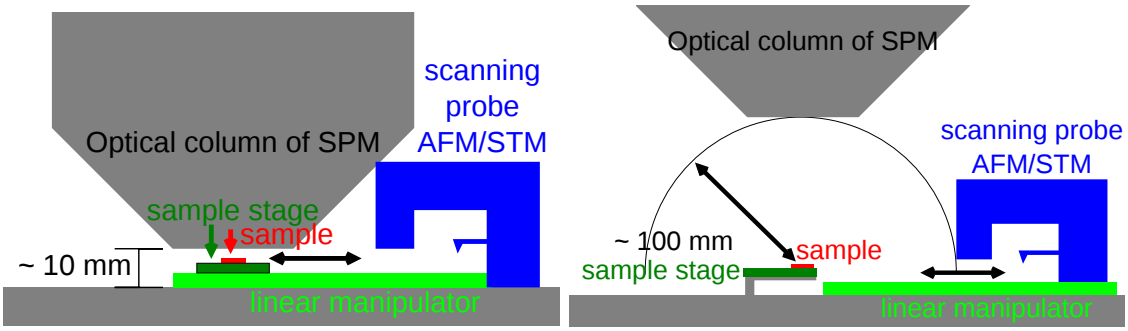

(a) transfer of sample (b) transfer of scanning probe device

Figure 37: A schematic use of scanning probe techniques as the supporting measurement technique of an SPM. With a supporting technique, the sample can be positioned laterally and vertically significantly faster than with the positron beam.

4.3 Proposed structure of SPM

The requirements for an SPM of the Aalto positron group are a positron beam diameter below 10 µm, a count rate of at least 50 cps, and a structure as simple as possible. In practice, the use of an SPM requires a supporting measurement technique for the vertical and lateral positioning of the sample (chapter 4.2.2). A commercial SEM (ZEISS/Opton, DSM 950) has been reserved for the optics of the SPM. This SEM is described in appendix A.

Beam pulsing in an SPM would be too complex for our intentions. So, the new SPM has to measure DBS. In our case, the higher moderating efficiency of a solid Ne moderator is not an option because of the higher complexity and the larger energy spread of moderated positrons. Hence, the new SPM will have W moderator. The moderator is a W single crystal cone surrounding the W thin film to increase the positron flux. The use of an optical column of a commercial SEM has been shown to be suitable by the BPM and the TPM and it significantly reduces the required workload. The electron guns of the BPM and the TPM are attached at different angles compared to the optical columns, which may be a reason why the TPM is unable to operate as an SEM. Thus, the new SPM has a 90° angle between the optical column and the electron gun.

Among the existing SPMs, the BPM meets all the outlined features. However, some modifications to the structure of the BPM are suggested. For example, the side-gap "single pole" lens of the MPM below the sample is considered as a way to achieve more free space above the sample and maybe reduce the beam spot size. The horizontal beamline construction, as in the TPM, is considered as a way to make the beam line more rigid and reduce its sensitivity to vibrations.

4.3.1 The positron source

If cracks in metals are to be a major target of studies, the diameter of the positron source can be increased from the source diameter of the BPM (500 µm). When studying cracks in metals, the annihilation data is typically averaged over several

grains in order to confirm that the data is not dominated by grain boundaries. Beam diameters of tens of micrometers have been typically been used [29,30,32,33,46,47, 51,54,55]. For some of the studies, the minimum diameter of the high flux beam spot of the BPM (20 µm) is already too small and the beam spot needs to be defocused.

If the diameter of the source is increased by a factor of 2 to 1000 µm, the diameter of the high flux beam should increase to approximately 40 µm. A larger of source diameter reduces the relative surface area of the moderator cone. The area of the thin film scales quadratically while the are of the cone scales linearly. The anticipated count rate can be calculated by weighting the increase of moderator surface with the related count rate, which is 1/3 for the cone part of the moderator:

$$\frac{1}{3} \cdot 2 + \frac{2}{3} \cdot 2^2 = \frac{10/3}{\approx} 3.33. \tag{17}$$

The anticipated count rate is roughly 6700 cps. The increase of the source diameter should not complicate attaining small beam diameters.

The only reason, which justifies a reduction of the source diameter, is the reduction of the gamma background produced by the positron source. The reduction of the diameter, and volume, of the positron source reduces quadratically the total activity, and the gamma background, while the reduction to the count rate of 1 µm beam diameter is relatively smaller.

The maximal length of the positron source material ($l_{s,max}$) can be estimated by calculating the amount of positrons, which can penetrate a certain length of NaCl, and selecting the desired trade-off between the increased amount of emitted positrons, the background and the cost of the source.

4.3.2 Important modifications and changes

There are some modifications and changes, which are to be made for the new, updated version of the BPM. First of all, the *in situ* annealing chamber is to be converted into an external annealing chamber. The moderator is then transferred within a small portable vacuum chamber. Though there is no direct malfunctions related to the *in situ* annealing chamber of the BPM, the annealing chamber adds a long extra vacuum chamber of 2 m, which both increases the sensitivity for vibrations and increases the size of the microscope. Replacing the *in situ* annealing chamber with a vacuum port allows attaching an additional vacuum pump to the positron source chamber. The external annealing chamber and the portable vacuum chamber can be used to anneal moderators for other positron beams and, as the W-moderator annealing is typically not done more often than every six months, it can even be shipped between different positron laboratories.

The baking of the vacuum chambers of an SPM enhances the quality of the vacuum. A better vacuum slows down the surface contamination and the degradation of the efficiency of the moderator, which reduces the required frequency of moderator annealing. The vacuum of the BPM during operation is only in the range of 10^{-4}-10^{-5} Pa [27] because the pumping speed is limited by the number of vacuum pumps. In the BPM, there are only a few possible locations where a vacuum pump

can be attached. The baking is to be realised because the required effort is minimal: the vacuum chambers of an SPM can be heated with externally attached resistance wires and the temperatures of sensitive components, such as magnetic lenses, can be monitored by incorporating simple temperature sensors into the structure of the SPM.

The software used to operate the BPM consist of multiple different programs with the oldest ones operating in the DOS-operating system. All the necessary software have to be implemented for the present computers. Otherwise, compatibility problems will eventually arise.

4.3.3 Appealing modifications requiring further study

A beam profile detector would highly accelerate the alignment and focusing of the positron beam. However, is problematic to find a detector capable of providing 1-20 µm resolution for positrons with a kinetic energy of 1-30 keV and, in addition, fit it within the 12 mm distance between the optical column and vacuum wall [27]. A beam profile detector would be be beneficial even with a resolution of $\sim$ 50 µm and a capability to detect the majority of positrons in the 1-30 keV energy range. Presently in the BPM, the focus of the positron beam is adjusted with a scintillator detector and a Mo-knife-edge [27].

The side-gap "single pole" objective lens of the MPM enables a sufficiently long distance between the optical column and the sample to suppress the contribution of the annihilations of the backscattered positrons. It might also enable a decrease of the beam spot size in an BPM-like SPM. Even attaining 2000 cps within a 1 µm beam spot could be possible by operating the SPM in the high flux mode and using two objective lenses, one in SEM-column and one below the sample.

Magnetic samples may disturb the focusing magnetic field and maybe only non-magnetic samples can be measured with the "single pole" objective lens below the sample. By having a linear manipulator for moving the Ge detector and magnetic lens, allows operating either with a long working distance and two objective lenses, when measuring non-magnetic samples, and with short (<10 mm) working distances and only the objective lens of the SEM-column, when measuring magnetic samples (Figure 38). The Ge detector may require shielding from the magnetic field of the "single pole" lens, but even the photomultiplier tube detector of the MPM has been able to operate with a double walled shielding [45]. It is possible that some remnant magnetisation might be induced into materials surrounding the "single pole" lens. However, the materials surrounding the second objective lens can be chosen to be such that they have a low magnetic hysteresis and the remnant magnetisation can be reduced by demagnetisation, i.e. applying an excitation of a varying sign and decreasing amplitude into the lens.

There are few possible drawbacks in the realisation of the additional magnetic lens into a new BPM-like SPM, which have to be evaluated beforehand. First, it is possible that there is interference between the objective lenses, which could degrade the operation of both lenses. Second, a magnetic lens between the sample and the Ge detector will decrease the solid angle coverage of the Ge detector and decrease

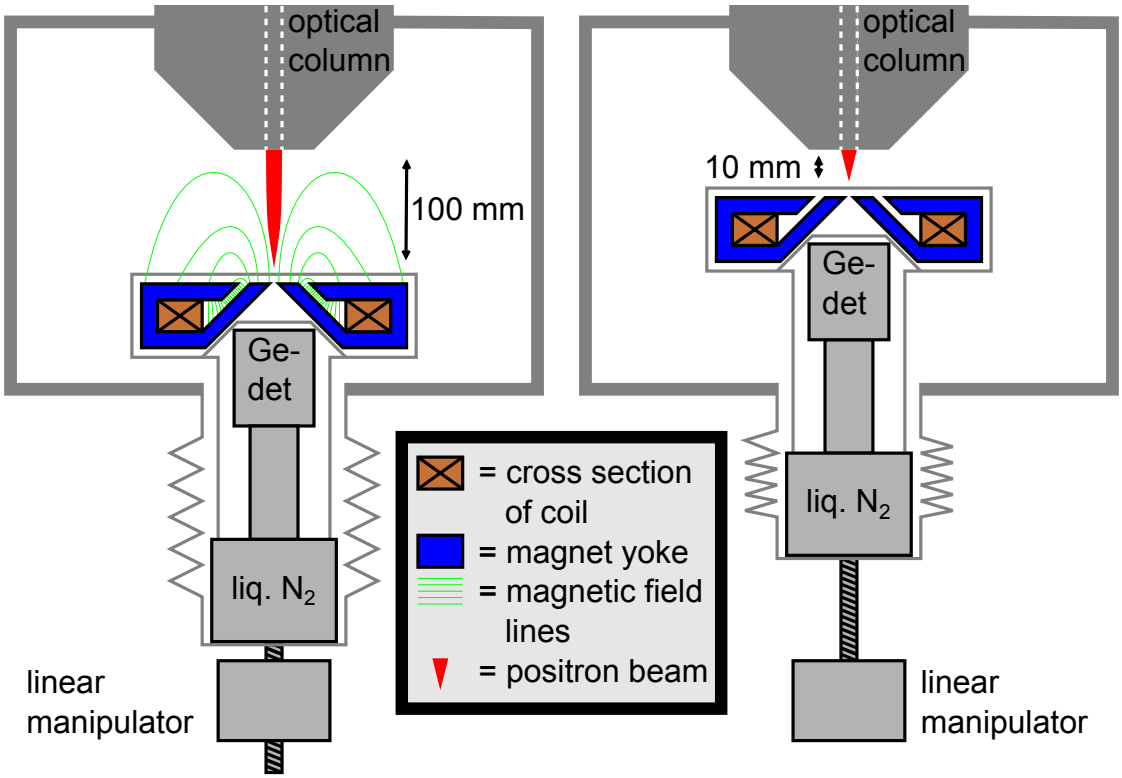

Figure 38: Schematic of a possible realisation of an objective lens behind the sample into a BPM-like SPM. There would be two operation modes, one with a long operating distance and both objective lenses for non-magnetic lenses and one with a short operating distance and only the objective lens of the SEM-column for magnetic samples.

the attained count rate. If the hole in the center of the magnetic lens is made large enough that a standard Ge detector of roughly 100 mm diameter fits completely inside the lens, the lens would not be able to produce a 1 µm beam spot anymore. Thus, a compromise between the quality of the magnetic lens and the solid angle coverage of the Ge detector has to be made. Then, it has to be verified if the compromise is still worth the effort.

It is also possible to design the SPM beam lines in the horizontal plane instead of a vertical configuration. The horizontal alignment enables more support points and is considered as a way reduce the amplitudes of possible oscillations.

4.3.4 Improvement ideas for consideration

A remoderation stage can be added into the SPM by introducing a thin film remoderator at the location of the present moderator without altering the rest of the SPM. The stage could be used to either reduce the size of the beam spot or to enable input from a positron source of a larger diameter or a higher energy spread.

Lenses with smaller aberrations could reduce the size of the positron beam spot.

For example, the BPM uses magnetic lenses, which are more than 20 years old. Also, the SEM reserved for the new SPM (ZEISS/Opton, DSM 950) is equally old. However, the magnetic lenses most essential for the beam spot are located within the optical column of the SEM and their replacement can be difficult.

4.4 Roadmap for the design and construction

The remaining work of the design and the construction of the new positron microscope can be divided into five stages:

1. **Verification of the feasibility of the uncertain modifications.** These modifications are summarised in Table 3 (further discussed in chapter 4.3.3). During this stage, all possible mechanical drawing of the BPM should be acquired. After this stage, the structure of the new SPM should be clear on the conceptual level.

2. **The design of mechanical components.** The existing mechanical drawings of the BPM has to be modified to include the improvements to be implemented. The components, which need to be designed, are shown in Table 4. Also, the location of the SPM should be known at this point. The SPM requires roughly a floor space of 5 m×5 m and a height of 3 m. The floor vibrations of the site have to be small.

3. **The construction of the SPM** includes the production of the necessary components and the assembly of the SPM. The magnetic optics are required at this point.

4. **The alignment and testing of the positron beam** require all the vacuum pumps, the power sources and the control software. The external annealing chamber has to be finished and a moderator has to be prepared at the beginning of this stage. The additional objective lens is required at the end of this stage when the positron beam is aligned up to the sample site.

5. **When the positron beam is ready for research** the Ge detector and the sample stage are needed to enable the actual PAS studies.

Table 5 lists subjects, which have to be bought during the project. Table 6 describes when the specific components should be manufactured or received. The remaining workload of the project is anticipated to be of the order of 5 man-years.

Table 3: The list of modifications (section 4.3.3) for which the feasibility has to be first verified. Later, the modifications, which are feasible, have to be designed and manufactured.

Name of component	Explanation
Beam profile detector	For the adjustment of the final focus. Does a suitable detectors exist?
Additional objective lens	Possible problems: crosstalk with the primary objective lens, layout of the lens and the Ge detector, remnant magnetisation
Horizontal alignment	Does it reduce sensitivity to vibrations?

Table 4: The list of components and tasks, which need to be both designed and constructed during the production of the new SPM.

Component/Task	Explanation
Annealing chamber	The external annealing chamber and the vacuum transport vessel
SPM Baking	Heating method and possible temperature sensors
Software	Updating for the present computers of the SPM
Body of SPM	Adding necessary changes to existing mechanical drawings

Table 5: The list of components, which need to be purchased for the new SPM. Figure 39 illustrates where different components of this table will be used. The numbers in the leftmost column refer to corresponding numbers in Figure 39.

#	no.	Component	Explanation
1	2	Beam Aligning Systems (BAS)	One for parallel shift and one for beam angle, same as in the BPM (ZEISS)
2	2	Condenser lenses	For positron and electron source branches, same as in the BPM (ZEISS)
3	2-3	Q-detectors	Consists of a scintillator + 2 photomultiplier tubes in coincidence. If a separate beam profile detector is used only 2 Q-detectors are needed
4	1	TEM-prism	For bending positron and electron beams, same as in the BPM (ZEISS)
5	1	Microscope stage	Three dimensional, 0.1 µm $\lesssim$ repeatability <1 µm
6	1	Ge detector	The shape and size may be affected by the additional objective lens
	4	Vacuum pumps	The BPM uses three turbo and one titanium sublimation pump
	11	Current sources	For external drive of magneto-optical elements: objective lens (1), Beam Alignment systems (5), condenser lenses (4), prism (1)
	2	HV-supplies	An accurate HV-supply for positron acceleration and a powerful HV-supply for moderator annealing

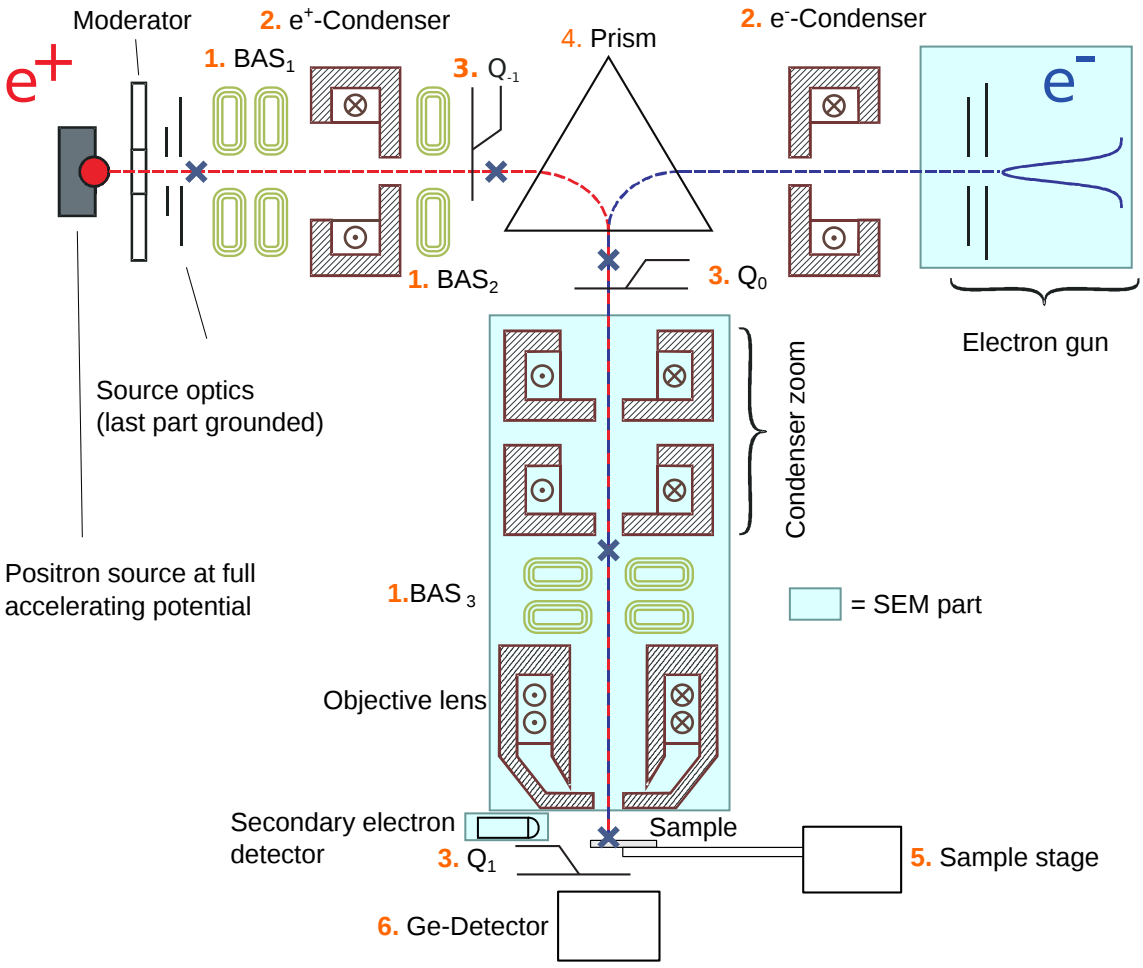

Figure 39: Diagram of the new SPM illustrating the locations of some components of Table 5. The numbers refer to components of Table 5. The figure is modified from [15].

Table 6: A timeline of the project. The letters V, D, M, P and X are used to denote the actions. The components and tasks are represented by the lines, while the columns represent the different stages of the project. The action should be done to the task or the component at latest during the stage. In the case of purchases, the item should be received during the corresponding stage.

V = verification of the feasibility of a modification
D = physical designing of the component
M = manufacturing of the component
P = purchase of the component
X = general task

Task/component	**Verification stage**	**Designing stage**	**Construction**	**Aligning of the beam**	**The beam is ready**
Mechanical drawings	X				
Beam profile detector	V	D		M/P	
Additional objective lens	V	D		M	
Horizontal alignment	V				
SPM Baking		D	M		
Body of SPM		D	M		
Location of SPM		X			
Annealing chamber		D	M		
Software				M	
Condenser lenses			P		
Beam aligning systems			P		
TEM-prism			P		
Q-detectors				P,M	
Microscope stage					P
Ge detector					P
Vacuum pumps				P	
Current sources				P	
HV-supplies				P	

5 Summary

In this work, three existing positron microscopes with spatial resolutions below 5 µm were reviewed. The detailed plans for a positron microscope at LLNL were also considered, though the microscope was never constructed. The focus of the review was the feasibility of constructing a new positron microscope.

The Munich positron microscope (MPM) has a completely custom-made, pulsed positron beam line, which can produce a 2 µm positron beam with a count rate of 80 cps. The MPM measures positron lifetime with a time resolution of 255 ps. It also possesses an electron gun for imaging as a scanning electron microscope (SEM).

The Bonn positron microscope (BPM) can produce a DC positron beam with a diameter of 1 µm and 50 cps. It measures Doppler broadening of the annihilation radiation. The BPM uses an optical column of a commercial SEM (ZEISS/Opton, DSM 960 (A)) for focusing of the positron beam. It can also operate as an SEM with a resolution of 12 nm.

The Takasaki positron microscope (TPM) also uses a column of a commercial SEM (TOPCON CORPORATION, SM-300) to focus the DC positron beam into a spot of 3.9 µm (30 cps). The TPM uses a solid Ne moderator, which is cooled down to 4 K. The TPM includes an electron gun but it has not been reported to perform electron microscopy.

The requirements for the new positron microscope are a positron beam with a diameter below 10 µm, a count rate of at least 50 cps and as simple structure as possible. In practice, a positron microscope also requires a supporting measurement technique for the vertical and lateral positioning of the sample.

Beam pulsing in an SPM would be too complex for our intentions, so the new SPM has to measure Doppler broadening. Although a solid Ne moderator has a five-fold moderating efficiency, it has an order of magnitude higher energy spread of moderated positrons than a W moderator. In addition, a solid Ne moderator also requires cooling down to 4 K and regular regrowth. Hence, the new SPM will have a W moderator. The moderator consists of a single crystal with a conical hole, in addition to a thin film, to increase the positron flux. The optical column of an SEM is used because is has been shown to be suitable for an SPM and it reduces the required workload. An SEM is used as the supporting technique. The electron gun is attached at a 90° angle to optical column as in the BPM because the 0° angle may a reason why the TPM is unable to operate as an SEM.

Among the existing SPMs, the BPM meets all the features above. The proposed SPM structure is based on the BPM but includes some modifications. Building a separate annealing chamber and transporting the moderator with a portable vacuum vessel allows removal of the 2 m long *in situ* annealing chamber of the BPM. This significantly reduces the size of the SPM and makes it less sensitive to vibrations. The baking of the vacuum chambers of the microscope enhances the vacuum of the BPM and lengthens the lifetime of the moderator while it only requires a small effort: integration of simple temperature sensors and heating elements into the microscope.

Some modifications, which require verification of their feasibility, are suggested. Introduction of an additional objective lens below the sample, similar to the one in

the MPM, allows a large free space in front of the sample and maybe a reduction of the positron beam diameter. The former suppresses the contribution of scattered positrons. A horizontal beam line is considered as a way to solidify the beam line and reduce the effects of vibrations. Additionally, a suitable beam profile detector would speed up the adjustment of the positron beam focus.

The SEM, which will be used for the focusing optics of the microscope, was initialised and tested during this work. A roadmap for the project has been outlined and a workload of the order of 5 man-years is anticipated.

References

[1] Brandes, G. R., K. F. Canter, T. N. Horsky, P. H. Lippel, and A. P. Mills Jr. "Scanning positron microbeam." Review of scientific instruments 59, no. 2 (1988): 228-232. http://dx.doi.org/10.1063/1.1140231

[2] Greif, H. and Haaks, M. and Holzwarth, U. and Männig, U. and Tongbhoyai, M. and Wider, T. and Maier, K. and Bihr, J. and Huber, B., *High resolution positron-annihilation spectroscopy with a new positron microprobe*, Applied Physics Letters, 71, 2115-2117 (1997), available: http://dx.doi.org/10.1063/1.120451

[3] David, A. and Kögel, G. and Sperr, P. and Triftshäuser, W., Lifetime Measurements with a Scanning Positron Microscope, Phys. Rev. Lett., volume 87, issue 6, 2001, http://link.aps.org/doi/10.1103/PhysRevLett.87.067402

[4] Masaki Maekawa, Atsuo Kawasuso, Construction of a positron microbeam in JAEA, Applied Surface Science, Volume 255, Issue 1, 31 October 2008, Pages 39-41, ISSN 0169-4332, http://dx.doi.org/10.1016/j.apsusc.2008.05.180

[5] Filip Tuomisto and Ilja Makkonen. "Defect identification in semiconductors with positron annihilation: Experiment and theory." Reviews of Modern Physics 85.4 (2013): 1583.

[6] Kimmo Saarinen, Pekka Hautojärvi, and Catherine Corbel. "Positron annihilation spectroscopy of defects in semiconductors." Semiconductors and Semimetals 51 (1998): 209-285.

[7] Hugenschmidt, Ch, *et al.* "The neutron induced positron source at Münich–NEPOMUC." Nuclear Instruments and Methods in Physics Research Section B: Beam Interactions with Materials and Atoms 221 (2004): 160-164. http://dx.doi.org/10.1016/j.nimb.2004.03.048

[8] Howell, R. H., R. A. Alvarez, and M. Stanek. "Production of slow positrons with a 100-MeV electron linac." Applied Physics Letters 40.8 (1982): 751-752.

[9] Antti Hakola: Ydin- ja alkeishiukkasfysiikka, Raportti TKK-F-B204 (2. painos). ISBN 978-951-22-9178-6

[10] Vehanen, A., K. G. Lynn, Peter J. Schultz, and M. Eldrup. "Improved slow-positron yield using a single crystal tungsten moderator." Applied Physics A 32, no. 3 (1983): 163-167.

[11] Mills Jr, A. Po, and E. M. Gullikson. "Solid neon moderator for producing slow positrons." Applied Physics Letters 49.17 (1986): 1121-1123. http://dx.doi.org/10.1063/1.97441

[12] Gramsch, E., J. Throwe, and K. G. Lynn. "Development of transmission positron moderators." Applied physics letters 51.22 (1987): 1862-1864. http://dx.doi.org/10.1063/1.98495

[13] Khatri, R., M. Charlton, P. Sferlazzo, K. G. Lynn, A. P. Mills Jr, and L. O. Roellig. "Improvement of rare-gas solid moderators by using conical geometry." Applied Physics Letters 57, no. 22 (1990): 2374-2376. http://dx.doi.org/10.1063/1.103856

[14] Lynn, K. G., E. Gramsch, S. G. Usmar, and P. Sferlazzo. "Development of a cone-geometry positron moderator." Applied Physics Letters 55, no. 1 (1989): 87-89. http://dx.doi.org/10.1063/1.101716

[15] Matt Haaks, *Materialforschung mit Positronen: Von der Doppler-Spektroskopie zur Vorhersage des Ermüdungsbruchs*, Helmholtz-Institut für Strahlen- und Kernphysik, Universität Bonn, 2010, available: agmaier.hiskp.uni-bonn.de/fileadmin/publications/2010_Habil_Haaks.pdf

[16] Maekawa, M., R. S. Yu, and A. Kawasuso. "Design of a positron microprobe using magnetic lenses." physica status solidi (c) 4, no. 10 (2007): 4016-4019. http://dx.doi.org/10.1002/pssc.200675821

[17] Gullikson, E. M., A. P. Mills Jr, W. S. Crane, and B. L. Brown. "Absence of energy loss in positron emission from metal surfaces." Physical Review B 32, no. 8 (1985): 5484. http://dx.doi.org/10.1103/PhysRevB.32.5484

[18] Wu, Y. C., Y. Q. Chen, S. L. Wu, Z. Q. Chen, S. J. Wang, and R. G. Greaves. "High moderation efficiency positron beamline." physica status solidi (c) 4, no. 10 (2007): 4032-4035. http://dx.doi.org/10.1002/pssc.200675825

[19] Katja Pennanen, "Termisten vakanssien tutkiminen vahvasti n-tyyppisessä piissä positroniannihilaatiospektroskopialla", Masters thesis, Helsinki University of Technology, 2005

[20] Haaks, Matz, *et al.* "Chemical sensitivity in positron annihilation with just one single Ge detector." physica status solidi (a) 202.4 (2005): R38-R40. http://dx.doi.org/10.1002/pssa.200510004

[21] Haaks, M., T. E. M. Staab, and K. Maier. "Analyzing the high-momentum part of positron annihilation Doppler spectra with a single germanium detector." Nuclear Instruments and Methods in Physics Research Section A: Accelerators, Spectrometers, Detectors and Associated Equipment 569.3 (2006): 829-836. http://dx.doi.org/10.1016/j.nima.2006.08.117

[22] Brusa, R. S., *et al.* "Doppler-broadening measurements of positron annihilation with high-momentum electrons in pure elements." Nuclear Instruments and Methods in Physics Research Section B: Beam Interactions with Materials and Atoms 194.4 (2002): 519-531. http://do.doi.org/10.1016/j.apsusc.2008.05.313

[23] Klobes, Benedikt, Björn Korff, Osman Balarisi, Patrick Eich, Matz Haaks, Karl Maier, Reinhard Sottong, Sven-Martin Hühne, Werner Mader, and Torsten EM Staab. "Probing the defect state of individual precipitates grown in an Al-Mg-Si alloy." Physical Review B 82, no. 5 (2010): 054113. http://dx.doi.org/10.1088/1742-6596/262/1/012030

[24] R Krause-Rehberg, F Börner, F Redmann, W Egger, G Kögel, P Sperr, W Triftshäuser, Improved defect profiling with slow positrons, Applied Surface Science, Volume 194, Issues 1–4, 21 June 2002, Pages 210-213, ISSN 0169-4332, http://dx.doi.org/10.1016/S0169-4332(02)00104-6

[25] Gibbs, Josiah Willard. Elementary principles in statistical mechanics: developed with especial reference to the rational foundation of thermodynamics. Cambridge University Press, 2010.

[26] Oka, Toshitaka, Satoshi Jinno, and Masanori Fujinami. "Analytical methods using a positron microprobe." Analytical Sciences 25.837 (2009). http://dx.doi.org/10.2116/analsci.25.837

[27] Dr. Matz Haaks, personal enquiry.

[28] U Männig, K Bennewitz, H Bihr, M Haaks, W Sigle, C Zamponi, K Maier, *Defect production by the TEM beam—the first application of the positron microprobe*, Applied Surface Science, Volume 149, Issues 1-4, 1 August 1999, Pages 217-220, ISSN 0169-4332, available http://dx.doi.org/10.1016/S0169-4332(99)00204-4

[29] M Haaks, K Bennewitz, H Bihr, U Männig, C Zamponi, K Maier, Measurements on cracktips in stainless steel AISI 321 by using a new positron microprobe, Applied Surface Science, Volume 149, Issues 1-4, 1 August 1999, Pages 207-210, ISSN 0169-4332, http://dx.doi.org/10.1016/S0169-4332(99)00202-0

[30] Karsten Bennewitz, Matz Haaks, Torsten Staab, Stephan Eisenberg, Thomas Lampe and Karl Maier, Positron annihilation spectroscopy - a non-destructive method for lifetime prediction in the field of dynamical material testing

[31] Zamponi, C. and Männig, U. and Staab, T. E. M. and Maier, K. and Eichler, S. and Hammer, R., Point defects as result of surface deformation on a GaAs wafer Applied Physics Letters, 83, 4128-4130 (2003), :http://dx.doi.org/10.1063/1.1625786

[32] Haaks, Matz; Müller, Ingo; Schoeps, Andreas; Franz, Hermann; Spatially resolved deformation studies on carbon steel employing X-rays and positron annihilation, http://dx.doi.org/10.1002/pssa.200622063 physica status solidi Vol 203 Issue 4 March 2006

[33] Eich, P., Haaks, M., Sindelar, R., Maier, K., Spatially resolved defect studies on fatigued carbon steel, physica status solidi (c) Volume 4, Issue 10, pages 3465-3468, September 2007 http://dx.doi.org/10.1002/pssc.200675814

[34] M. Haaks, Scanning positron microscopy: Non-destructive imaging of plastic deformation in the micrometer range, CIRP Annals - Manufacturing Technology, Volume 57, Issue 1, 2008, Pages 537-540, ISSN 0007-8506, http://dx.doi.org/10.1016/j.cirp.2008.03.109

[35] Klobes, B., B. Korff, O. Balarisi, P. Eich, M. Haaks, I. Kohlbach, K. Maier, R. Sottong, and T. E. M. Staab. "Defect investigations of micron sized precipitates in Al alloys." In Journal of Physics: Conference Series, vol. 262, no. 1, p. 012030. IOP Publishing, 2011. http://dx.doi.org/10.1088/1742-6596/262/1/012030

[36] Weinersmith, Zach. Saturday Morning Breakfast Cereal, retrieved January 20, 2015, http://www.smbc-comics.com/?id=2088

[37] G Kögel, SPM-Group, The München scanning positron microscope, Applied Surface Science, Volume 116, 2 May 1997, Pages 108-113, ISSN 0169-4332, http://dx.doi.org/10.1016/S0169-4332(96)01038-0

[38] Piochacz, C.; Egger, W.; Hugenschmidt, C.; Kögel, G.; Schreckenbach, K.; Sperr, P.; Dollinger, G. Implementation of the Münich scanning positron microscope at the positron source NEPOMUC physica status solidi (c), vol. 4, issue 10, pp. 4028-4031

[39] A. Zecca, R. S. Brusa, M. P. Duarte-Naia,, G. P. Karwasz,, J. Paridaens, A. Piazza, G. Kögel, P. Sperr, D. T. Britton, K. Uhlmann, P. Willutzki and W. Triftshäuser, A Pulsed Positron Microbeam, EPL (Europhysics Letters) Volume 29 Number 8, http://dx.doi.org/10.1209/0295-5075/29/8/005

[40] Peter Sperr *et al.*, On the Electronic Design and the Performance of a Ramp Generator for a Pulsed Low Energy Positron Beam, 1994, Materials Science Forum, 175-178, 993

[41] P. Sperr, G. Kögel, P. Willutzki, W. Triftshäuser, Pulsing of low energy positron beams, Applied Surface Science, Volume 116, 2 May 1997, Pages 78-81, ISSN 0169-4332, http://dx.doi.org/10.1016/S0169-4332(96)01032-X

[42] D.T. Britton, K. Uhlmann, G. Kögel, Magnetic positron optics, Applied Surface Science, Volume 85, 2 January 1995, Pages 158-164, ISSN 0169-4332, http://dx.doi.org/10.1016/0169-4332(94)00326-2

[43] Uhlmann K. ; Britton D. T. ; Kögel G., A through the lens reflection remoderator for positrons, Optik (Stuttgart) Y. 1994, vol. 98, No. 1, pages 5-10

[44] Bleeker, A. J. and Kruit, P., A condenser objective lens with asymmetric polepieces to facilitate the extraction of secondary and Auger electrons, Review of Scientific Instruments, 62, 350-356 (1991), http://dx.doi.org/10.1063/1.1142126

[45] K Uhlmann, D T Britton and G Kögel, A new optical column for a scanning positron microscope Measurement Science and Technology Volume 6 Number 7 1995 http://dx.doi.org/10.1088/0957-0233/6/7/012

[46] W Egger, G Kögel, P Sperr, W Triftshäuser, S Rödling, J Bär, H.-J Gudladt, Vacancy clusters close to a fatigue crack observed with the München scanning positron microscope, Applied Surface Science, Volume 194, Issues 1–4, 21 June 2002, Pages 214-217, ISSN 0169-4332, http://dx.doi.org/10.1016/S0169-4332(02)00106-X

[47] W. Egger, G. Kögel, P. Sperr, W. Triftshäuser, J. Bär, S. Rödling, H.-J. Gudladt, Measurements of defect structures of a cyclically deformed Al–Mg–Si alloy by positron annihilation techniques, Materials Science and Engineering: A, Volumes 387–389, 15 December 2004, Pages 317-320, ISSN 0921-5093, http://dx.doi.org/10.1016/j.msea.2004.02.070

[48] Hugenschmidt, C. "The status of the positron beam facility at NEPOMUC." In Journal of Physics: Conference Series, vol. 262, no. 1, p. 012002. IOP Publishing, 2011. http://dx.doi.org/10.1088/1742-6596/262/1/012002

[49] C Piochacz et al, Enhancement and Transformation of the Phase Space Density of the NEPOMUC Positron Beam, Journal of Physics: Conference Series, Volume 505, conference 1, 2014, http://dx.doi.org/10.1088/1742-6596/505/1/012027

[50] Munroe, R, The difference, XKCD, a webcomic of romance, sarcasm, math and language, retrieved 20.1.2015 http://xkcd.com/242/

[51] Maekawa, M., Y. Yabuuchi, and A. Kawasuso. "Evaluation of stainless steel under tensile stress using positron microbeam." Journal of Physics: Conference Series. Vol. 225. No. 1. IOP Publishing, 2010. http://dx.doi.org/10.1088/1742-6596/225/1/012033

[52] Maekawa, M., and A. Kawasuso. "Observation of spatial distribution of vacancy defects in semiconductor by positron microscope and electron beam induced current measurement." Journal of Physics: Conference Series. Vol. 443. No. 1. IOP Publishing, 2013. http://dx.doi.org/10.1088/1742-6596/443/1/012041

[53] Kawasuso, A., T. Ishimoto, M. Maekawa, Y. Fukaya, K. Hayashi, and A. Ichimiya. "A coherent positron beam for reflection high-energy positron diffraction." Review of scientific instruments 75, no. 11 (2004): 4585-4588. http://dx.doi.org/10.1063/1.1806651

[54] Yabuuchi, A., M. Maekawa, and A. Kawasuso. "Positron microbeam study on vacancy generation caused by stress corrosion crack propagation in austenitic stainless steels." Journal of Physics: Conference Series. Vol. 262. No. 1. IOP Publishing, 2011. http://dx.doi.org/10.1088/1742-6596/262/1/012067

[55] Yabuuchi, A., M. Maekawa, and A. Kawasuso. "Vacancy defects in a stress-corrosion-cracked Type 304 stainless steel investigated by positron annihilation spectroscopy." Journal of Nuclear Materials 419.1 (2011): 9-14. http://dx.doi.org/10.1016/j.jnucmat.2011.08.012

[56] Aihara, Jun, *et al.* "Microstructures and Positron Annihilation Spectroscopy of Nearly Stoichiometric ZrC Coating Layers for Advanced High-temperature Gas-Cooled Reactor Fuel." Journal of the American Ceramic Society 94.12 (2011): 4516-4522. http://dx.doi.org/10.1111/j.1551-2916.2011.04785.x

[57] Stoeffl, W., P. Asoka-Kumar, and R. Howell. "The positron microprobe at LLNL." Applied surface science 149, no. 1 (1999): 1-6. http://dx.doi.org/10.1016/S0169-4332(99)00162-2

[58] Howell, Richard H., W. Stoeffl, A. Kumar, P. A. Sterne, T. E. Cowan, and J. Hartley. "High current pulsed positron microprobe." In Materials Science Forum, vol. 255, pp. 644-646. 1997. http://dx.doi.org/10.4028/www.scientific.net/MSF.255-257.644 https://e-reports-ext.llnl.gov/pdf/232150.pdf

[59] Asoka-Kumar, P., R. Howell, W. Stoeffl, and D. Carter. "High intensity positron program at LLNL." In The fifteenth international conference on the application of accelerators in research and industry, vol. 475, no. 1, pp. 361-365. AIP Publishing, 1999. http://dx.doi.org/10.1063/1.59156 https://e-reports-ext.llnl.gov/pdf/234263.pdf

[60] Scanning electron microscope product web page, TOPCON CORPORATION, retrieved 12.12.2014. http://www.topcon.com.sg/industrial/sm.html

[61] Periodic table, Nickel, Royal Society of Chemistry, retrieved 15.2.2015. http://www.rsc.org/periodic-table/element/28/nickel

[62] Piochacz, C., and C. Hugenschmidt. "A novel setup for the pulsing and energy enhancement of a positron beam." In Journal of Physics: Conference Series, vol. 443, no. 1, p. 012093. IOP Publishing, 2013. http://dx.doi.org/10.1088/1742-6596/443/1/012093

[63] Operating manual of DSM 950 scanning electron microscope, ZEISS/OPTON

A ZEISS/Opton, DSM 950 SEM

The SEM reserved for construction of the SPM is DSM 950 (ZEISS/Opton). It consists of a separate microscope and operating modules (Figure 40). The microscope contains a secondary electron detector, operates with acceleration voltages from 490 V to 30 kV and has a maximum resolution of 5 nm (30 kV). The focus of the electron beam can be adjusted from 2 to 50 mm beneath the objective lens. However, the best resolution is attained with a short working distance. The operating manual of the DSM 950 describes comprehensively the initialisation and the operation of the microscope. [63]

Figure 40: DSM 950 (ZEISS/Opton) scanning electron microscope consists of separate microscope and operating modules. The controls of the vacuum system are located in the front side of the microscope module. The controls of the electron beam are located in the operating module.

The recorded image consists of 512×512 pixels with an 8 bit gray-scale resolution. The sample can be scanned either with a TV mode (25 frames/s), slow scans from 1 s to 360 s per image or by averaging up to 256 TV-rate images. Besides scanning a 2-D image, the microscope can scan a line, the electron beam can be locked onto a single spot or the beam can be controlled externally by two analogous +-10 V voltages.

Thus, DSM 950 can also perform electron lithography and, if accompanied with a suitable X-ray detector, energy-dispersive X-ray (EDX) spectroscopy as well. The measured image is shown on the CRT screen of the SEM, it can be received from "BAS OUT" and "SYNC OUT" BNC-terminals at the backside of the operating module of the DSM 950 or from RS-232 serial port with DITI DOS-software (ZEISS). [63]

A.1 Electron optics

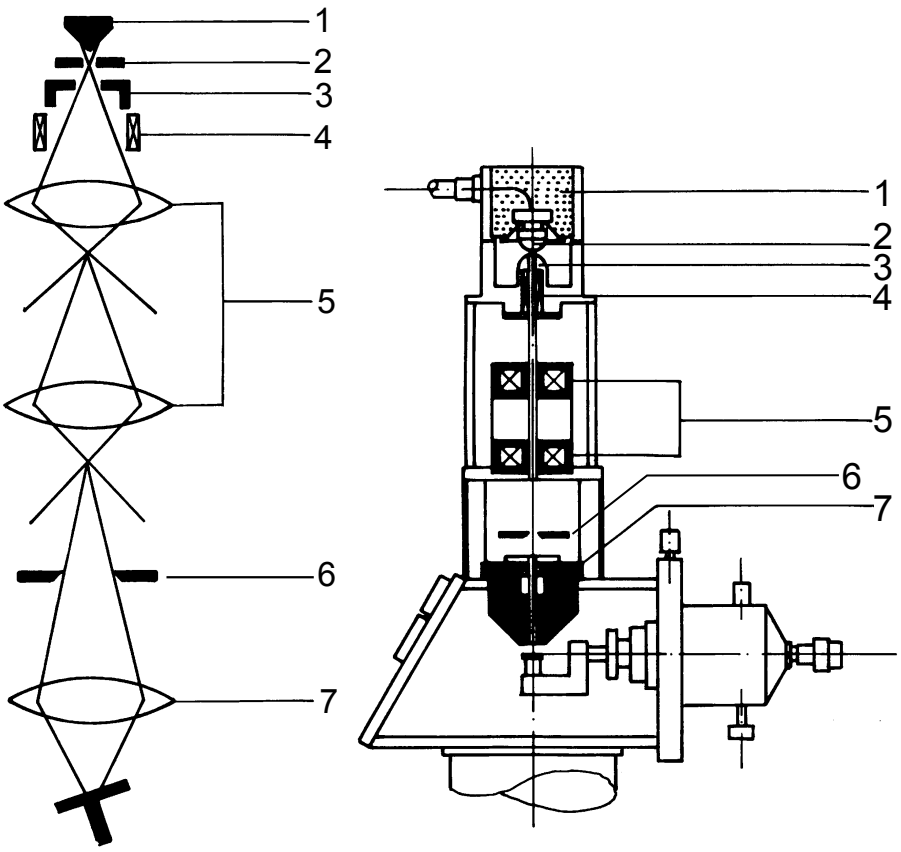

(a) (b)

Figure 41: A diagram (41a) and a cross section (41b) of the optical column of the DSM 950 (ZEISS/Opton) [63]. The numbers refer to the same elements in both the both figures: (1) Electron source, (2) Wehnelt cylinder, (3) anode, (4) beam alignment coils, (5) condenser lenses, (6) aperture, (7) objective lens.

The operation of the DSM 950 is illustrated in Figure 41. The optical components of the DSM 950 are located outside the vacuum system. The electron source (1 in Figure 41) consists of a tungsten hair pin filament inside a Wehnelt cylinder (2 in Figure 41). The electrons are accelerated after the source with an anode (3 in Figure 41) on the ground potential. Next, the electron beam enters a liner tube, which is

located within a vacuum tube and can also be removed for cleaning. The liner tube also includes constant apertures. [63]

There are beam alignment coils (4 in Figure 41) around the top part of the liner tube. With these, the electron beam can be deflected perpendicularly to the beam line. They are used to complete the alignment of the electron source. [63]

A pair of condenser lenses (5 in Figure 41) changes the diameter of the electron beam at the location of the objective aperture (6 in Figure 41). The aperture removes the part of the electron beam, which hits the aperture outside the aperture hole. The excitation of the condenser lenses is changed when the user changes the "resolution" setting from the operating module. The currents of both lenses are adjusted simultaneously to keep the location of the cross-over behind the second condenser lens approximately constant. A higher resolution setting reduces both the size and the flux of the electron beam. The aperture is located within a holder, which allows a manual change and alignment of the aperture *in situ*. The holder has four apertures with diameters of 200 µm, 160 µm, 120 µm and 70 µm. [63]

The objective lens (7 in Figure 41) focuses the electron beam on the sample. The vertical location of the focus can be adjusted with the "focus" setting of the operating console. The objective lens also houses two sets of crossed saddle coils, which operate as scanning coils (crossed squares in Figure 42, 1 and 2 in Figure 42b). The upper set of coils (1 in Figure 42b) deflects the electron beam away from the optical axis. The lower set of coils (2 in Figure 42b) deflects the beam back through the center of the objective lens (3 in Figure 42b) to the sample (4 in Figure 42b). An eight-pole stigmator is also incorporated within the scanning coil system. The stigmator is used to correct the shape of the electron beam (astigmatism). [63]

A.2 Requirements

The DSM 950 SEM requires an environment with a constant temperature within the range 15-25 °C, a relative humidity lower than 60 % and floor vibrations less than 3 µm peak-to-peak, regardless of frequency. The magnetic fields have to be weaker than $5 \cdot 10^{-7}$ T peak-to-peak. The SEM needs 3 kVA of electrical power with a voltage of 220 V (+10/-15 %). The power line should have a slow-blow fuse of 25 A. As the SEM includes parts with high voltages, microscope has to be grounded with an additional conductor with a cross section of at least 4 mm^2. [63]

Cooling is required for the turbomolecular pump, magnetic lenses and the power elements of the electronics. The heat output of the SEM to the circulating coolant is approximately 1 kW and the coolant has to flow at least 2 l/s with a pressure of 2-3 bar. [63] A 50 % mixture of ethane-1,2-diol and water type is used as the coolant with a Neslab M33 chiller with a temperature control of the coolant. The DSM 950 has a signal output to activate the chiller only when the cooling is necessary, and it should be connected to the chiller (Figure 43). The direction of the coolant flow is marked with up- and downwards pointing arrows (Figure 44) but the documentation does not reveal which one indicates the input and which one the output of the coolant. [63]

Venting the vacuum chamber with nitrogen gas instead of air significantly reduces the evacuating time. A nitrogen gas supply can be inserted into a valve shown in

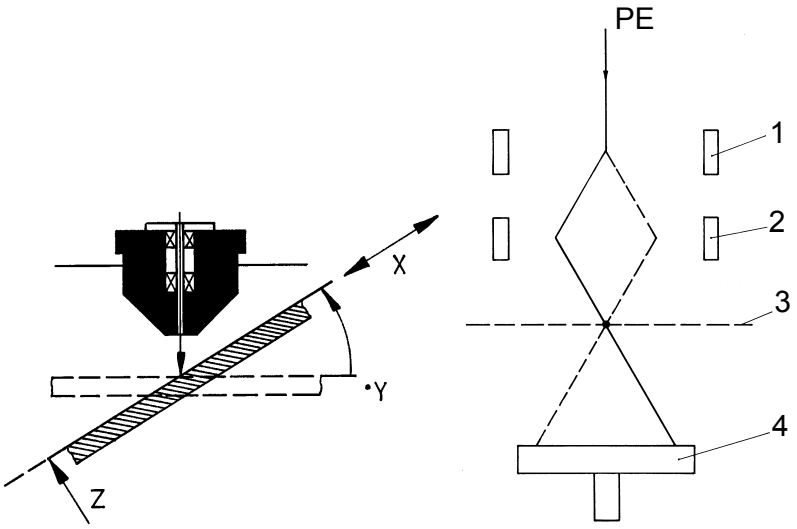

(a) (b)

Figure 42: 42a: A cross section of the objective lens with scanning coils (crossed rectangles) and the sample stage with the possible manipulation directions [63]. 42b Electron beam scanning [63]: (1) and (2) scanning coils, (3) intersection with the center of objective lens, (4) sample stage.

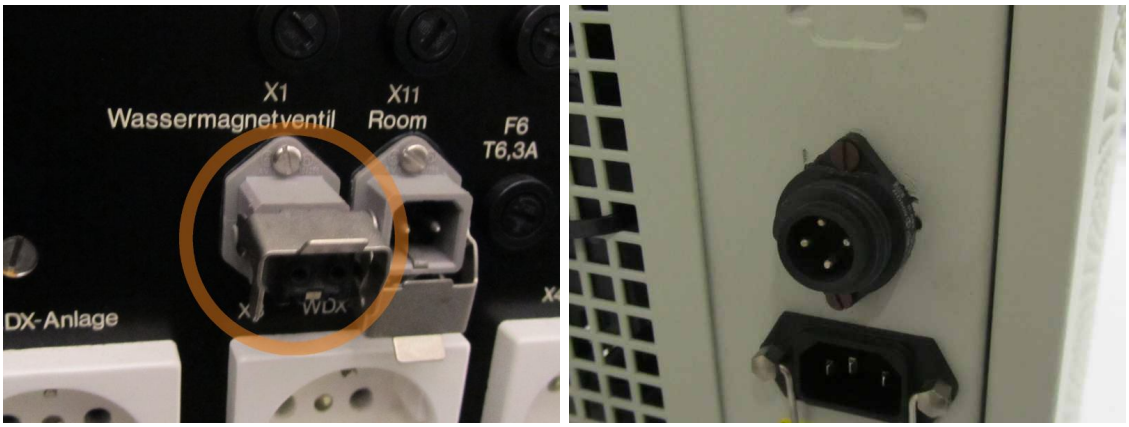

(a) Coolant control connector in the back panel of the DSM 950

(b) Coolant control connector in the back panel of the Neslab M33 chiller

Figure 43: Automatic coolant control in the DSM 950 and the Neslab M33 chiller.

Figure 44. The pressure of the nitrogen has be between 0.2 and 0.3 bar. The nitrogen consumption is with an open chamber is 3 l/s at with the nitrogen pressure of 0.2 bar. The nitrogen can be supplied from a gas cylinder with pressure reducing valves. [63]

The DSM 950 has a shock-damping system consisting of four air-filled shock-absorbers. The shock-damping system reduces sensitivity to floor vibrations but the microscope can be utilised for non-extreme resolution imaging also with empty

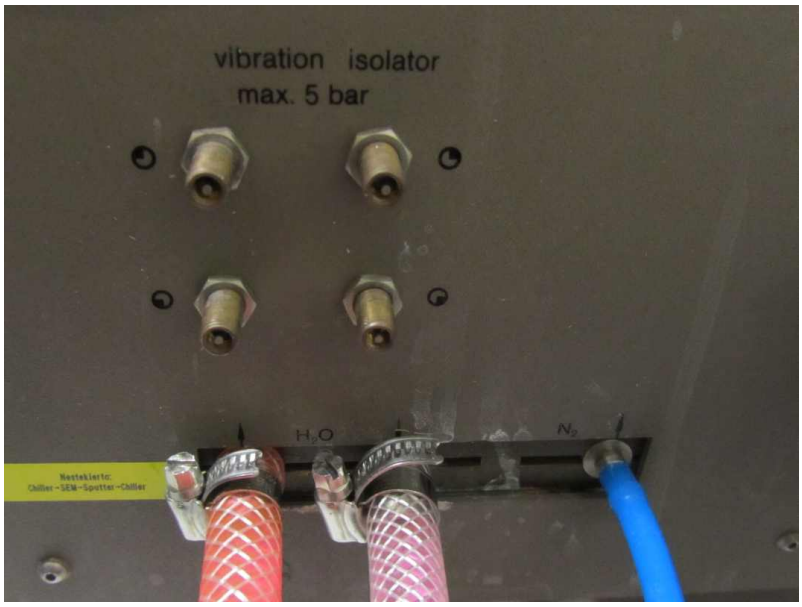

Figure 44: Connectors on the back-side of the DSM 950 for coolant, nitrogen gas for venting and compressed air for the shock-damping system.

shock-absorbers. The maximum air pressure of the shock-absorbers is 5 bar, as marked above the vents (Figure 44). In the case of the shock-absorbers need frequent filling, the valves should be cleaned [63].

The main vacuum pump of the DSM 950 is a Pfeiffer TPH 170 turbo pump. It needs a prevacuum of approximately 1 Pa, which has to be provided with an external vacuum pump.